



# FINAL REPORT

**Grant Agreement number: ACP0-GA-2012-321495**

**Project acronym: HEXAFLY**

## Project title: High-Speed Experimental Fly Vehicles

## Funding Scheme: FP7: Collaborative Project: Small or Medium-Scale Focused Research Project Theme 7: TRANSPORT

**Date of latest version of Annex I against which the assessment will be made:**

**Scientific representative of the project's coordinator:**

**Name: Dr J. Steelant**

**Title: Senior Engineer**

**Organisation: European Space Agency – European Space Research and Technology Centre (ESA-ESTEC)**

**Tel: +31/71/565.5552**

**Fax: +31/71/565.5421**

**E-mail: Johan.Steelant@esa.int**

**Project website address: www.esa.int/techresources/hexafly**

## APPROVAL

| **Title** | **issue** | revision |
|---|---|---|
| HEXAFLY: Final Report | 1 | 0 |

| **Author(s)** | **date** |
|---|---|
| J. Steelant (ESA) | |
| C. Walton (GDL) | |
| L. Serre (ONERA) | |

| **Approved by** | **date** |
|---|---|
| J. Steelant (ESA) | |

I, as scientific representative of the coordinator of this project and in line with the obligations as stated in Article II.2.3 of the Grant Agreement declare that:

- The attached final report represents an accurate description of the work carried out in this project;
- The project (tick as appropriate):

  X has fully achieved its objectives and technical goals;

  ☐ has achieved most of its objectives and technical goals with relatively minor deviations[1];

  ☐ has failed to achieve critical objectives and/or is not at all on schedule[2].

- The public website is up to date, if applicable.
- To my best knowledge, the financial statements which are being submitted as part of this report are in line with the actual work carried out and are consistent with the report on the resources used for the project (section 6) and if applicable with the certificate on financial statement.
- All beneficiaries, in particular non-profit public bodies, secondary and higher education establishments, research organisations and SMEs, have declared to have verified their legal status. Any changes have been reported under section 5 (Project Management) in accordance with Article II.3.f of the Grant Agreement.

Name of scientific representative of the Coordinator: J. Steelant

Date: 31/ 07/ 2014

Signature of scientific representative of the Coordinator: .....

1 If either of these boxes is ticked, the report should reflect these and any remedial actions taken.

2 If either of these boxes is ticked, the report should reflect these and any remedial actions taken.

# Table of contents

## List of Figures



## List of Tables

## Nomenclature

*Acronyms*

| | |
|---|---|
| CFD | Computational Fluid Dynamics |

*Roman Symbols*

| | |
|---|---|
| T | temperature [K] |

*Greek Symbols*

| | |
|---|---|
| ρ | density [kg $m^{-3}$] |

*Superscripts and subscripts*

| | |
|---|---|
| $_i$ | species index |

# 1 Publishable Summary

Civil High-speed transportation has always been hampered by the lack of range potential or a too high fuel consumption stemming from a too low cruise efficiency. Indeed, looking into the performance of classically designed high-speed vehicles, their performances drop nearly linearly with flight Mach number as indicated by the red line on *Fig. 1*. Over the last years, however, radical new vehicle concepts were proposed and conceived having a strong potential to alter this trend. This innovative approach is based upon a well elaborated integration of a highly efficient propulsion unit with a high-lifting vehicle concept. The realization of both a high propulsive and aerodynamic efficiency is based upon the minimization of kinetic jet losses while striving to the best uniformity but minimal induced velocity for lift creation. The dashed green line in *Fig. 1* illustrates the potential of this innovative design methodology whereas the green line indicates what has been achieved as a revolutionary, high speed civil air transportation concepts worked-out along this new approach.

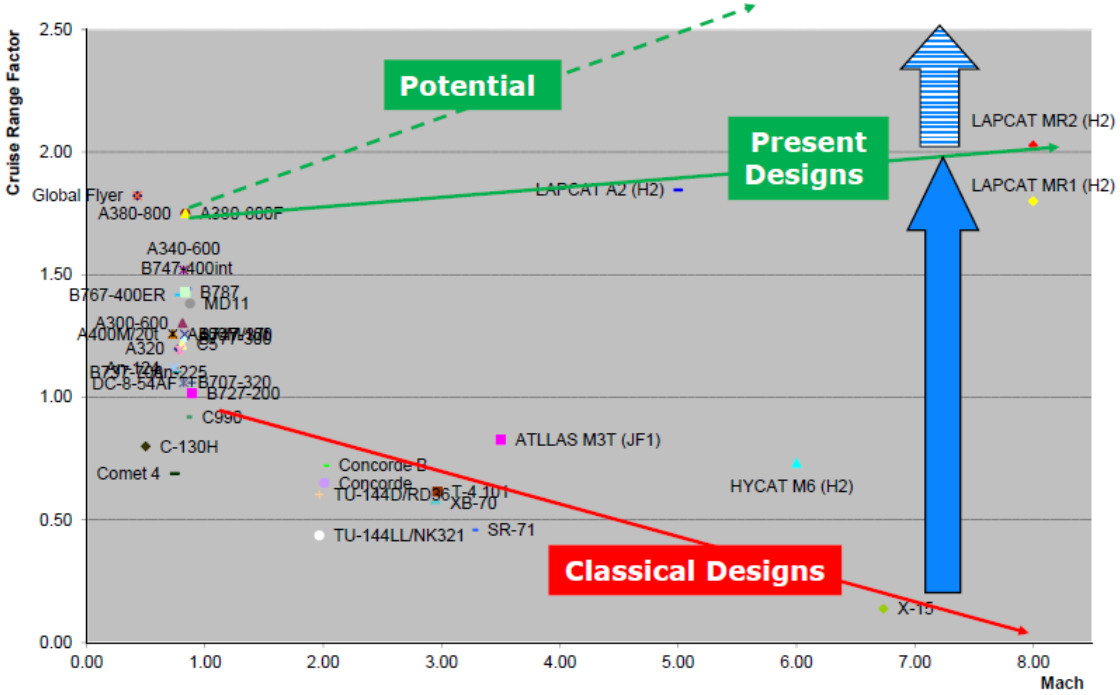


**Fig. 1: Long-range potential of high-speed vehicles in function of flight Mach number: Red: achievable with classical designs with minimal integration; Green: present designs based upon strongly integrated propulsion-vehicle designs with a potential limit (dashed line)**

Performing a test flight will be the only and ultimate proof to demonstrate the technical feasibility of these new promising high-speed concepts versus their potential in range and cruise. This would result into a major breakthrough in high-speed flight and create a new era of conceptual vehicle designs.

At present, the promised performances can only be demonstrated by numerical simulations or partly experimentally. As high-speed tunnels are intrinsically limited in size or test duration, it is nearly impossible to fit even modest vehicle planform completely into a tunnel (*Fig. 2*). Therefore experiments are limited either to the internal propulsive flowpath with combustion but without the presence of high-lifting surfaces, or to complete small-scaled aero-models but without the presence of a combusting propulsion unit. Though numerical simulations are less restrictive in geometrical size, they struggle however with accumulated uncertainties in their modelling of turbulence, chemistry and combustion making complete Nose-to-Tail predictions doubtful without in-flight validation. As a consequence, the obtained technology developments are now limited to a technology readiness level of TRL=4 (components validated in laboratory).

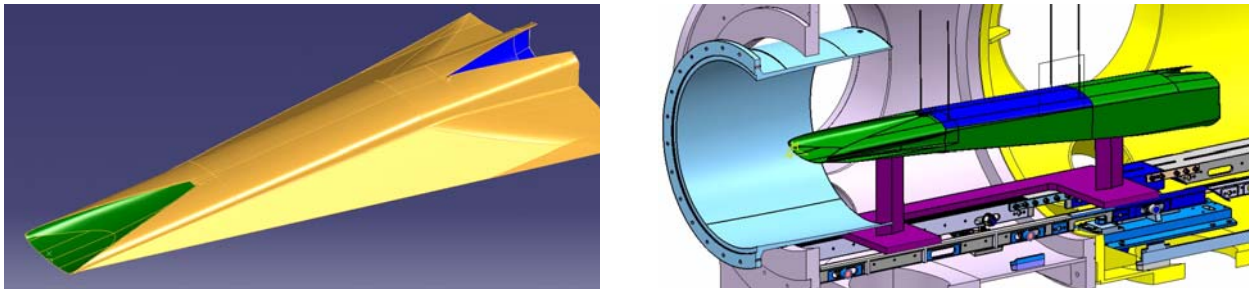

**Fig. 2: Left: example of a completely integrated vehicle concept with intake (green), nozzle (blue) and fuselage-wings (gold), Right: corresponding internal flowpath model maximized within tunnel without aero-planform (1.5m long)**

## 1.1 Project Objectives

The HEXAFLY project aims to achieve a first maturation and a proof of concept to experimentally fly-test these radically new conceptual designs accompanied with several breakthrough technologies on board of a high-speed vehicle. This approach would increase drastically the Technology Readiness Level (TRL) up to 6 (System demonstrated in relevant environment).
The emerging technologies and breakthrough methodologies strongly depending on experimental flight testing at high speed can be grouped around the 6 major axes of HEXAFLY:

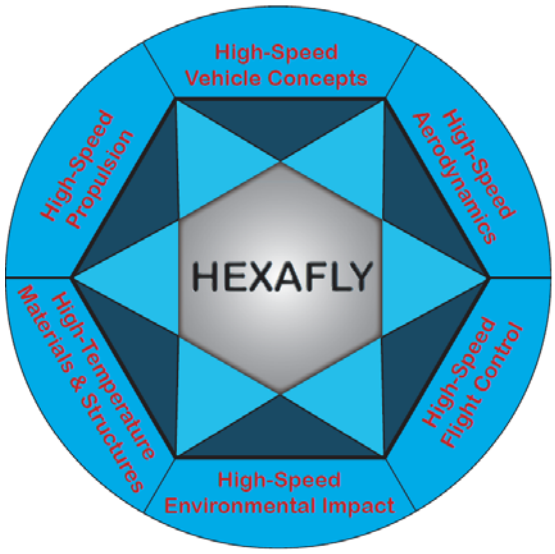


1. ***High-Speed Vehicle Concepts*** to assess the overall vehicle performance in terms of cruise-efficiency, range potential, aero-propulsive balance, aero-thermal-structural integration, etc...
2. ***High-Speed Aerodynamics*** to assess e.g. compressibility effects on transition, aerodynamic vehicle shapes with high L/D, stability, etc…
3. ***High-Speed Propulsion*** to evaluate the performances of high-speed propulsive devices such as intakes, air-breathing engines (ABE), nozzles (SERN) including phenomena such as high-speed combustion, injection-mixing processes, etc…
4. ***High-Temperature Materials and Structures*** to flight test under realistic conditions high temperature lightweight materials, active/passive cooling concepts, reusability aspects in terms oxidation, fatigue, etc…
5. ***High-Speed Flight Control*** requiring real-time testing of GNC (Guidance Navigation Control) in combination with HMS/FDI technologies (Health Monitoring Systems/ Fault Detection and Isolation)
6. ***High-Speed Environmental Impact*** focusing on reduction techniques for sonic boom and sensitivities of high-altitude emissions of $H_20$, $CO_2$, NOx on the stratosphere.

To mature this experimental flight testing, a scientific mission profile will be defined followed by a proof-of-concept based upon:

- a preliminary design of a high-speed experimental flight vehicle covering the 6 major axes
- selection and integration of the ground-tested technologies developed within LAPCAT I & II, ATLLAS I & II and other national programs
- identification of the most promising flight platform(s)

allowing to address following items:

- identification of potential technological barriers to be covered in a follow-up project
- assessment of the overall ROM-costs to work the project out in a follow-up project
- the progress and potential of technology development at a higher TRL

The vehicle design will be the main driver and challenge in this project. The prime objectives of this experimental high-speed cruise vehicle shall aim for

- an integrated conceptual design demonstrating a combined propulsive and aerodynamic efficiency
- a positive aero-propulsive balance at a cruise Mach number of 7 to 8 in a controlled way
- making optimal use of advanced high-temperature materials and/or structures
- an evaluation of the sonic boom impact by deploying dedicated ground measurement equipment

Once conceived, the level of acceleration from Mach 5 up to a cruise speed of Mach 8 can be determined.

The level of complexity and the number of technologies to be potentially integrated largely depends on the affordable size of the flight vehicle. The presently available ground facilities within Europe limit the size to ~1.5m length whereas ~4.5m seems to be an affordable upper limit stemming from presently on-going flight experiments in the US and Russia. Though a larger scale can accommodate a higher density of technology and measurements points, the smaller scale will excel in terms of a lower complexity, weight, size and cost. Therefore, a trade-off is necessary to actually evaluate how the above listed objectives can be realized within an achievable technical and financial scope. Therefore, HEXAFLY is a necessary step prior to embarking onto a larger experimental flight project by identifying, sorting out and alleviating any potential technological risk upfront.

This will require a:

- definition of one preliminary experimental flight vehicle layout but scaled at a small (~1.5m) and a larger scale (e.g. ~4.5m) based upon the available aero- and propulsive databases of the Mach 8 vehicle concept investigated within the LAPCAT II project
- definition of flying test-beds to perform the job: i.e. ground-launched (e.g. sounding rockets) and/or air-launched boosters (e.g. Raduga-D2 booster released from Tu-22 supersonic aircraft):
    - sounding rockets for both scales
    - air-launched only for the largest scale
- identification of existing flight experimental configurations as a building platform for partly or full integration of a pre-defined vehicle concept
- evaluating how far ground-test results can or need to be extrapolated towards real flight conditions by means of numerical tools and/or ground facilities, e.g. wall temperature effects, scaling…

The databases, simulation tools and methodologies developed within LAPCAT I & II and ATLLAS I & II will be fully exploited to achieve the above listed requirements and to highlight potential technological hurdles. Furthermore, the two proposed scales for the very same vehicle geometry allow assessing the increased density of gauges and inclusion of additional new technologies on the largest vehicle scale versus the technical and financial risks.

Besides the vehicle and platform definition, the suitability of the launch site and test range need to be assessed in terms of potential limitations on the mission and scientific objectives, i.e. flight corridors, TTC (telemetry, tracking and command), safety aspects (termination) and recovery. In a first step, test ranges within Europe and Russia will be favoured. The Andoya test range in Norway, the Esrange and the NEAT range in Sweden are equipped and suitable for ground-launched flight tests in Europe. For air-launch ranges however, no sufficient downrange capability is available within Europe whereas Russia can open some of its test ranges to Europe for experimental flight tests as formerly done for NASA and now for France.

All of the above investigations shall be performed in enough depth to evaluate the ROM-costs for the two flight vehicle scales, their integration and the corresponding launch methodologies. The outcome will provide an overview of the most promising routes towards high-speed flight testing in function of size, complexity and cost. Equipped with these results, the European community on high-speed aircraft will be further aligned and able to profile themselves uniformly towards any international collaboration on flight testing as promoted by the European Commission, in particular Russia, Japan and Australia.

A *duration of 18 months* for this project is set forward in order to:

- define the requirements and operational conditions for the scientific mission,
- perform a preliminary layout of a flight vehicle able to test technologies along the 6 major axes,

- define the required flying platform with the needed adaptations
- to address potential technology barriers
- evaluate the ROM-costs of the different vehicle/platform combinations

## 1.2 Progress and Achievements

Please include for each subsection a description of the *work performed* since the beginning of the project, a description of the *main results* achieved so far, the *expected final results* and their *potential impact and use* (including the socio-economic impact and the wider societal implications of the project so far: don't hesitate to make links to other (short-term) applications such as for subsonic airliners, .....).

*Experimental Flight Vehicle Definition*

The study began with some preliminary trajectory simulations performed by DLR-Moraba and Gas Dynamics Ltd. For this initial profile the VS-40 two-stage sounding rocket was used for the launch system, with the resulting flight conditions used as inputs to some of the component modelling studies, including the Nose-to-Tail CFD studies and the combustion chamber thermal modelling.

The Nose-to-Tail analyses confirmed that the vehicle operation at fuel-on conditions is associated with boundary layer separation issues at the combustor entrance. However, a stable solution with net thrust was obtained at an equivalence ratio of 0.8 assuming transitional flow on the forward intake surfaces.

The thermal analysis led to the final proposed solution of Cu/Zr alloy protected by a TBC for the combustion chamber, whilst for the injection struts the best solution appears to be Molybdenum struts covered by an ablative insulated layer in the first part of the trajectory.

Following the generic system studies, a more detailed design study of the experimental vehicle was undertaken. This began with an assessment of the vehicle control system using some of the aerodynamic performance figures derived from the Nose-to-Tail analyses. The final V47 configuration was shown to be statically stable for longitudinal aerodynamics with a static margin of 6.6%, and also statically stable for lateral-directional aerodynamics. Linear lateral dynamics was neutrally stable (Dutch Roll) and not damped due the modelling approximations made, but a possible active control system based on asymmetrical deflection of ailerons (no rudders) was proposed to increase the Dutch Roll damping.

A structural analysis of the experimental flight vehicle was developed by DLR-St in a first design iteration. For this study the vehicle was split into several substructures, such as nose and inlet section (including intake leading edges), fuselage and associated support structure, rudders, wings (and wing leading edges), internal flow path and ailerons. Each of these components has to fulfil different requirements (e.g. oxidation resistance, mass, structural stability and integrity) and therefore, different materials needed to be applied to satisfy the specific needs of the mission. Subsequently, a first structural model was set up and both a mechanical and a transient thermo-mechanical finite element analysis were performed. A final structural layout was adapted by ESA-ESTEC to assure the integration of all subsystems and thermo-mechanical constraints stemming from the different components.

*Flight Platform Definition*

Two ground-based solutions were conceived, i.e. an unguided and guided sounding rocket Launch Vehicles. The unguided VS-40 requires a spin stabilized vehicle which requires a spin balanced payload. Due to the highly unsymmetrical layout of the EFTV spin balancing is nearly impossible. Therefore unguided, spin stabilized Launch Vehicle are excluded for further use in HEXAFLY.

The initial guided options have been the Brazilian S40 and the VS-40, both equipped with the same Thrust Vector Control (TVA). The S40 did not match the scientific objectives of providing Mach 7 at 90km apogee (limitation to Mach 5). On the other hand the VS-43 does.

Independent if the Launch Vehicle is guided or unguided, the following on-board subsystems are necessary to support the mission: Telemetry, TV, GPS, and Ignition Units for separation. In addition stabilizing Fins and Payload Fairing are required too.

In case of a guided Launch Vehicle the above subsystems are completed during the boosted flight phase with Thrust Vector Assembly, requiring Guidance Navigation and Control (GNC) and Thrust Termination, as well as Radar Transponder. In the unpowered flight phase, stabilization is archived with a Cold Gas System.

The Launch Vehicle can be launched from a single rail launcher or a launch stool. The single rail launcher has the disadvantage that retractable launch lugs need to be implemented. Since the conical skirt diameter of the VS-43 is of 1.3 m the retractable launch lugs would get rather large and the retraction process is fault-prone. Launching from a launch stool is therefore recommended, which offers the opportunity to protect the entire payload with a hammerhead Fairing rather than an ogive nosecone with overlaying wing-tip protection covers. A split version is not recommended since the stiffness will be reduced and separations complexity increased.

For the Air Launched option, the aerodynamic stability is an issue, due to the large lifting surfaces of the EFTV at both scales. This point is to be addressed specifically to enable better understanding of the integration constraints. This study would require further information about the evolution of the booster's center of gravity. These issued should be addressed with Raduga designers.

It seems possible to integrate a large size vehicle as EFTV-A, but the mass should be reduced significantly with respect to today's evaluation of 1,4 t for L=4,5m (mass value to be considered as a pessimistic upper limit).

## 1.3 Next Steps

The outcome of the *HEXAFLY*-study indicated that the proposed vehicle propelled on the basis of a scramjet was technically realizable. After a trade-off, the most promising configuration was a 3m long vehicle being brought to a cruise altitude of 32km, on the basis of a sounding rocket. With this size, it was shown that the proposed vehicle has the potential to perform a stable and trimmed cruise flight demonstrating an aero-propulsive balance, i.e. Thrust ≥ Drag and Lift ≥ Weight.
Similarly, all needed subsystems were defined and sized to perform the job at a conceptual design level. Though the team indicated that the concept and the related technologies have enough maturity as an unpropelled glider, the project identified also some key technological barriers which require a deeper investigation when aiming for a self-supporting and self-propelled vehicle. Grouped along the 6 major axes of the project, the following technology developments are set as objectives for a future study:

1. ***High-Speed Vehicle Concepts:*** to assess the vehicle performance in terms of aero-thermal-structural integration, aero-propulsive loads, etc... based upon a detailed multi-disciplinary design for an experimental flight test vehicle
2. ***High-Speed Aerodynamics:*** to assess the effects of transition on drag to better estimate the ranges of T-D balance, the aerodynamic handling characterization wrt to flight stability,
3. ***High-Speed Propulsion:*** to resize and optimize the combustor/injector geometry by including now the effect of heated walls, the need of hydrogen storage at high pressure and its regulation
4. ***High-Temperature Materials and Structures:*** particular components such as leading edges, combustor and ailerons require particular attention in material choice, sizing and thermal protection
5. ***High-Speed Flight Control:*** the change in engine-on and -off conditions as well as the dorsal mounting of the engine require particular flight control algorithms to assure a flight-stable operation
6. ***High-Speed Environmental Impact:*** to design pressure probes released from the vehicle to measure the sonic boom impact close to the vehicle.

An important element in setting up this flight experiment is the collection and transmission of the experimental data acquired on board. Special attention will be given to the in-flight measurement techniques, the data acquisition and the related telemetry.

# 2 Project Objectives

## 2.1 Experimental Flight Vehicle Definition

The ultimate objective of the HEXFALY project was to design an experiment for flight testing a small-scale hypersonic vehicle. As defined in the Description of Work the project was split into two distinct work-packages, with WP2 focussed on the flight vehicle design, and WP3 addressing the launch platform definition.

Within WP2 there were two primary objectives:

1. Define the goals and requirements for the flight experiment;
2. Layout a vehicle on two different scales (at ~1.5m length, and 3-4.5m length) and assess the impact on the scientific objectives and the overall cost.

The mission requirements were defined within WP2.1, and detailed under D2.1.1. These formed the basis for the subsequent flight vehicle definition under WP2.2, which was to be based on one of the Mach 8 concepts developed under the FP7 funded LAPCAT-II project. As noted above the vehicle was to be assessed at two different scales, with the small-scale vehicle launched from a ground based platform, and the larger scale vehicle mounted on a ground or air-launched platform. A third option was also developed using an existing flight-testing platform, such as LEA.

The broad development plan for the vehicle was a two-fold process, beginning with some generic studies to assess the suitability of the sub-systems in a flight test environment, before lying out the different flight-test options. The description of progress in section ## is broadly aligned with this philosophy.

## 2.2 Flight Platform Definition

Once the mission requirements and the overall vehicle layout are known, one needs to select the potential launching platforms able to bring the flight experiment at the desired speed, altitude and attitude. Two kinds of launching platforms will be evaluated: a ground-based (sounding-rockets) and an air-based (booster concept such as Raduga, …)

The mounting of the flight vehicle will have an impact on the interface with the platform and its overall aero-propulsive performance. Mechanical and aerodynamic design changes are required on the platform which needs to be taking into account in the final trajectory, mission and operation assessment. This WP will conclude with an estimation of the ROM-costs for the different platforms and mission profiles.
For the two different scales of vehicles, two corresponding ground-launched flying platforms need to be selected, adapted and dimensioned to fulfil the mission profile successfully in terms of altitude, attitude and speed. The interface requirements between the payload and sounding rocket will be defined and assessed for each of the scaled vehicles. Finally also an evaluation of the needed ground-based operations, the data retrieval, the potential test ranges, etc. will be assessed.

The experience gained by the partners on an air-launched flying test bed will be applied to assess the adaptations needed to accommodate the up-scaled larger scale experimental vehicle (~4.5m). The interface requirements between the payload, the booster and the air carrier will be defined and assessed for the large vehicle scale and the integrated FEC-option.

Finally also an evaluation of the needed ground-based operations, the data retrieval, the potential test ranges, etc. will be assessed.

This overall assessment will allow sketching out the general layout for the differnt platforms with the integrated flight experiment and provide enough information to assess the overall cost to perform the flight campaign.

# 3 Work Progress and Achievements

## 3.1 Experimental Flight Vehicle Definition

*Introduction*

As noted in section 1.1, the development plan for the vehicle was a two-fold process, beginning with some generic studies to assess the suitability of the sub-systems in a flight test environment, before lying out the different flight-test options. The description of progress in this section is broadly aligned with this philosophy, beginning with a review of the generic system studies, which consisted of:

1. Preliminary trajectory modelling;
2. CFD modelling of both the external vehicle aerodynamics, and the internal engine performance; and
3. Thermal assessment of the combustion chamber.

The report then goes on to describe the layouts of the different flight test options, and their supporting studies. In the discussion that follows three different vehicle architectures are defined:

1. A free flight experiment using the large scale vehicle (EFTV);
2. Vehicle mounted on the LEA platform (ELTV).
3. A captive-carry trial using the small scale vehicle launched on a sounding rocket (ECTV);

It should be noted that there are two variations of the free-flight vehicle; the air-launched version referred to as the EFTV-A; and the ground launched option called the EFTV-G.

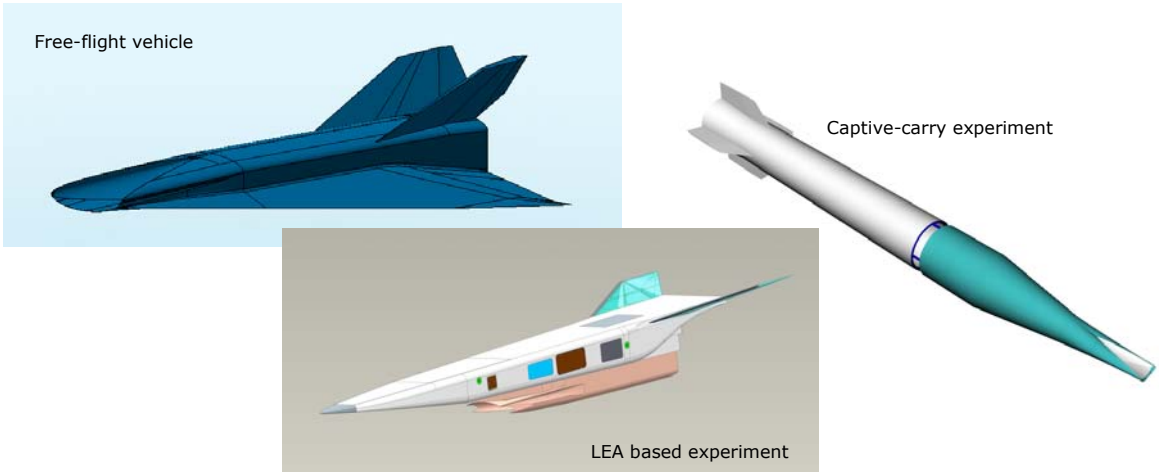


*Figure 1: Different vehicle architectures for the flight test.*

*Background*

At this point it is perhaps useful to briefly review the Mach 8 concept developed under LAPCAT-II, on which the HEXAFLY flight-test configuration is based. As shown in **Figure 2** this civil transport aircraft was intended to carry 300 passengers and crew over a range in excess of 15,000km. The vehicle uses an air-turbo rocket to take-off and accelerate to Mach 4.5, before switching to a dual-mode ramjet to reach the target cruise condition of Mach 8 at an altitude of 35km. With a span 41m and an overall length of over 90m, the vehicle gross take-off weight is estimated to be in excess of 400 tons.

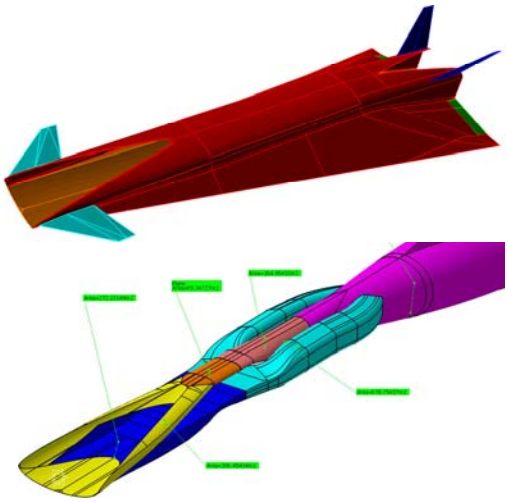

*Figure 2: Mach 8 concept vehicle from LAPCAT-II (courtesy ESTEC)*

As part of the LAPCAT-II project a scaled down version of this vehicle was free-jet tested in the HEG shock-tunnel facility at DLR-Gottingen, as shown in Figure 3. A free-flight model was developed in which the data-acquisition, instrumentation, and fuel system was carried on-board the test vehicle, and over the short test period of the facility (~3-4ms) the vehicle demonstrated that the engine thrust was sufficient to overcome the vehicle drag.

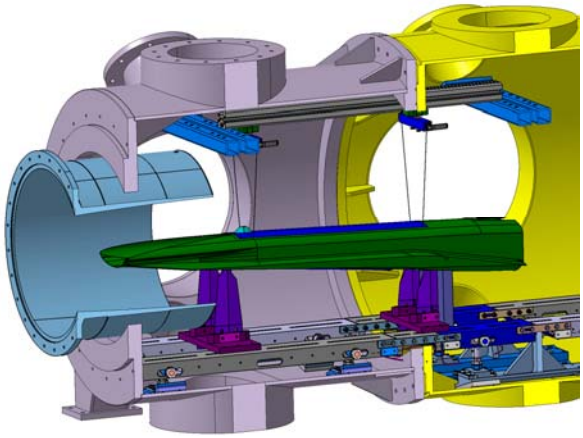

*Figure 3: Sub-scale testing of the LAPCAT vehicle, courtesy DLR.*

*Generic System Studies – Trajectory Modelling*

Work under WP2 began by identifying the target conditions for the flight test campaign. . These were finalised in the 'Mission Requirements Document' (MRD, D2.1.1), which for the ground launched free-flying system were defined as:

1. Mach 7 to 8 with a target flight Mach number of 7.4.
2. An altitude between 27-33km, with a target of 31.9km.
3. A target flight path angle of 0°.

Although the launch platform is primarily an output from WP3, the flight vehicle definition that is developed under WP2 requires some knowledge of the trajectory profile for the experiment. For that reason some preliminary trajectory simulations were performed by DLR-Moraba and Gas Dynamics Ltd, and the resulting flight conditions were used as inputs to some of the component modelling studies.

Following the kick-off meeting in early October 2012, DLR-Moraba provided an initial trajectory profile for a free-flying ground launched system, using the VS-40 two-stage sounding rocket. This is the same launch platform employed for the SHEFEX-II flight test, consisting of an S-40 solid

fuelled first stage motor containing approximately 4tonnes of propellant, and a smaller S-44 second stage motor carrying about 800kg of propellant.

With the experience gained on the SHEFEX-II platform, DLR adapted the launch profile in an attempt to achieve the target test conditions identified in the MRD. **Figure 4** below shows the profile presented by DLR at the first project meeting in Oberpfaffenhofen. It is broadly similar to the SHEFEX-II launch profile although in this case the booster is launched at a slightly shallower flight path angle of ~82°, carrying the vehicle to an apogee of approximately 140km. Before ignition of the second stage motor a precession manoeuvre is performed in order to reduce the pitch angle to about 45°. The second stage motor therefore acts like a retro-rocket by reducing the rate of descent and increasing the horizontal velocity of the vehicle. Following motor burn-out of the second stage, the payload continues on a ballistic descent, reaching Mach 7 at an altitude in excess of 30km.

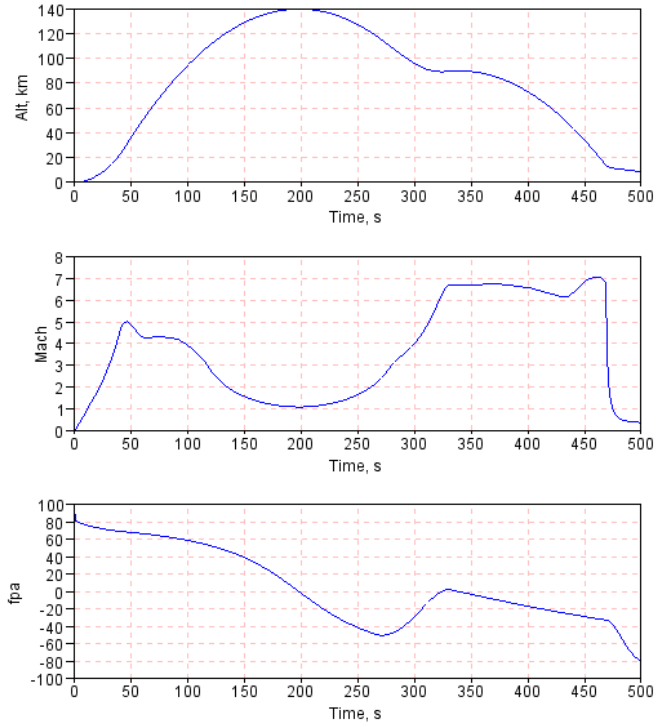


*Figure 4: Altitude (top), Mach number (middle) and Flight Path Angle (bottom) for preliminary Hexafly trajectory, courtesy DLR-Moraba.*

In terms of the Mach number and altitude the booster is therefore capable of achieving the test conditions stipulated in the MRD. However, the flight path angle during the test would be around -30°; as opposed to the level flight condition desired in the MRD. For that reason GDL were tasked with examining alternative trajectories for the ground launched system, using lift during the re-entry phase of the mission to increase the flight path angle.

Figure 5 shows a trajectory profile that comes close to achieving the target conditions for the experiment. The first stage of the profile is broadly similar to that provided by DLR-Moraba with a gross take-off mass of just under 7tonnes, and a steep initial flight path angle in excess of 80°. However, after separation of the first stage motor it is assumed that a precession manoeuvre is employed to drop the pitch angle down to about 5°, much further than the 45° used in the preliminary simulation. By the end of the second stage burn the vehicle has accelerated to 2.4km/s at an altitude of approximately 128km.

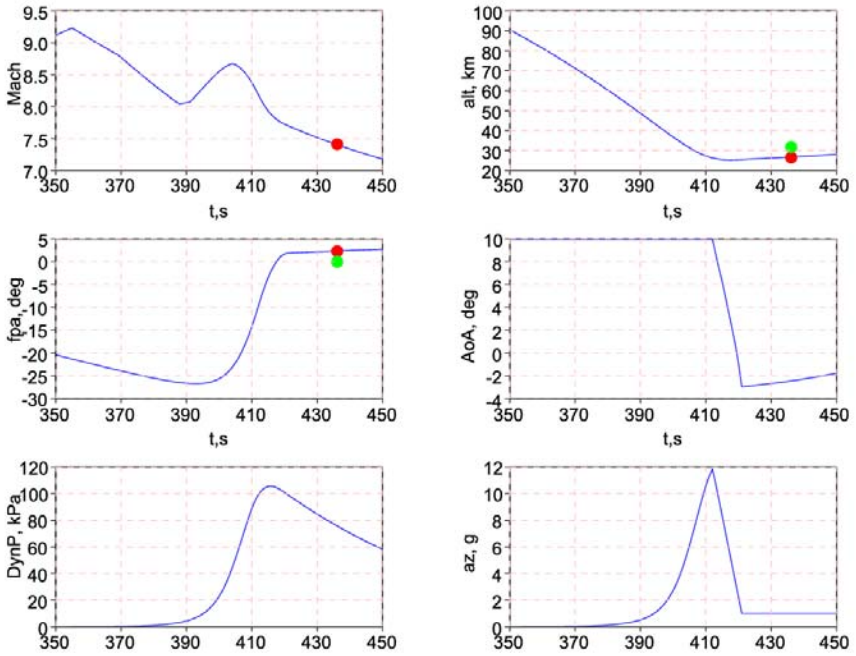


***Figure 5: Trajectory profile for a free-flying EFTV with a 400kg payload. Mach number (top left); Altitude (top right); Flight path angle (middle left); AoA (middle right); Dynamic pressure (bottom left) and vertical acceleration (bottom right).***

During the descent back into the atmosphere, it is assumed that cold gas thrusters can be used to re-orient the vehicle to set a pre-determined initial angle-of-attack for the turn. It is also assumed that once the dynamic pressure starts to build, aerodynamic controls are employed to gradually reduce the angle-of-attack, so that the vehicle achieves a flight path angle of zero degrees on completion of the turn. In this case the payload pulls through zero degrees flight path angle and climbs a little to the target test conditions, so that the peak dynamic pressure occurs a short time before the test window. The payload is within the range specified in the MRD as it passes through Mach 7.4, but to achieve this target requires an angle-of-attack of at least 10° and the ability to rapidly adjust the incidence as the dynamic pressure starts to build. However, the model suggested that it may be possible to use Lift during the re-entry to achieve a 0° flight path-angle for the test, and the model was therefore used to define input conditions for both the control system design and the combustion chamber thermal analysis (described later in the report).

*Generic System Studies – Nose-to-Tail Analyses*

The aerodynamic database used for the trajectory model was derived from a CFD computation prepared by ESTEC. ESTEC had the task of setting up the aerodynamic database at the design conditions in the Mission Requirements Document (M=7.35, H=31.9 km). This detailed CFD data was then used by CIRA for carrying out their stability analysis including the sizing of the fins and ailerons, which was carried out in parallel to this study. The simulations were all carried out on a geometry with an intake leading edge radius of 1 mm and zero flap deflection and angles of attack of zero, -2, +2, and sideslip angles of zero and -2 were studied. For all cases, non-reactive simulations (fuel-off) and reactive simulations (H2 in air combustion) were carried out.

In the following three figures the flow field around the flight configuration and within the combustion chamber is shown exemplarily for AoA=0, SoA=0, and ER=1. In Figure 6 the Mach number is displayed by line contours around the vehicle. Figure 7 shows the hydrogen injection in the combustion chamber and in Figure 8 the surface temperature from the top and bottom view is plotted.

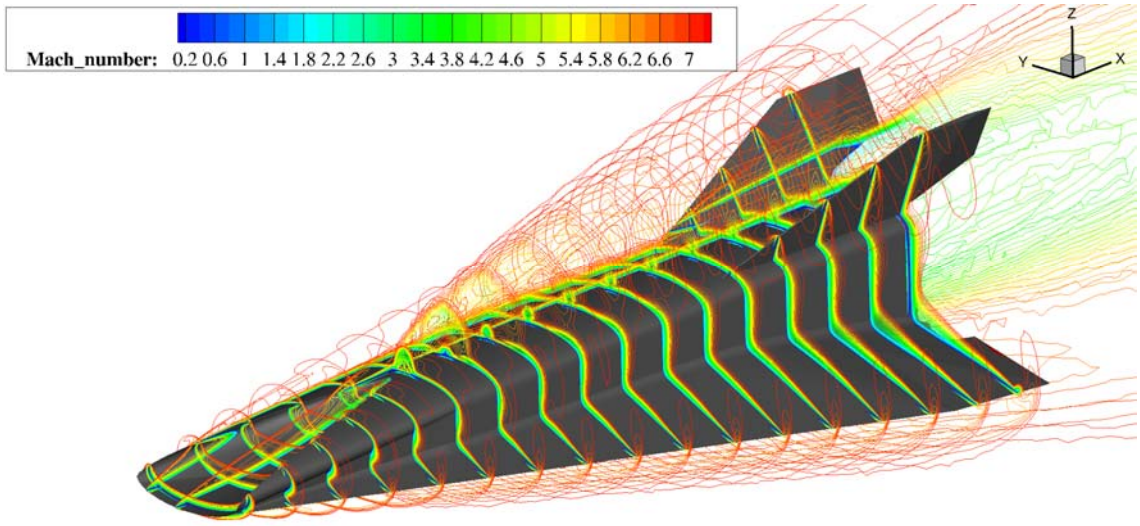


***Figure 6: HEXAFLY flight configuration (L=2.88 m) zero degree angle of attack, zero degree sideslip angle. Line-contours of Mach number;***

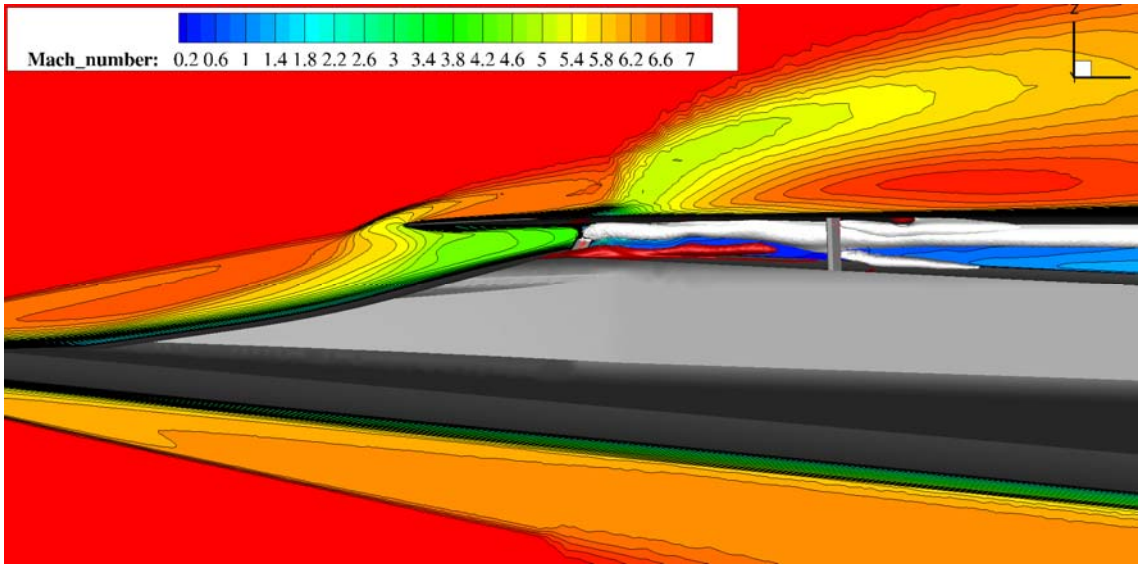


***Figure 7: HEXAFLY flight configuration (L=2.88 m) zero degree angle of attack, zero degree sideslip angle. Contours of Mach number***

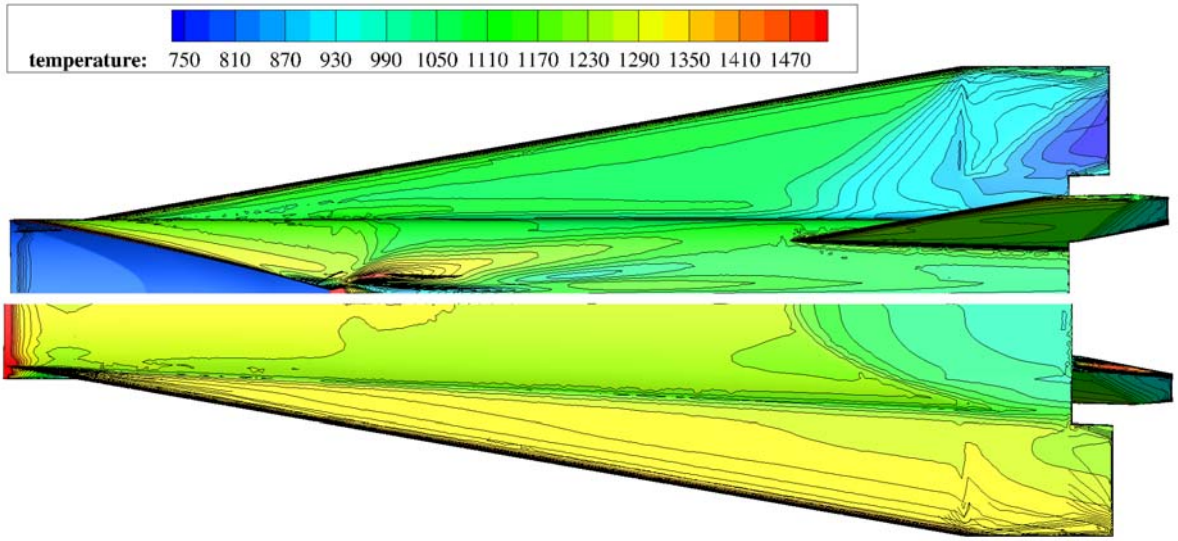


***Figure 8: HEXAFLY flight configuration (L=2.88 m) zero degree angle of attack, zero degree sideslip angle. Contours of surface temperature number on top and bottom.***

The most important aerodynamic coefficients of the HEXAFLY configuration are given in the following figures Figure 9 to Figure 12. The coefficients were calculated as:

Drag coefficient: $C_D = \frac{D}{A_{ref}\, q}$

Lift coefficient $C_L = \frac{L}{A_{ref}\, q}$

Moment coefficients $C_M = \frac{M}{A_{ref}\, L_{ref}\, q}$

The reference quantities for the aerodynamic database are:

- Dynamic pressure: 32979 Pa
- Reference area: 2.44 $m^2$
- Reference length: 2.876 m

The lift coefficient, drag coefficient and pitching moment coefficient are given in Figure 9. All curves show a relatively linear behaviour which is typical for the studied waverider geometry. The drag coefficient becomes negative for AoA=-2 which means positive net thrust of the configuration at this angle of attack. Also, by decreasing or increasing the AoA by 2 degree the lift basically doubles or halves.

In the next figure the aerodynamic efficiency (lift over external vehicle drag) is shown both for fuel-on and fuel-off simulations at SoA=0. The highest L/D observed is at +2 degree angle of attack where it reaches approximately 5.5 which is still quite high for a flight Mach number at 7.35. Also for the cruise condition at AoA=0 the L/D is still above 5, only for pitching the vehicle down where the lift decreases significantly the L/D is small at around 3. It has to be noted that these figures are for a configuration with vertical stabilizers, but also with no deflection of the ailerons.

The centre of pressure (COP) is given in Figure 11 with respect to the leading edge, meaning that 100 % represents the aft of the vehicle. At zero degree angle of attack the COP is at 62.2 %, when pitching the waverider down it moves backwards. For pitching-up manoeuvres the COP only small changes in the COP can be seen.

For the cases at non-zero sideslip angle (SoA=-2) the behaviour of the vehicle is very similar to the ones with SoA=0 (Figure 12). Non-zero roll moments and yaw moments exist of course and are given in detail in deliverable D2.2.2.

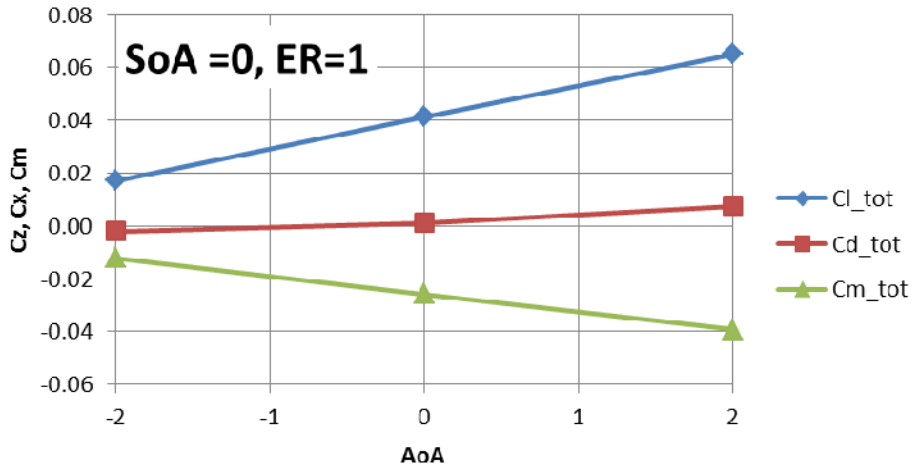


***Figure 9: HEXAFLY configuration lift coefficient, drag coefficient, pitching moment coefficient for SoA=0 as a function of angle of attack***

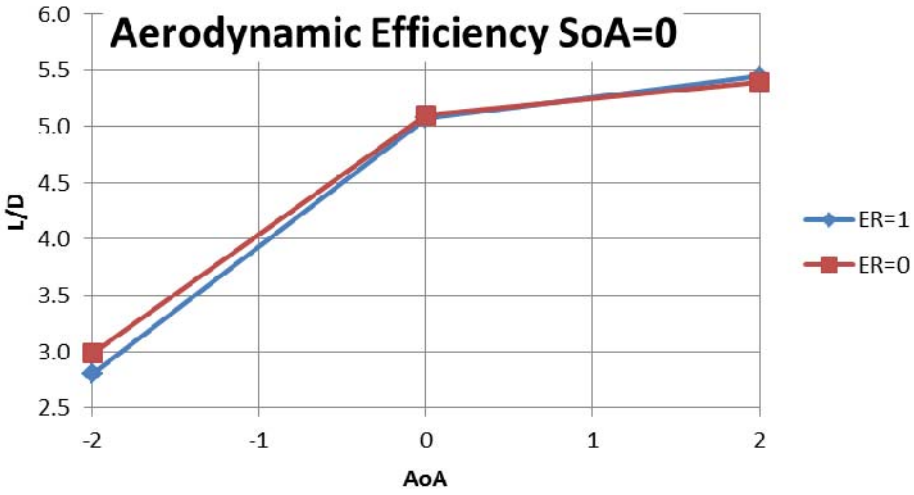


***Figure 10: HEXAFLY configuration aerodynamic efficiency (L/D) for SoA=0 as a function of angle of attack***

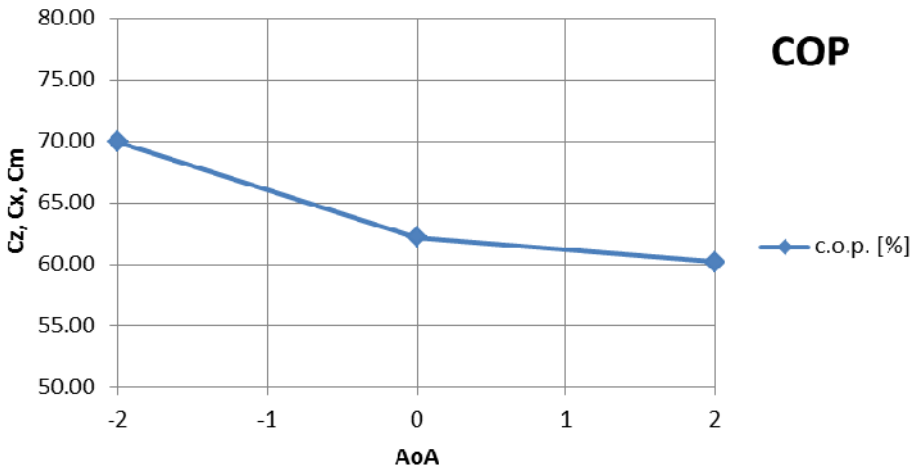


***Figure 11: Evolution of centre of pressure as a function of angle of attack for ER=1, SoA=0***

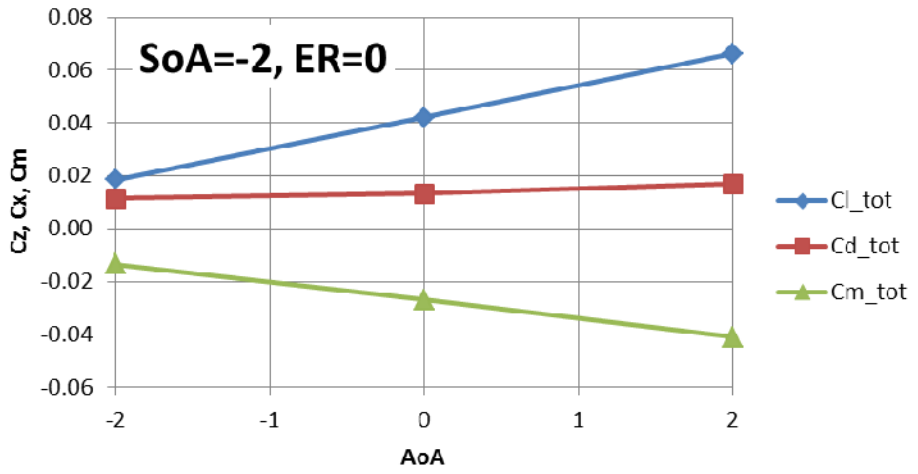


***Figure 12: HEXAFLY configuration lift coefficient, drag coefficient, pitching moment coefficient for SoA=-2 as a function of angle of attack***

DLR's numerical investigations of the complete vehicle were performed with the hybrid structured/unstructured DLR-Navier-Stokes solver TAU. The geometry and the computational grid were provided by ESA-ESTEC, and represent the complete sub-scale flight vehicle (l=3.15m) including the fuel injection struts. The leading edge radii were 1mm. A half-configuration with a symmetry boundary condition in the x-z plane was used to reduce computational cost.

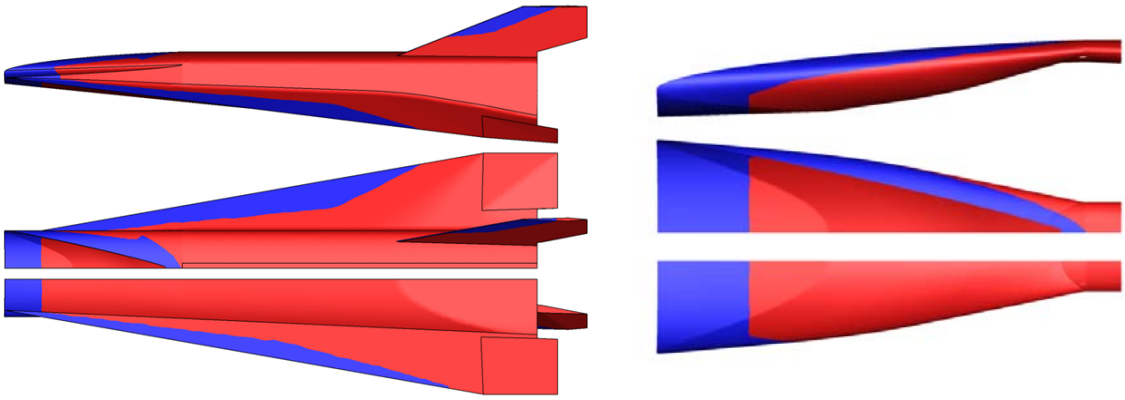

Figure 13 shows a schematic of the vehicle surface. In the transitional computations, the boundary layers in the blue regions are laminar. The right part of the figure illustrates the locus of the transition line on the internal intake surface.

***Figure 13: Schematic of the computational domain (vehicle surface).***

The unstructured computational grid consists of about 7.4 million volumes. Structured prismatic sublayers were used at the viscous walls. A dimensionless wall spacing of $y^+$ = O(1) was used to ensure sufficient resolution for the low Reynolds number turbulence model. The grid was refined in the vicinity of shocks to improve the resolution of the intake flow field. The internal feeding system of the fuel injectors was not included in the computational domain. The hydrogen supply was modelled by using Dirichlet-boundary surfaces at the appropriate location on the struts (exits of the fuel-injection-nozzles. All total of four nose to tail computations was performed:

(1) Fuel-off, turbulent flow
(2) Fuel-off, transitional flow
(3) Fuel-on, equivalence ratio = 1.0, turbulent flow
(4) Fuel-on, equivalence ratio = 0.8, transitional flow

All computations were performed with the free stream conditions summarized in Table 1 at an angle of attack of zero degree. The hydrogen injection conditions are set to Mach 2 and a total temperature of 300K (static temperature of 167K) and static densities of 1.282 kg/m³ and 1.026 kg/m³ for the equivalence ratios of 1 and 0.8, respectively. The hydrogen injector size was designed such that these flow conditions result in a fuel mass flux distribution is 65% on the front (semi-strut) injectors and 35% on the back (full-strut) injectors. The outer vehicle walls were assumed to be in radiative equilibrium (epsilon = 0.3), the intake surface was assumed to be at a constant temperature of 800K, adiabatic walls were used to model the internal flow path.

| | |
|---|---|
| Static pressure | $p_\infty$ = 1828 Pa |
| Static temperature | $T_\infty$ = 222.3 K |
| Static density | $\rho_\infty$ = 0.02852 kg/m$^3$ |
| Mach number | $Ma_\infty$ = 7.350 |
| Flow velocity | $u_\infty$ = 2202 m/s |

***Table 1: Free stream conditions***

Computational results for the transitional and turbulent fuel-off cases are summarized in Figure 14. The Mach number contours in the left part show that the shock wave on the pressure side of the vehicle is aligned with the wing tip which validates the waverider design of the outer aerodynamic shape. The right part of Figure 7 shows contours of axial velocity at different cut planes on the intake for the transitional (left) and turbulent (right) cases. A small separation bubble forms in the transitional flow at the upstream end of the compression surface as illustrated by the red iso-surface of axial flow reversal. Further, a region of decelerated flow develops in both cases in the center of the compression surface. This decelerated flow is very likely to be the source of unstart

issues at large equivalence ratios that were observed to be associated with the present vehicle design. Unstart occurs after massive flow separation at the combustor entrance which is promoted by the plume of decelerated flow visible in Figure 7.

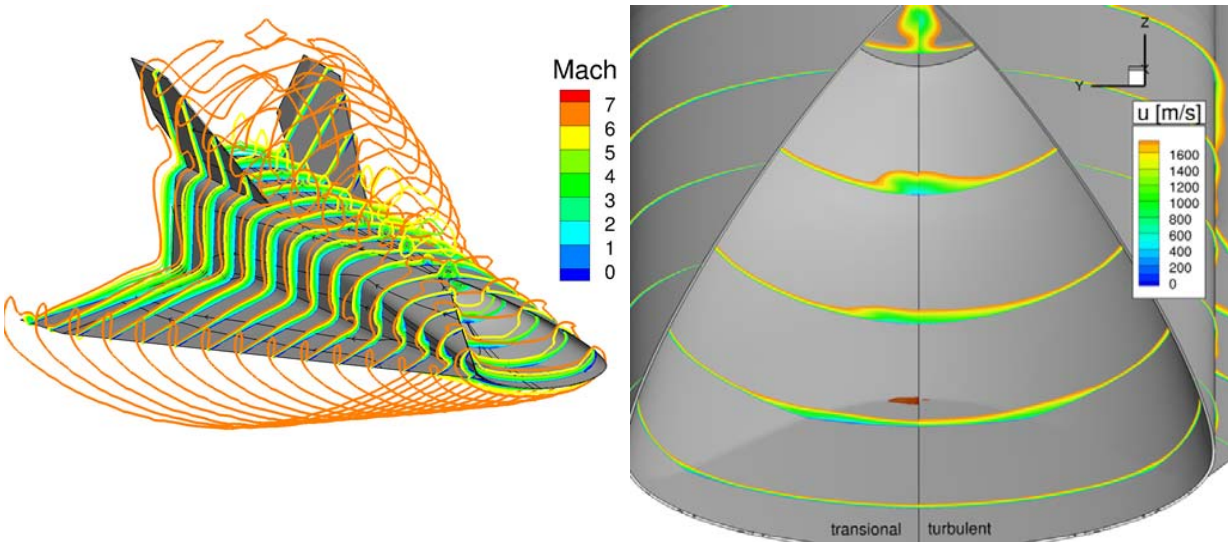


***Figure 14: Turbulent and transitional flow fields at fuel-off conditions: Mach number (left) and velocity (right) contours.***

The source of the decelerated flow plume at the centre of the compression surface is significant cross flow which develops close to the intake surface. The cross flow patterns are shown in the left part of Figure 15 (skin friction lines) and differ significantly for the turbulent and transitional boundary layer assumptions. For reference and comparison, the surface streamlines of an Euler computation are added in the right part of Figure 8. The flow close to the surface converges at the symmetry plane of the intake which lifts the decelerated fluid from the boundary layer into the bulk flow. The main driver of the cross flow is the swept intersection of the compression surface which with the flat plate insert of the intake. In the turbulent case, the cross flow starts at this intersection line. In the transitional case with a larger subsonic region of the upstream boundary layer, the cross flow is more distributed and starts to occur further upstream.

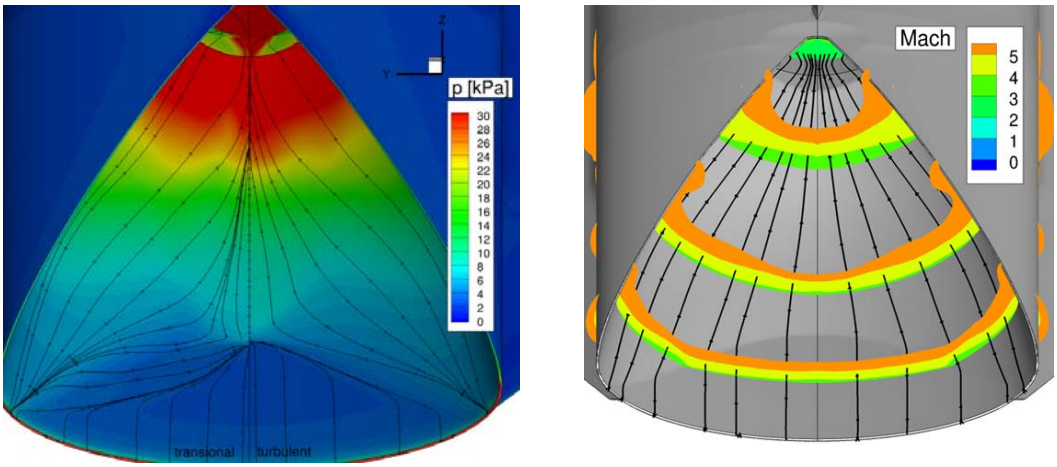

***Figure 15: Left: turbulent and transitional flow fields at fuel-off conditions: Surface pressure distribution and skin friction lines; Right: Surface stream lines and Mach number contours for an Euler solution***

Figure 16 illustrates the flow field of the turbulent case at an equivalence ratio of 1. A large area of separated flow develops on the intake as is shown by the red iso-surface of axial flow reversal in the left part of the figure and the Mach number plot on the symmetry plane in the right part. This flow separation remained stable in the computation and leads to a significant increase of spillage. The impact of the increased spillage on the external flow is clearly visible in the Mach number contours on the suction side in the left part of Figure 9. Further, the mass capture of the combustor is reduced from 2.79 kg/s to 1.78 kg/s. No thrust is generated at this operating condition and the vehicle drag amounts to 660N.

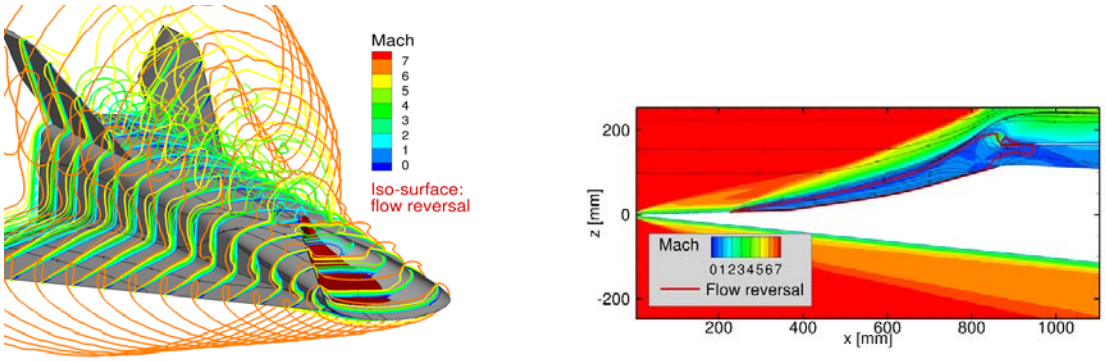


***Figure 16: Turbulent flow field of the equivalence ratio=1 case. Right: Symmetry plane in the vicinity of the combustor entrance***

Mach number contours and the iso-surface of axial flow reversal for the transitional case at an equivalence ratio of 0.8 are shown in the left and right part of Figure 17, respectively. The shape of the reversed flow / flow separation pattern in the right part of the figure correlates strongly with the structure of the plume of decelerated flow from the fuel-off cases. The flow separation does not affect the mass capture of the intake and the flow spillage. The flow structure at the suction side of the vehicle is identical to the fuel-off cases.

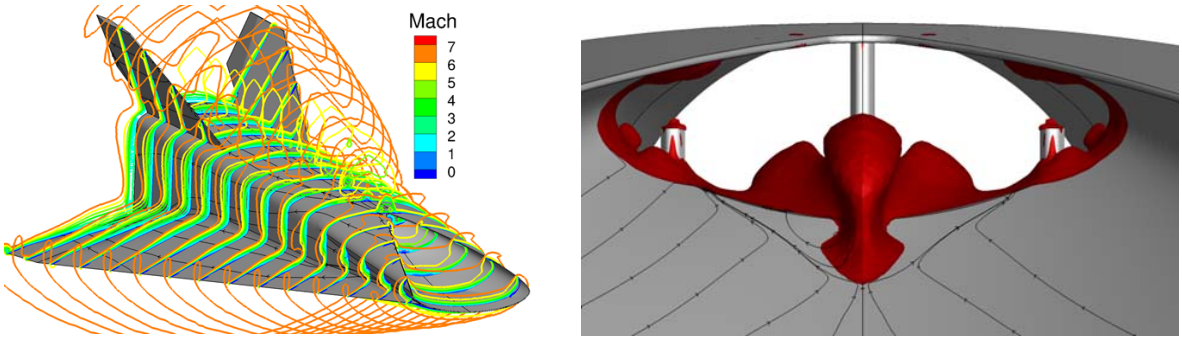


***Figure 17: Transitional flow field of the equivalence ratio = 0.8 case. Right: Front view of the combustor entrance, iso-surface of flow reversal***

Figure 18 is a detailed view of the flow field in the combustion chamber. The red iso-surface of 1% H2 mass-fraction shows the locus of the fuel jets. The distribution of O2 mass fraction at the cut planes confirms a distribution of the reaction zone over the entire combustor cross section resulting in a large combustion efficiency. 3.4% of the injected hydrogen remains unburned at the exit of the thrust nozzle. The sonic line shows that a significant amount of combustion occurs in subsonic flow. A maximum of 75% of the combustor cross section is subsonic in the region between the

semi-strut and the full-strut injectors. The vehicle delivers a thrust of 200N at this operating condition. The aerodynamic forces of all considered computational cases are summarized in Table 2.

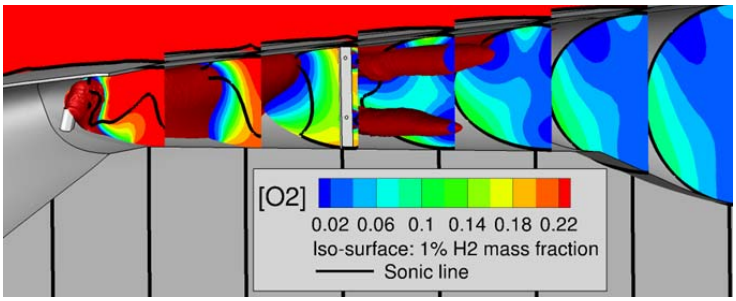


***Figure 18: Combustor flow field of the transitional equivalence ratio = 0.8 case***

| Case | Drag [N] | Viscous Drag [N] | Lift [N] |
|---|---|---|---|
| $\alpha$ = 0°; EQR = 0; turbulent | 2010 | 1060 | 7190 |
| $\alpha$ = 0°; EQR = 0; transitional | 1930 | 985 | 7270 |
| $\alpha$ = 0°; EQR = 1; turbulent (unstart) | 661 | 985 | 5530* |
| $\alpha$ = 0°; EQR = 0.8; transitional | -199 | 1170 | 6890* |

***Table 2: Aerodynamic forces***

To summarize, the performed CFD analyses confirm that the vehicle operation at fuel-on conditions is associated with severe boundary layer separation issues at the combustor entrance. This problem originates from the development of a large region of decelerated flow on the intake. The reason of the accumulation of low speed flow at the intake center is the occurrence of cross flow in the intake boundary layer. The associated cross flow pattern strongly depends on the boundary layer properties Transitional flow tends to stabilize the boundary layer at the combustor entrance due to a shift of cross flow to the upstream region of the intake and the reduced boundary layer thickness in the downstream part of the intake. A stable solution with net thrust was obtained at an equivalence ratio of 0.8 and transitional flow assumption on the intake.

*Generic System Studies: Combustor Thermal analyses and Propulsion Feed System*

The possible technology to be used for the engine of the HEXAFLY vehicle was investigated based on the available materials and structures, and associated modelling. This concerns the walls, the leading edges, the injection struts, the inlet, the chamber, and the nozzle. Two main loops were conducted; one using a preliminary trajectory profile based on the VS-40 launch system; and a second one using the single stage S-43 launch system.

Using the preliminary launch profile for the VS-40 provided by GDL (Figure 5), a generic heat load was computed with semi-empirical engineering methods and set for the thermal computations of the different solutions (Figure 19).

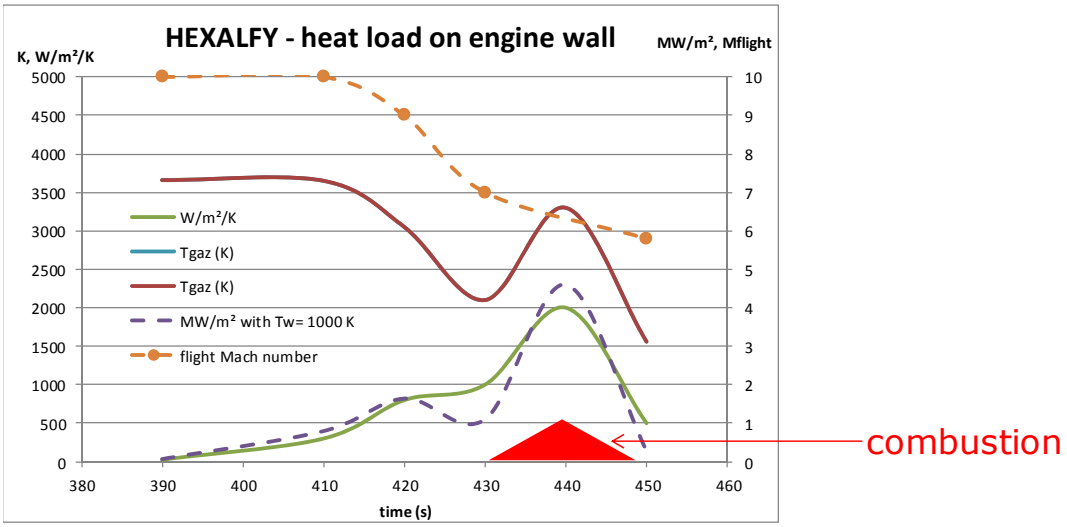


***Figure 19: Associated heat load on the combustor wall***

For the current study we have focussed on heat sink materials for the combustor walls (either metallic or CMC materials), with the addition of thermal barrier coatings (TBC). Active cooling solutions were not considered in the current study, because of their complexity and additional weight penalty. An example on a generic experimental test leg at Mach 8 is given below, where the surface weight of each wall solution is plotted versus the time of combustion realizable before the material limits are exceeded (generally the oxidation temperature).

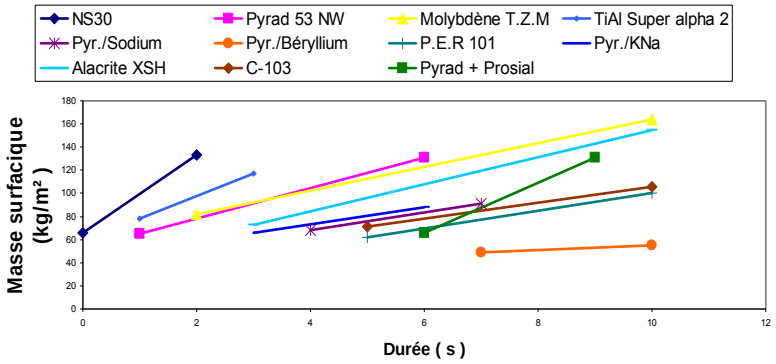


***Figure 20: Example of previous scan of wall technology for Mach 8 scramjet flight experiment***

As a heat sink solution has been chosen, each solution is computed in unsteady conduction with the time dependent hot boundary condition of Figure 19, assuming adiabatic wall on the (back) opposite side. For each solution, the thickness of the material and its TBC, if any, is varied and optimized. The material models are based on an in-house data-base. This method has been extensively used and checked, especially within the European program ATLLAS2. An example of the computed temperature for a solution based on Stainless Steel protected with TBC is shown below on the left while a more thermally diffusive (and heavier) solution with Cupper/zirconium alloy is shown on the right. The red arrows indicate the duration of combustion.

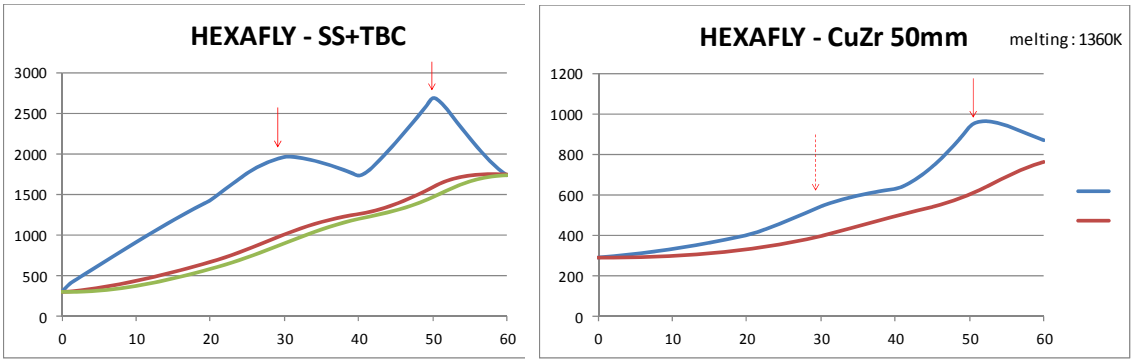


***Figure 21: Example of heat sink wall solutions: temperature versus time***

The following picture shows two examples of trying to optimize the CuZr alloy option; on the left by increasing the wall thickness; and on the right by adding a TBC (a classical barrier based on ZrO2 is considered here).

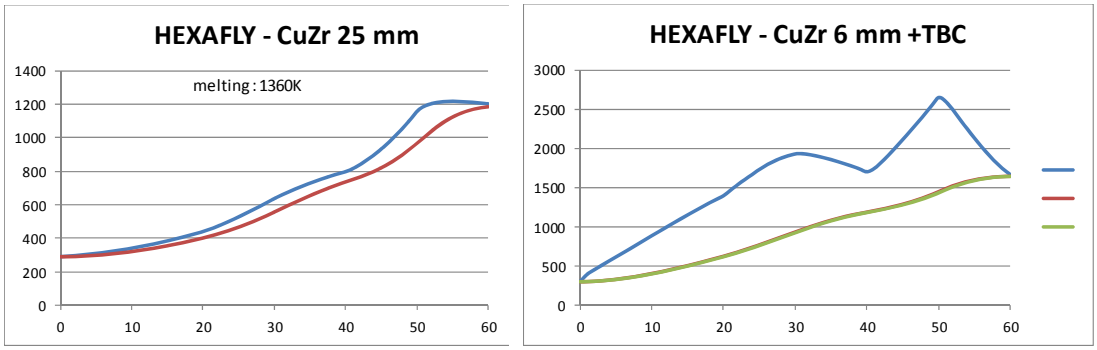


***Figure 22: Example of CuZr alloy solution scanning***

In this solution, we have two limits: the CuZr alloy hot temperature has to be below its melting temperature of 1360K; and the TBC (if any) is demonstrated for this type of duration and environment up to 2300K only. An example with a CMC material (C/C/SiC) under the same heat load, is shown below.

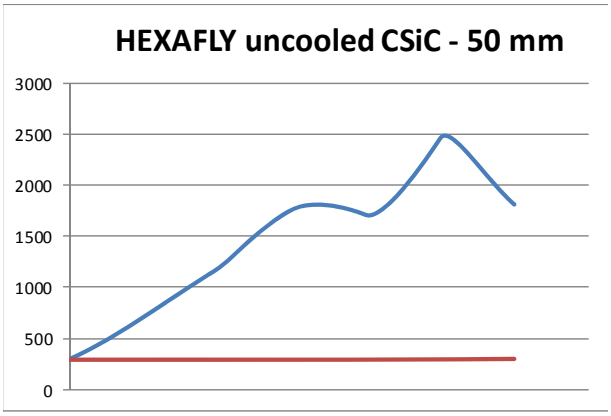


***Figure 23 : CMC wall along the considered test trajectory***

Following these initial computations we also considered the option of closing the intake for the first part of the trajectory. Furthermore, after some discussion with the other partners, additional options were also considered:-

- CuZr 6 mm + TBC (closed cover till 30 to 39s)

- Aluminium alloy with TBC (different thicknesses)
- SS 10 mm thick + TBC
- Inconel + TBC : 6 and 10 mm : close to SS

Associated with the initial closure of the intake, we have now different solutions that could work as shown in Figure 24 to Figure 26.

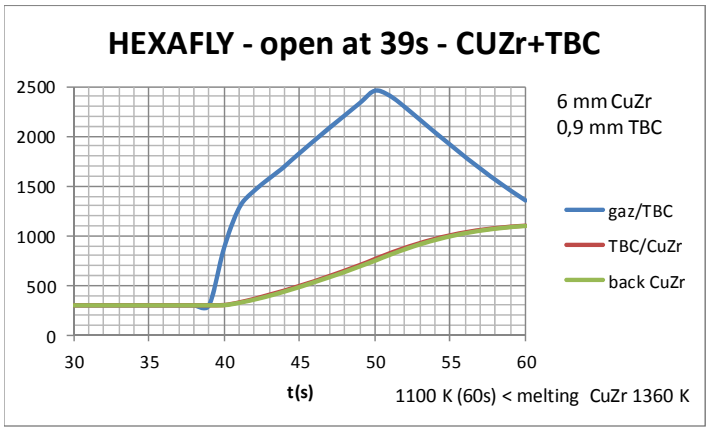


***Figure 24: Example of a viable combustor wall solution***

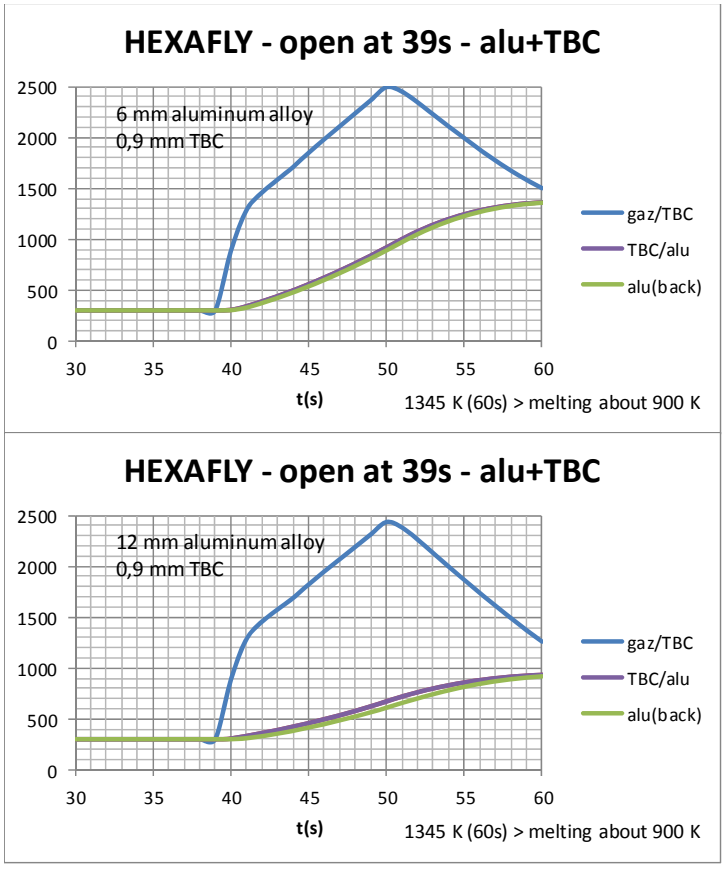


***Figure 25: Aluminium under TBC for different thicknesses (here 6 and 12 mm)***

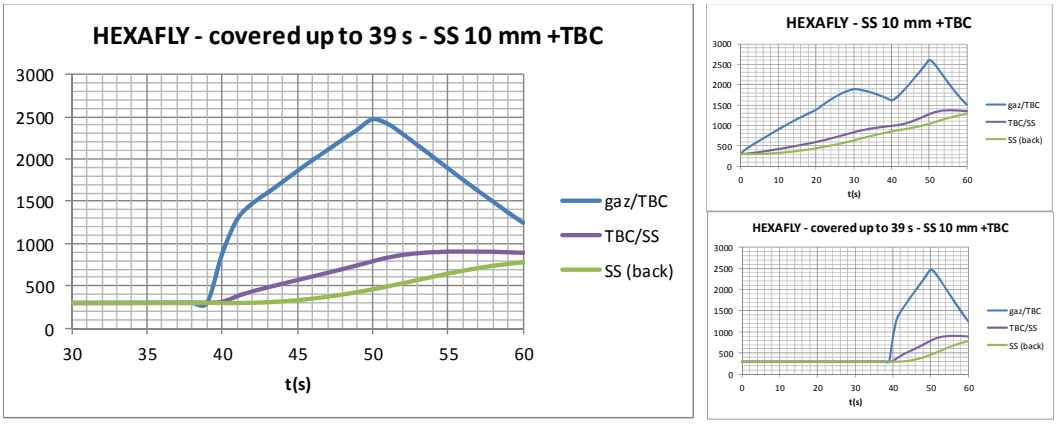


***Figure 26: 10 mm Stainless Steel wall with TBC and inlet closure***

The same kind of work was conducted on the injection struts. The local heat loads were derived from the chosen trajectory and the work performed in ATLLAS2 on a generic strut which is not so different from the HEXAFLY ones.

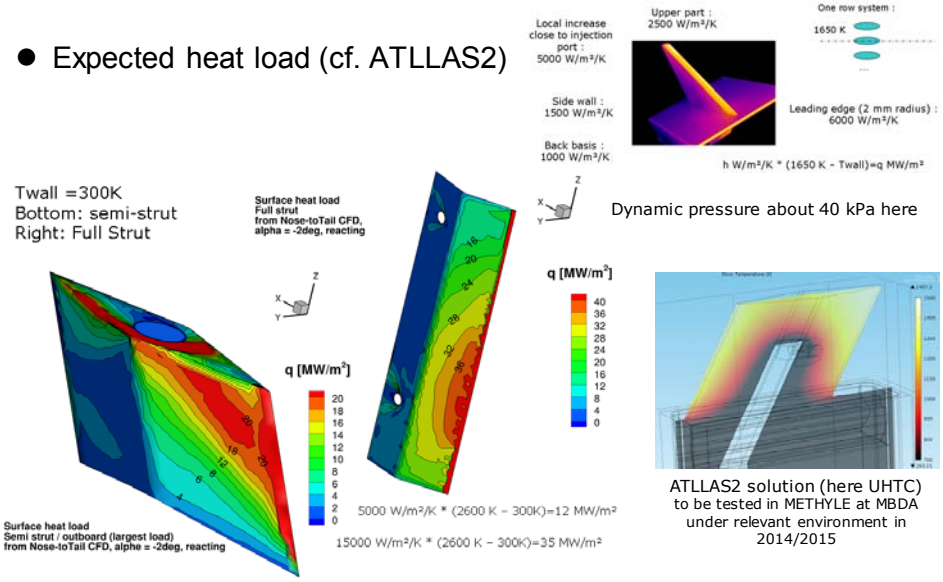


***Figure 27 : injector studies and heat loads in ATLLAS2***

The most loaded part is obviously the leading edge of the strut. The heat transfer coefficient could reach 5000 W/m²/K or 10 000 W/m² depending on the leading edge radius (R=2 mm for example) and on the local flow conditions (shock/shock interaction, combustion before the second row of struts). An example of results is given below, with the wall temperature and thermal heat loads trajectory on the left and two different heat sink leading edge computations of injection struts at the right.

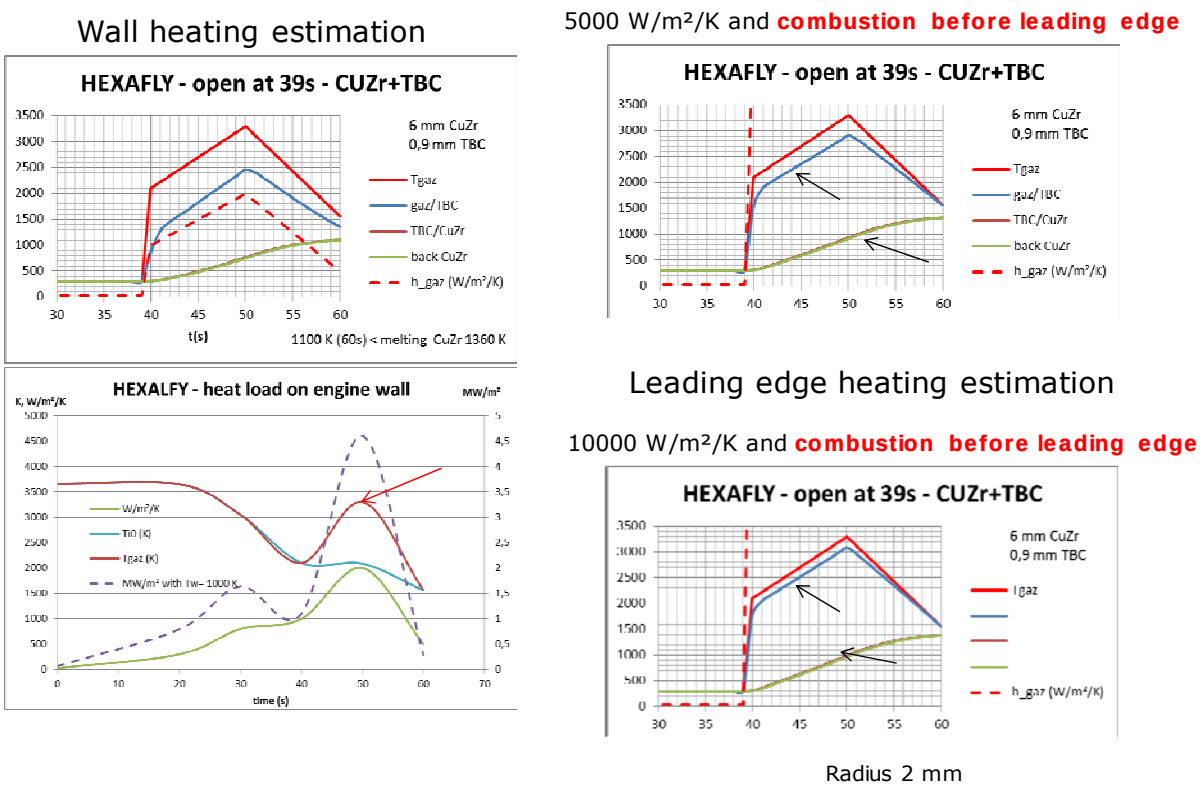


***Figure 28: Predicted wall and strut temperatures***

If we assume the strut does not afford any combustion, some examples are given below.

10000 W/m²/K and **NO combustion before leading edge**

Radius 2 mm

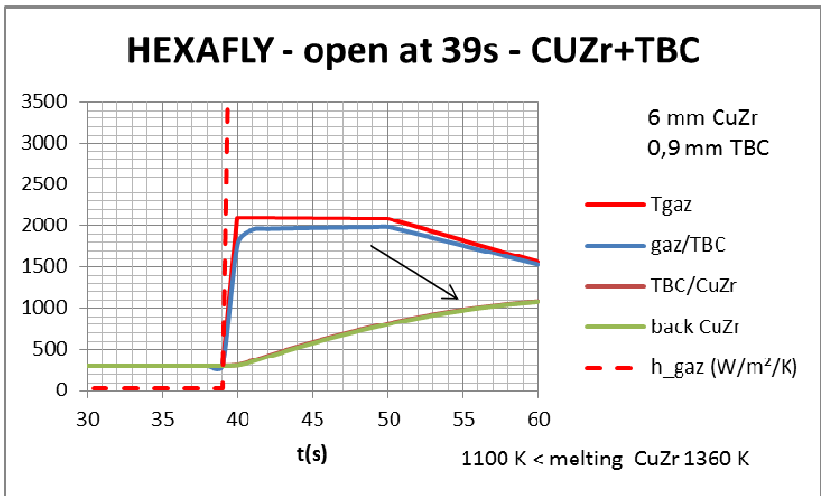


***Figure 29 : CuZr injection strut protected by thick 0.9 mm TBC even on its leading edge***

The same study was performed with a Molybdenum leading edge. As can be seen on the computed temperature below, this solution could work only if there are no hot gases from combustion impinging on the leading edge.

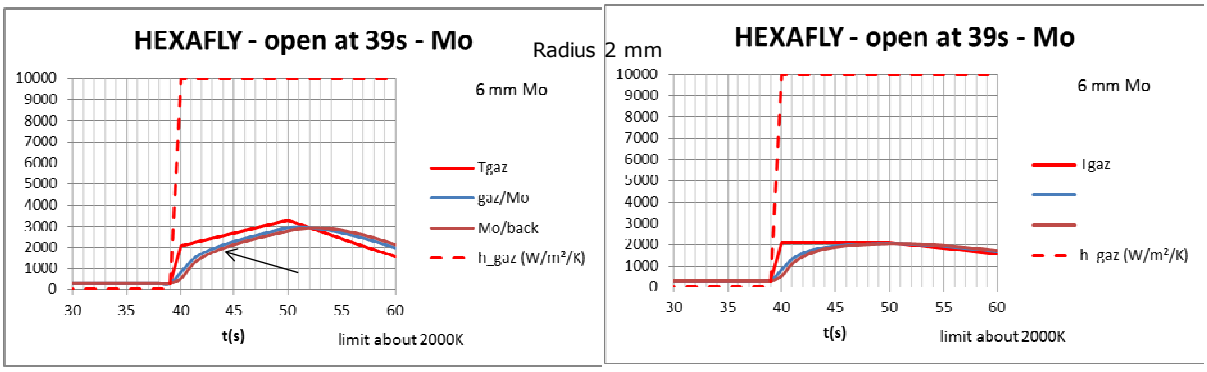


10000 W/m²/K and **combustion before leading edge** 10000 W/m²/K and **NO combustion before leading edge**

***Figure 30: Thermal assessment of Molybdenum injector leading edge***

In the second part of the study, a thermal assessment was performed for an updated trajectory using the S-43 launcher. As shown below, the corresponding heat loads are less strong for the engine, due to the change of the trajectory and also a decrease of the active test leg and combustion 'triangle' duration.

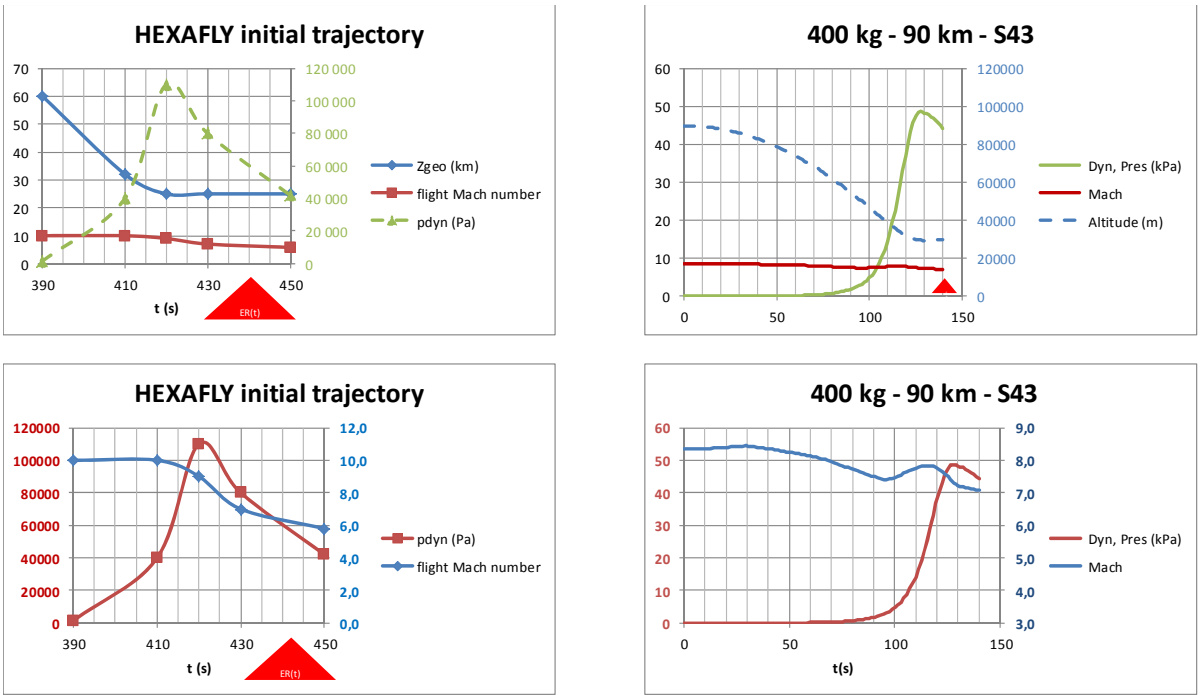


Previous version up to Final Review Final version (May 2014)

***Figure 31: New trajectory (right) compared to the first one (left)***

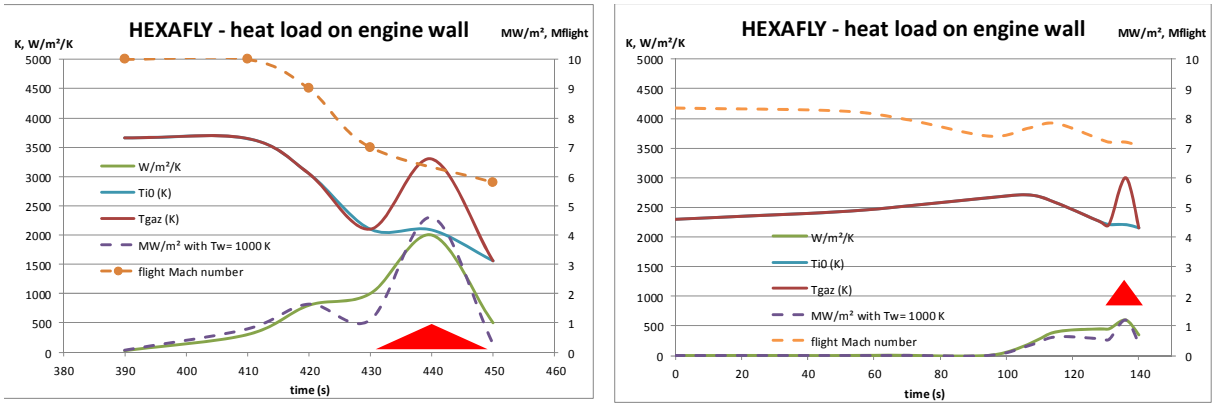


Previous version up to FR Short Final version (May 2014)

***Figure 32: Updated (right) and initial (left) heat loads for the engine***

Following a similar analysis to the VS-40 profile led to the final proposed solution of Cu/Zr alloy protected by a TBC for the combustion chamber. For the injection struts (in the absence of covering the intake, which is not mandatory with the S43 trajectory), the best solution appears to be Molybdenum struts covered by an ablative insulated layer in the first part of the trajectory. The total weight of the Cu-made internal flowpath is 88.8kg with the following splits:

| Item part | Weight [kg] | CAD nomenclature |
|---|---|---|
| Nose+intake | 49.2 | Solid nose intake + tip solid nose |
| Combustor | 15.9 | Inlet CC + CC front |
| 2D nozzle | 11.1 | CC back |
| 3D nozzle | 12.5 | CC tail |

**Tab. 1: Component weights for flight control subsystem**

The proposed thicknesses for the different components are listed below:

| Item part | Material | Thickness [mm] | ZrO Coating thickness [mm] | Total in CAD [mm] |
|---|---|---|---|---|
| Intake | CuZr | 4.5 | 0.8 | 5.5 |
| Intake | C-C/Sic | 5 | 0 | N/A |
| Intake LE=2mm | CuZr | 1.1 (LER) | 0.9 | - |
| Combustor | CuZr | 7 | 0.8 | 7.8 |
| Injector | Mo | 2 (LER) | - | 2 |
| 2D-Nozzle | CuZr | 4.5 | 0.8 | 5.5 |
| 3D-Nozzle end | CuZr | 2.5 | 0.8 | 3.5 |
| Nozzle tail | Ti | 3.2 | 0.8 | 4 min. |

**Tab. 2: Component weights for flight control subsystem**

To accommodate enough hydrogen on-board, it was obvious from the start that a high-pressure H2 tank was needed (≥ 700bar). Though these tanks are existing and available from the shelf, a dedicated pressure regulator needs to be developed to provide the $H_2$ at 16-30bar at the injector. The particularity in the present design is the large $H_2$ mass flow rate (i.e. 0.039 g/s to 0.095 g/s) which is not common. Furthermore a specific regulator with a closed feed-back loop is needed to assure the foreseen ER which is dependent on the altitude and speed. The pressure regular consists of 2 stages: the first one is screwed inside the tanks (M25) for a pressure staging to 75-100 bar whereas the 2nd one brings it to its final set-value. So far the analysis is based upon an ER=1, but one should actually aim for a larger ER not only to have a higher mixing efficiency (smallest at ER=1) and hence a larger thrust but also to build in some margin for the measurement uncertainties wrt the atmospheric conditions and flight speed. With the available hydrogen on-bard and the specific design, the experimental campaign with combustion can last from 3 sec at 27km up to 9 sec at 32km (Fig. 3).

The feed-lines consist of 1" pipes. The potential accumulation of frost onto the lines (cooled down by the H2 expansion) is considered not risky due to the low ambient pressure and low vapour content at ~30km altitude and the short exposure time and the heat sink capacity of the feed lines (~20K/s).

One particular note is linked to the massive temperature drop in the tank which can cause initiation of cracks in the liner once the temperature drops below -45$^0$C (Fig. 3). This would be a matter of concern for multiple re-use of the bottle, but not here for the unique flight test. However, the qualification process will need to take this into consideration once testing the complete propulsion system.

The part item list is given in **Tab. 3** and the overall layout of the internal flowpath, tank and pressure transducer are given in Fig. 4.

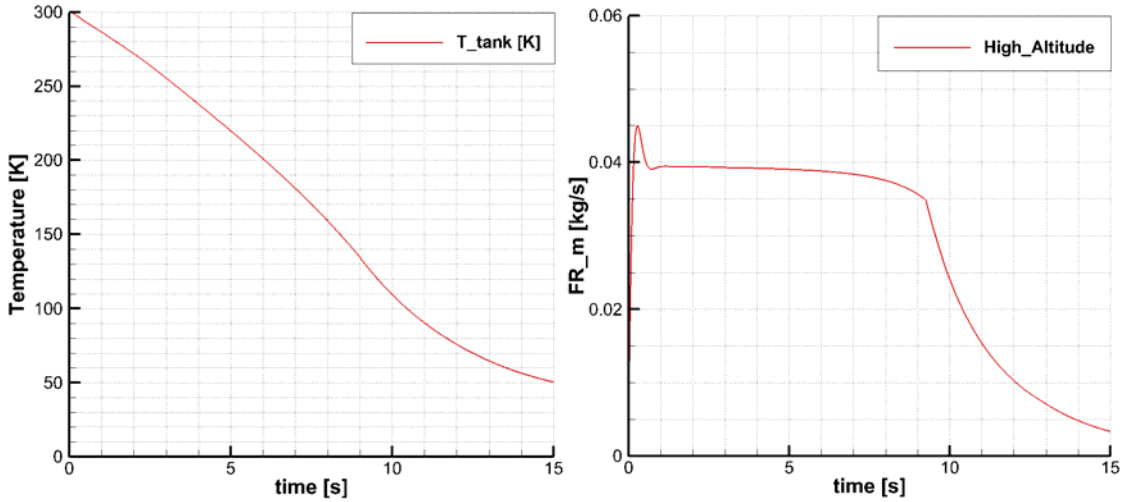


***Fig. 3: Tank temperature and mass flow rate evolution at high altitude flight (32km)***

| Item part | Weight [kg] |
|---|---|
| Tanks (2) | 10.0 |
| Tank Connectors | 3.2 |
| Pressure regulator | 1.3 |
| Flow controller | 4.0 |

**Tab. 3: Component weights for propulsion subsystem**

***Fig. 4: Structural Internal flowpath layout along with the propulsion feed system***

*Detailed System Studies – EFTV Design (Control System, CIRA)*

With the completion of the generic system studies, work began to be focussed on the layout of the different configurations. Recall that three variants of the vehicle were developed under WP2; a free flight experiment using the large scale vehicle (the EFTV); a vehicle based on the LEA platform (the ELTV); and a captive-carry trial using the small scale vehicle launched on a sounding rocket (the ECTV). We will begin by describing the activities surrounding the EFTV, starting with the control system study performed by CIRA.

The main results of the CIRA activity have been the different configurations of the EFTV-G, developed jointly with the designer ESA-ESTEC and deeply analysed in terms of aerodynamic performance, flight stability and control, from Kick-Off Meeting to the Final Review of the HEXAFLY project. They are reported in the following table, together with an indication of the major modifications characterizing each configuration.

| configuration | $L_{ref}$ [m] | rear bottom | Scramjet flowpath | aileron | vertical tail | C.o.G. |
|---|---|---|---|---|---|---|
| Preliminary wing-body | 2.873 | original | original | no | no | 50% |
| T4y6° | 2.873 | original | original | flap#2 | T4, 6-deg toe | 55% |
| FB-T4-F3 | 2.873 | flat | tilted -1.92 deg | flap#3 | T4, no toe | 50% |
| V47 | 2.873 | flat | tilted -1.92 deg | flap#4 | T4, no toe, small modification of TE | 50%, 56% |

***Table 3: EFTV-G versioning***

The final EFTV-G configuration released at the HEXAFLY Final Review is shown in Figure 33.

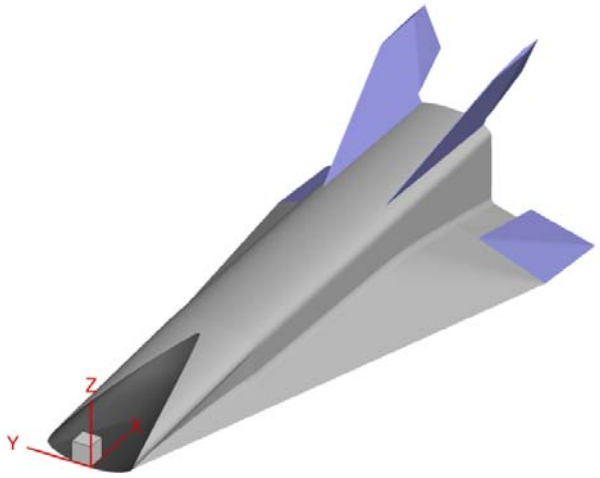


*Figure 33: EFTV-G final vehicle layout with control surfaces integrated (vertical tail and ailerons)*

The aerodynamic data for the EFTV-G configurations were provided by ESA-ESTEC (based on aero-propulsive nose-to-tail CFD simulations) and/or calculated by CIRA using a viable engineering tool (SPREAD) based on surface inclination methods, developed, verified and validated along the LAPCAT-II project.

The starting configuration (see Figure 34) was the simply scaled down LAPCAT-II Mach=8 vehicle without any control surfaces and with nominal CoG at 50% of the vehicle's reference length. Even though statically stable (with a static margin of 7.8%, see Figure 35) in longitudinal flight, it emerged the absolute necessity to design:

i) a vertical tail to assure the static and dynamic lateral-directional stability in both motor-off and motor-on conditions;

ii) ailerons to both assure static longitudinal stability and trim the vehicle in the considered flight conditions;

iii) and eventually a combination of control surfaces to quickly damp the roll/yaw coupling (see Figure 36) in both motor-off and motor-on conditions.

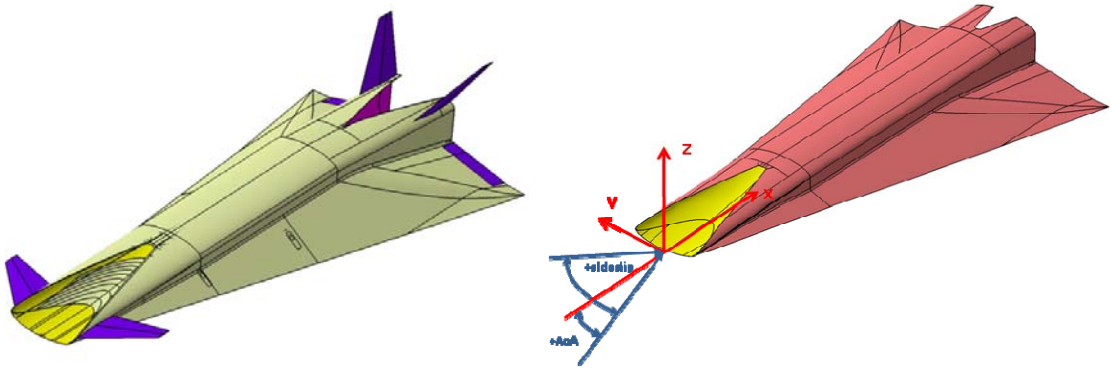


*Figure 34: Full-scale vehicle (left) and reduced-length vehicle (right) without control surfaces*

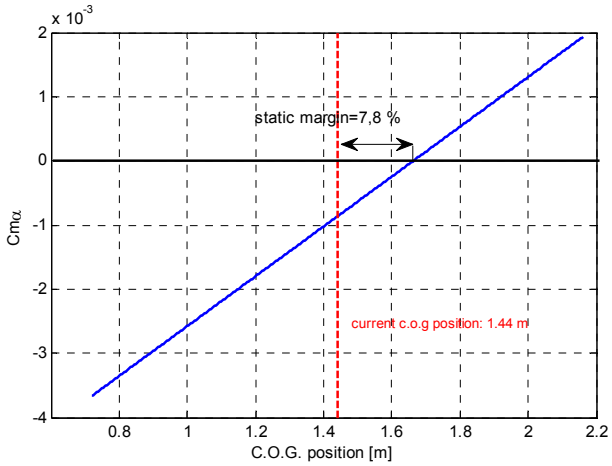


*Figure 35: Preliminary EFTV-G $C_{m\alpha}$ evaluation in function of CoG variation*

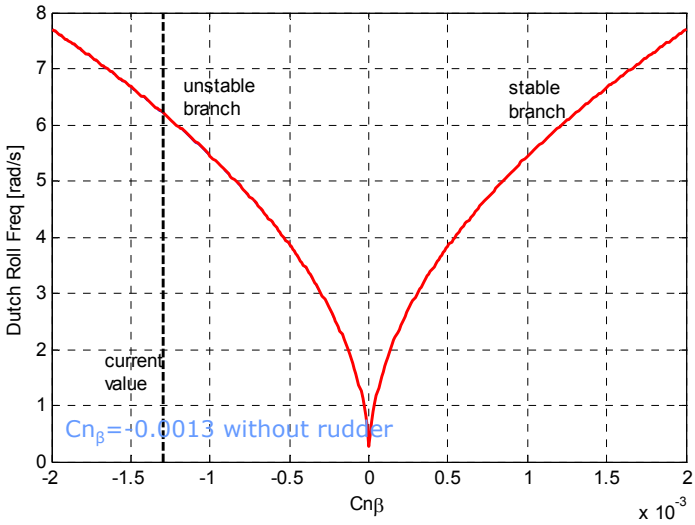


*Figure 36: Preliminary EFTV-G Dutch-Roll frequency in function of $C_{n\beta}$*

With the **T4y6°** configuration, design loops for a vertical tail with fixed fins (see Figure 37 and Figure 38) and ailerons (see Figure 39) were performed, and at the same time the nominal CoG was moved forward, from 50% to 55% of the vehicles reference length. The configuration was statically stable with a longitudinal static margin of 3.9%, the pitch-trim was obtained with the help of the vertical tail, the ailerons were used only to provide longitudinal control (see Figure 40 and Figure 41), and lateral-directional static stability was assured at non-negative values of angle of attack. Linear lateral dynamics was neutrally stable (Dutch Roll) and not damped due the modelling approximations made. CAD files (see Figure 42 and Figure 43) and AEDB of the T4y6° configuration were delivered by CIRA in occasion of the HEXAFLY project PM1. A drawback of the T4y6° configuration was the fact that a toe angle of the fins was necessary to produce a down-force balancing the strong pitching-down moment of the aeroshape, so avoiding negative aileron deflections larger than 20 deg to pitch trim the vehicle. Of course, this was possible only with a large loss of aerodynamic efficiency.

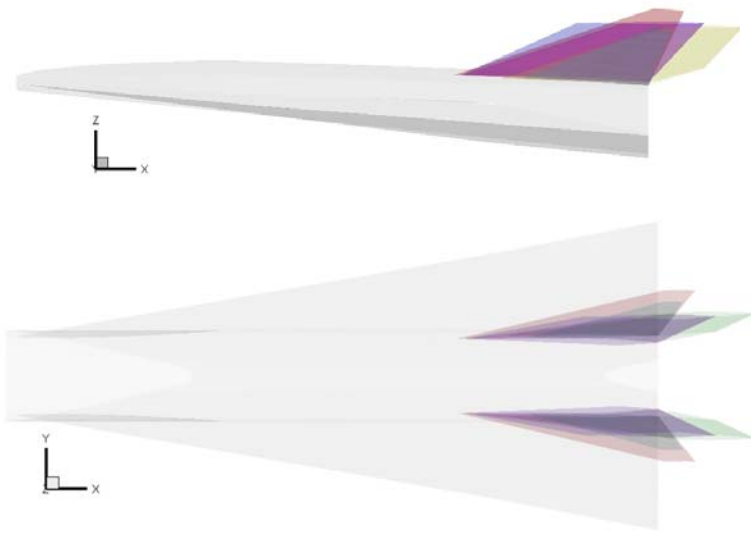

*Figure 37: Comparison of the VT configurations in transparency (clockwise: side, front, back, top views)*

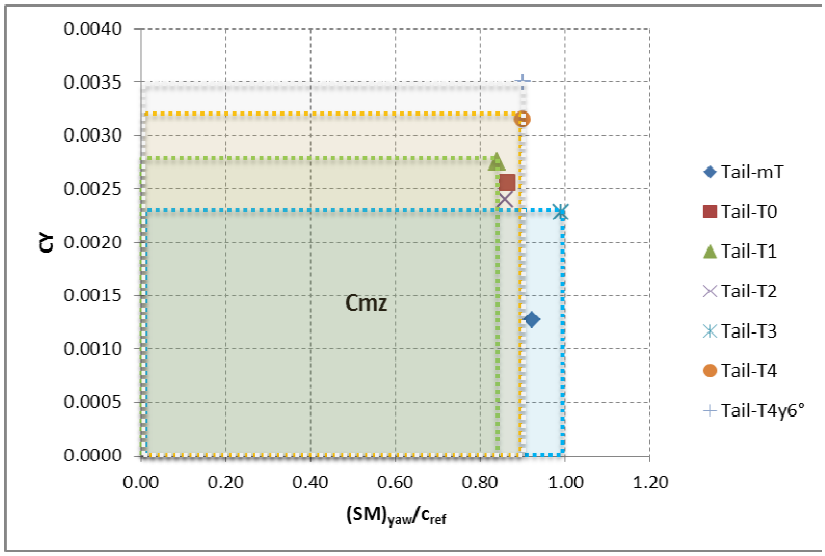


*Figure 38: Comparison of the Vertical Tail configurations in terms of yawing moment provided*

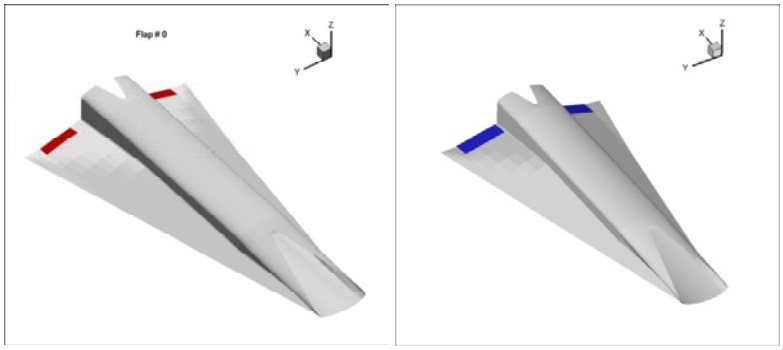

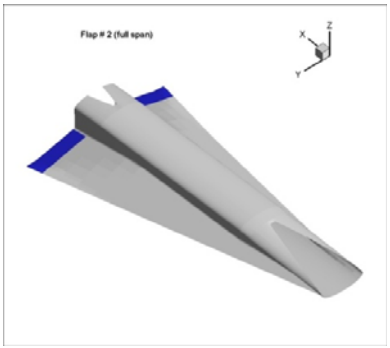


*Figure 39: Aileron configurations investigated (flap#0, left; flap#1, middle; flap#2, right)*

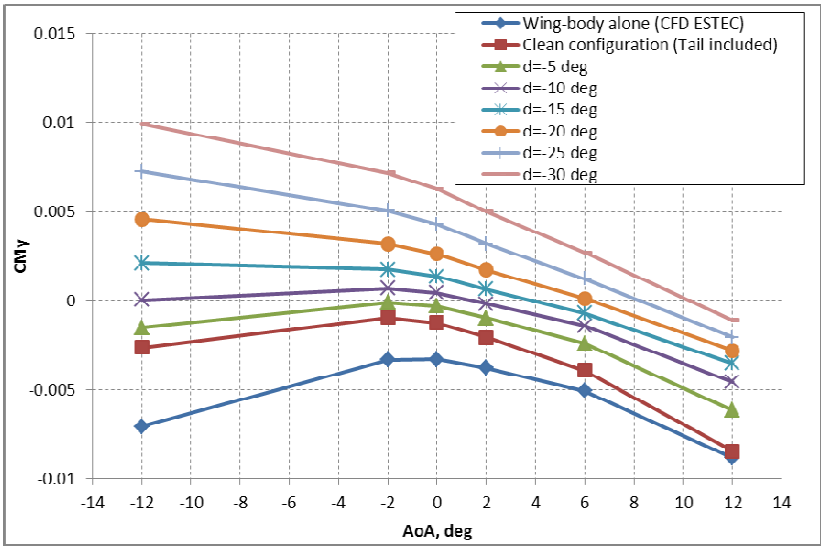


*Figure 40: Pitching moment coefficient vs. AoA, effect of aileron deflection*

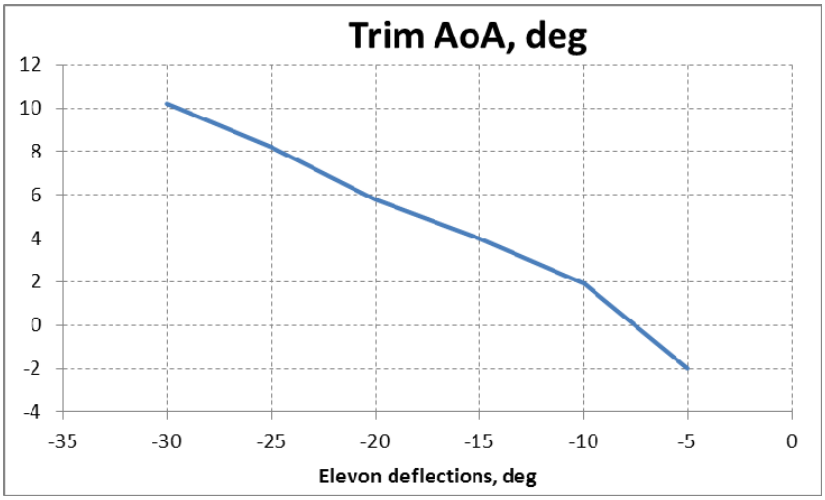


*Figure 41: EFTV-G evolution of trim AoA as function of aileron's deflection*

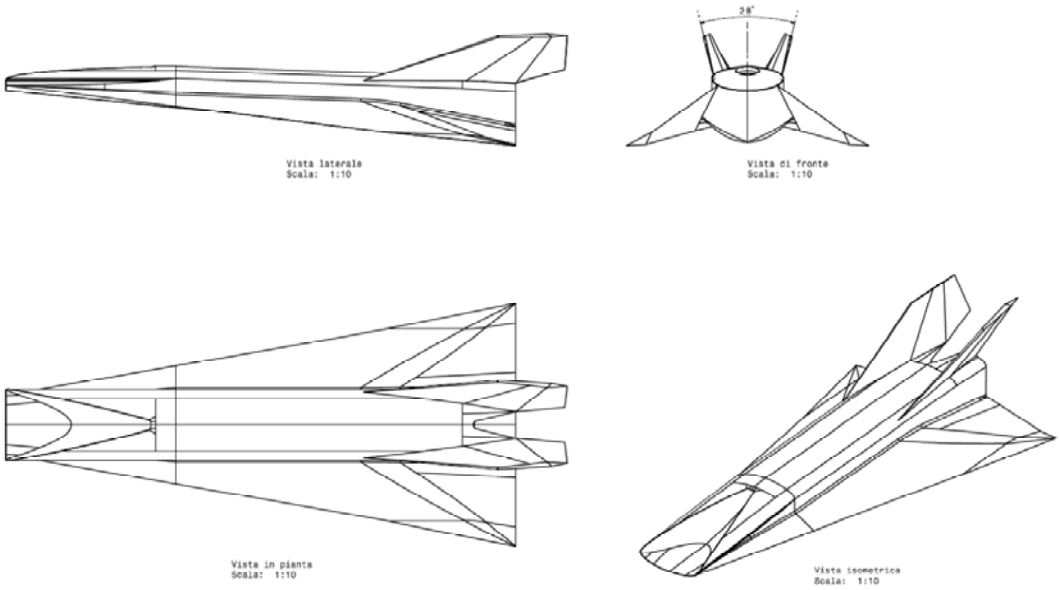


*Figure 42: EFTV-G T4y6° configuration*

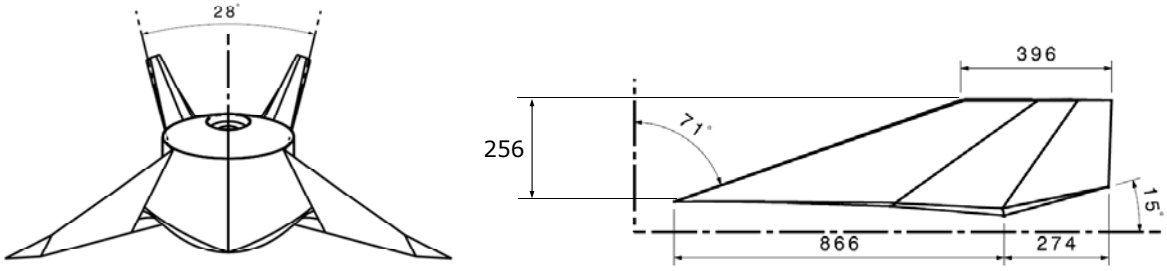


*Figure 43: Detail of T4y6° vertical tail*

In order to recover aerodynamic efficiency it was decided to fly at non-negative angle of attack (nominally AoA=0 deg), to maximize thrust vector pitch-trim stabilizing effect and to minimize fin toe angle of the vertical tail. The main structural aeroshape modification was the rotation of the scramjet engine flowpath, tilted by -1.92 deg (see Figure 44 and Figure 45), that caused an increase of lateral surfaces of the vehicle, while a flat bottom was chosen for the rear part of the vehicle basing on considerations about longitudinal static stability, together with nominal CoG at 50% of the vehicle's reference length.

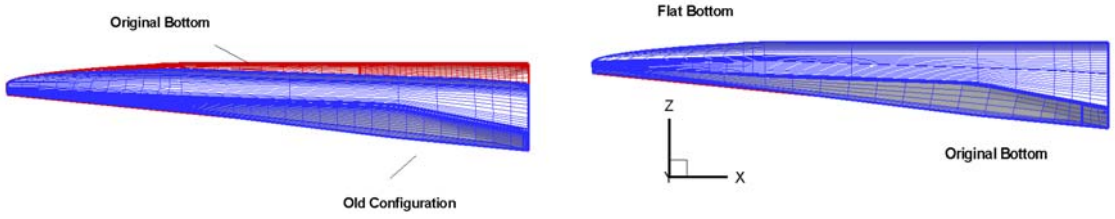


*Figure 44: EFTV-G different aeroshapes: side view*

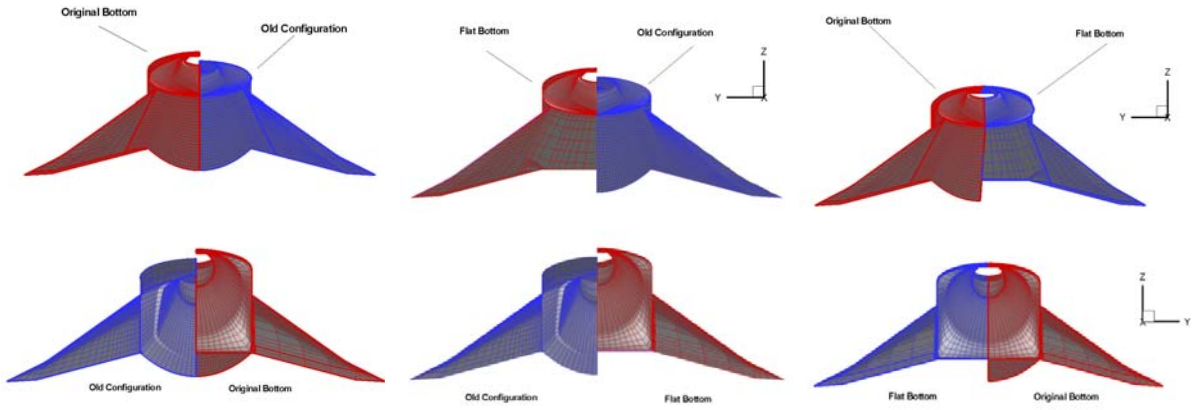


*Figure 45: EFTV-G different aeroshapes: front view (top row) and rear view (bottom row)*

New definition and sizing of vertical tail (without fin toe angle) and ailerons (double sized) defined the **FB-T4-F3** configuration whose nominal motor-on experimental flight condition was AoA=AoS=0 deg. CAD files and AEDB of the FB-T4-F3 configuration were delivered by CIRA in occasion of the HEXAFLY project PM2, see Figure 46 and Figure 47.

A detailed aerodynamic analysis was also performed, see from Figure 48 to Figure 50, both longitudinal and lateral-directional, and different effects of engine, sideslip, clean and trimmed configuration were assessed both on aerodynamic efficiency and trimming capabilities of the configuration. The configuration resulted statically stable with a longitudinal static margin of 5.9% and also statically stable for lateral-directional aerodynamics. Linear lateral dynamics was neutrally stable (Dutch Roll) and not damped due the modelling approximations made. A possible active control based on asymmetrical deflection of ailerons (no rudders) was also proposed to increase the Dutch Roll damping.

Finally, hinge-moments were characterized for a preliminary selection and sizing of servo-actuators (electrical motors) to actuate ailerons, see Figure 51.

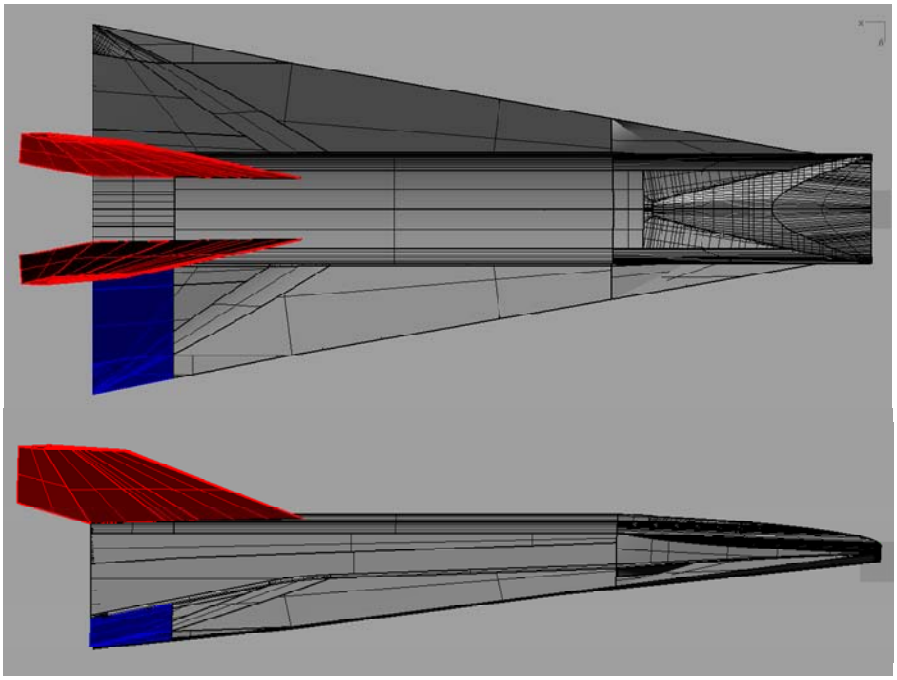

*Figure 46: EFTV-G FB-T4-F3 configuration*

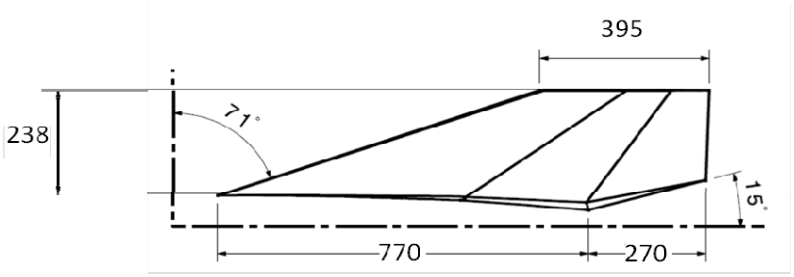


*Figure 47: Detail of FB-T4-F3 vertical tail*

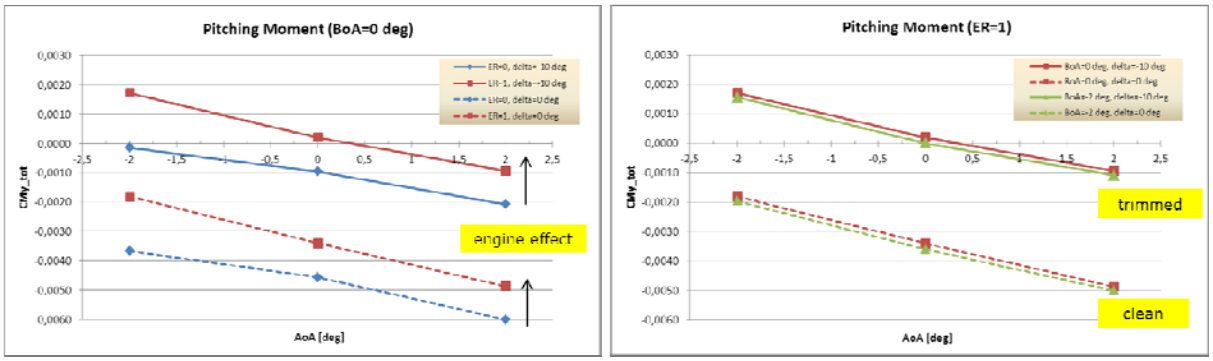


*Figure 48: EFTV-G FB-T4-F3 pitching moment coefficient evolution vs. angle of attack (no sideslip, left; motor-on, right)*

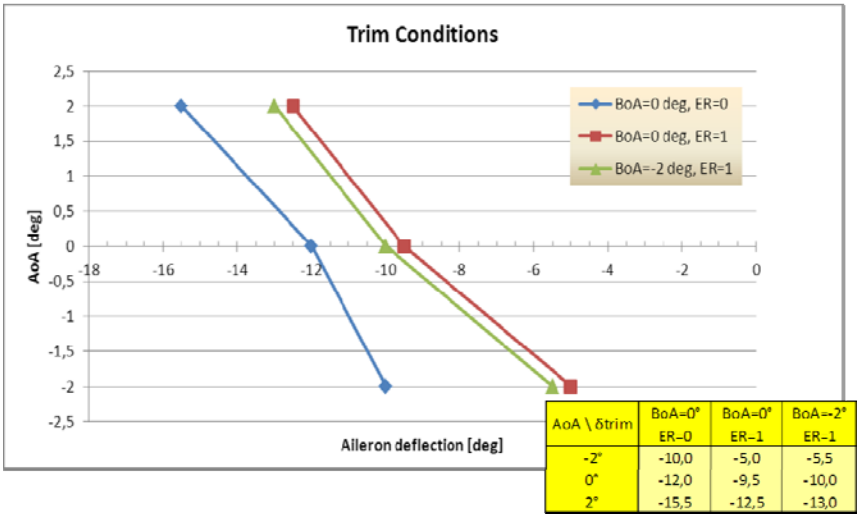


| AoA \ δtrim | BoA=0° ER=0 | BoA=0° ER=1 | BoA=-2° ER=1 |
|---|---|---|---|
| -2° | -10,0 | -5,0 | -5,5 |
| 0° | -12,0 | -9,5 | -10,0 |
| 2° | -15,5 | -12,5 | -13,0 |

*Figure 49: EFTV-G FB-T4-F3 evolution of trim AoA as function of aileron's deflection*

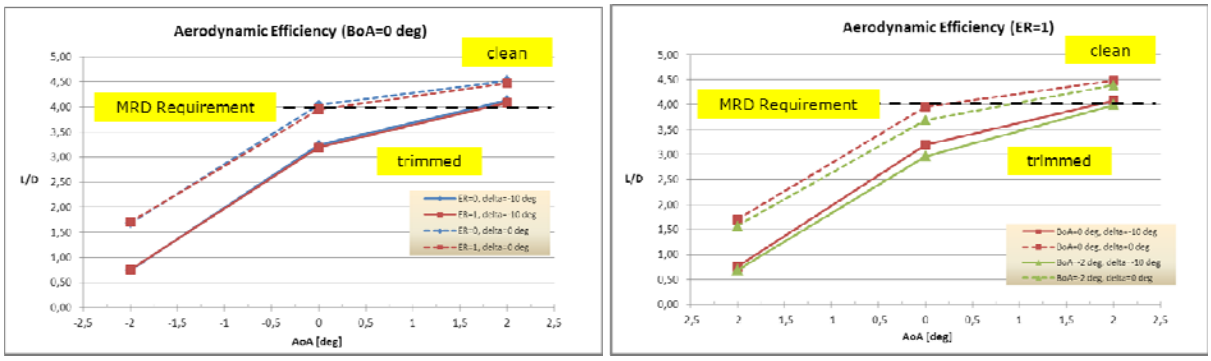


*Figure 50: EFTV-G FB-T4-F3 lift-to-drag ratio evolution vs. angle of attack (no sideslip, left; motor-on, right)*

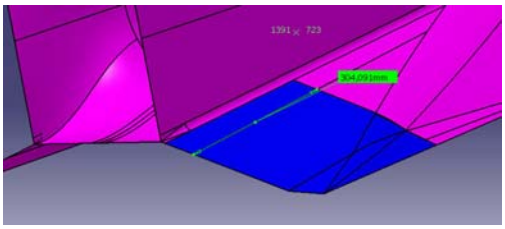

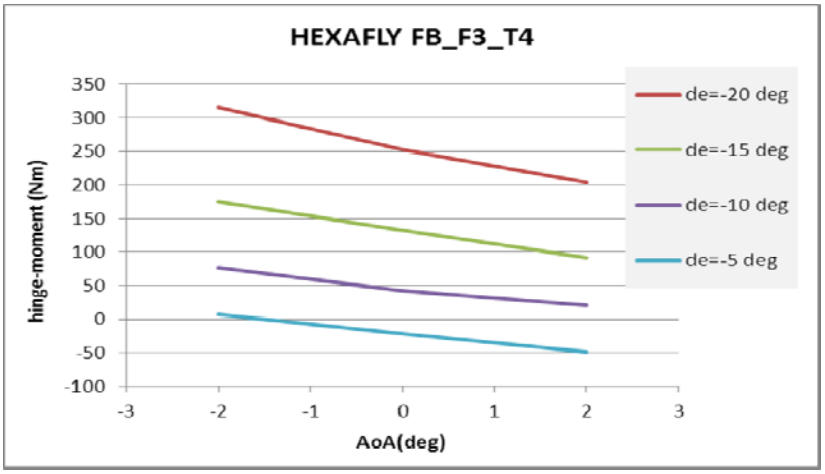


*Figure 51: EFTV-G hinge-moments in function of angle of attack (flight nominal conditions)*

The last **V47** configuration differed from the FB-T4-F3 only for some modifications to ailerons (smaller span, same surface, cantilever), wing span (slightly reduced) and fins (trailing edge small modification), see Figure 52. Being confirmed the nominal motor-on experimental flight condition, and the nominal CoG at 50% of the vehicle's reference length, the aerodynamic performance of the new aileron shape was analysed and was confirmed (see Figure 53).

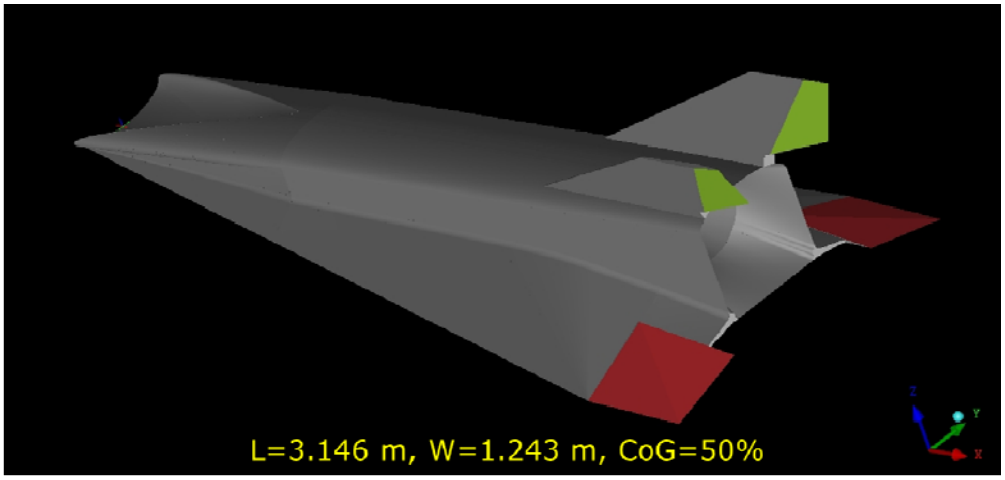


*Figure 52: V47 EFTV-G vehicle with modified ailerons and vertical tail*

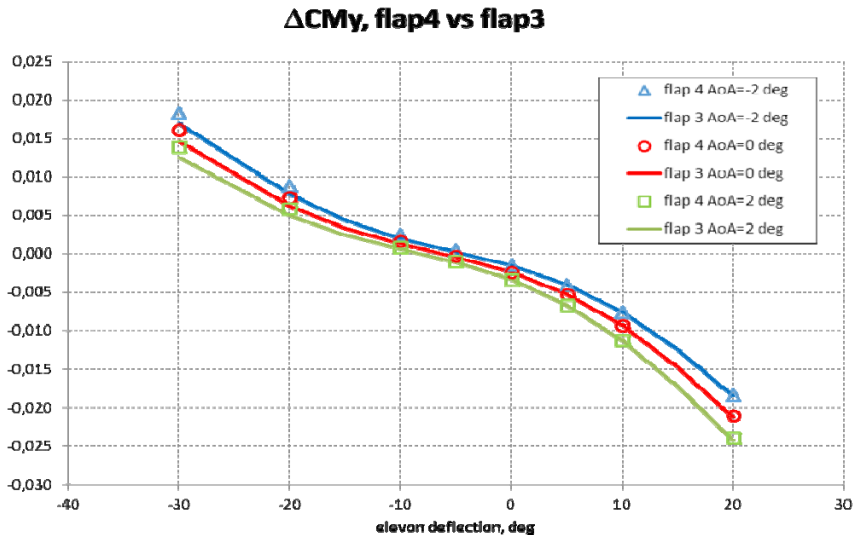


*Figure 53: Flap#4 vs. Flap#3 (ΔCL, top left; ΔCD, top right; ΔCMy, bottom)*

The flight stability analysis was based on the last CFD-based AEDB released by ESA-ESTEC. The configuration resulted statically stable with a longitudinal static margin of 6.6% and also statically stable for lateral-directional aerodynamics (a decreased dihedral effect was observed for V47 w.r.t. FB-T4-F3 vehicle). Linear lateral dynamics was neutrally stable (Dutch Roll) and not damped due the modelling approximations made. A possible active control based on asymmetrical deflection of ailerons (no rudders) was also proposed to increase the Dutch Roll damping. A possible CoG location (56%) to have a “neutrally stable” vehicle (SM≈0, see Figure 54) was also considered for V47 vehicle, with the following effects: short period pole in the origin of the complex plane (zero pitch-stiffness), more than halved aileron’s deflection for trimming the vehicle, decreased yaw stiffness, decreased Dutch Roll frequency.

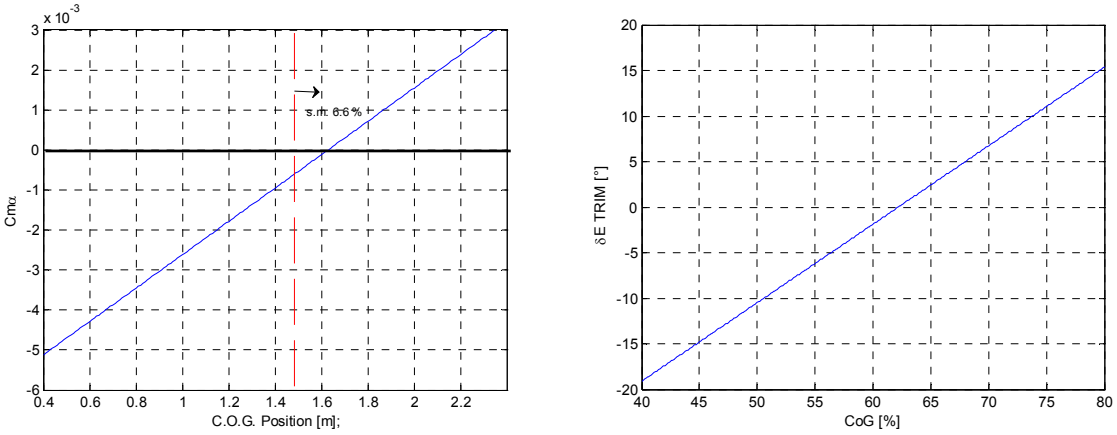


*Figure 54: V47 EFTV-G $C_{m\alpha}$ evaluation (left) and trim deflection (right) in function of CoG variation*

Flight Control equipment (IMU, magnetometer, FCC, servo-actuators, actuation lane) was preliminarily defined and inputs for configuration and CAD files were given, see Table 4 and Figure 55.

| # | Part name | Mass (kg) | Volume (m³) | Gx (m) | Gy (m) | Gz (m) | Power (W) | VDC (V) |
|---|---|---|---|---|---|---|---|---|
| 1 | IMU-1 | 2 | 0,005 | 1,938 | -0,091 | -0,100 | 30 | 28 |
| 2 | IMU-2 | 0,5 | 0,001 | 2,405 | 0 | -0,147 | 5 | 28 |
| 3 | FCC | 2 | 0,004 | 1,938 | 0,091 | -0,100 | 5 | 28 |
| 4 | Act. Moog 1 | 4,6 | 0,004 | 2,220 | -0,103 | -0,147 | 180 | 28 |
| 5 | Act. Moog 2 | 4,6 | 0,004 | 2,220 | 0,103 | -0,147 | 180 | 28 |

***Table 4: Flight Control inputs for EFTV-G V47 configuration file***

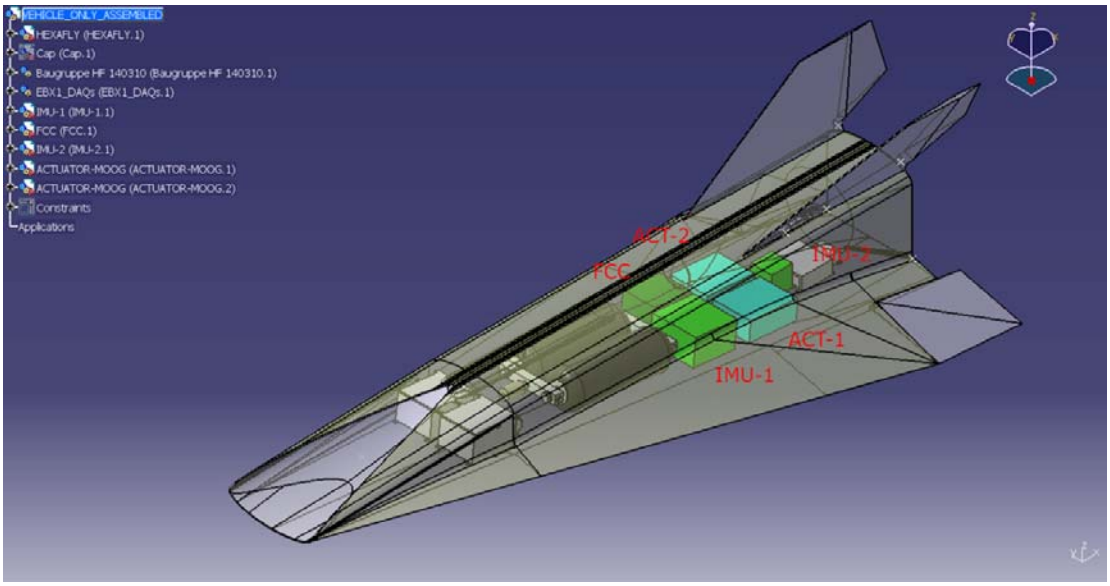


*Figure 55: EFTV-G V47 internal subsystems*

*Detailed System Studies – EFTV Design (Structural Layout, DLR-Stuttgart)*

The vehicle design for this current study is based on the LAPCAT II vehicle approach developed by ESA-ESTEC, DLR *et al*. It consists of aerodynamically optimised shapes for the outer vehicle with an integrated internal scramjet flow path. The aim of this study was to set up a structural model without taking the internal propulsion flow path into account. Contrary to the aerodynamic model designed in LAPCAT II, the mechanical model consists of volumetric bodies with a wall thickness, a mass and also a centre of mass. For first design variants, the STEP-configuration 'HEXAFLY_3m_Prelim_Flight_Configuration.stp' was used, provided by ESA on 19.10.2012. The vehicle had a total length of 2985.4 mm (referred to as 3m in the following text).

DLR BK was using the CAD software *UNIGRAPHICS NX 7.5*, for this reason the STEP geometry was imported here and transformed into a volumetric body afterwards. This turned out to be unfavourable as the imported aerodynamic surface model consists of many curved surfaces which cause bumpy surfaces. Those irregularities in turn cause singularities and open points (not water-tight) in the surface, which make the generation of volumetric bodies very costly and time-consuming.

For the experimental flight vehicle (EFTV), several substructures like nose and inlet section including inlet leading edges, fuselage including support structure, rudders, wings and wing leading edges, internal flow path (not considered in this study) and ailerons were identified, see Figure 56. Each of these components has to fulfil different boundary conditions in regard to e.g. oxidation resistance, mass, structural stability and integrity. Therefore, different materials needed to be applied tailored to the specific needs.

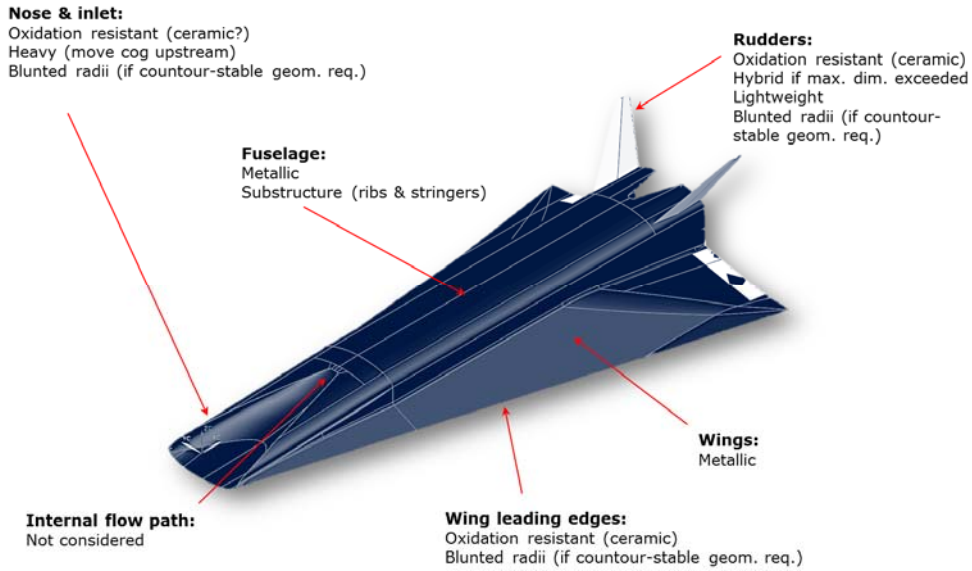


***Figure 56: EFTV design approach***

Subsequently, a first structural model was set up. Hereby, the internal flow path was excluded from a mechanical analysis and only shown for illustration reasons. In doing so, the vehicle was split into the parts (Figure 57) nose section, support structure with substructure and wings, tail section and ceramic-based hot parts, such as wing leading edges, rudders and ailerons.

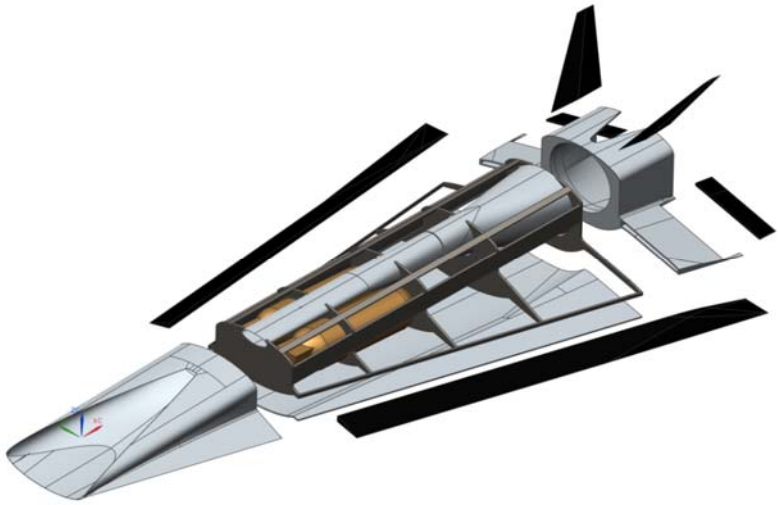

***Figure 57: EFTV v0 configuration, exploded views without fuselage/wing skin***

For this first vehicle approach, both a mechanical and a transient thermo-mechanical finite element analysis have been performed. Particularly thermally induced stress reach high levels, which have to be taken care of at future design iterations (see right-hand side of Figure 58). On the other side, mechanical stresses do not seem to be critical yet as depicted in the left-hand side of Figure 58.

One of the major findings of the vehicle design and the associated finite element analysis was the identification of critical items which have to be eliminated further on.

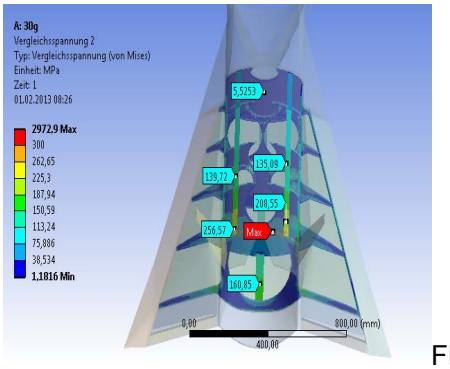


FEA, mechanical stress levels

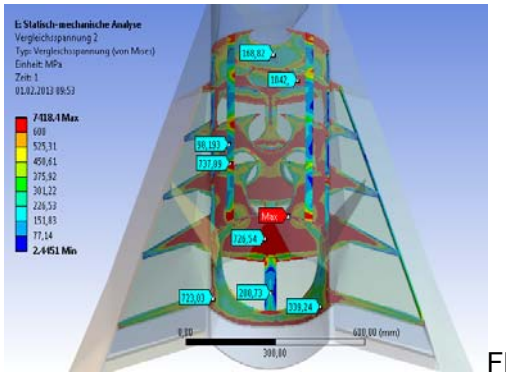


FEA, thermal stress levels

***Figure 58: EFTV v0, FEA results***

Within the scope of the project, several design variants have been considered and analysed, which enabled the estimate vehicle masses, centers of gravity as well as moments of inertia which are crucial for other design disciplines. It turned out, that the masses of both nose and tail section are the main design drivers here. Therefore, alternative concepts such as split or hollow nose sections have been investigated, as can be seen in Figure 59.

(a) Split nose

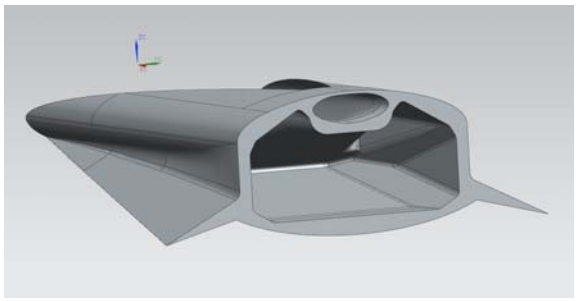

(b) Hollow nose

***Figure 59: EFTV, nose section design alternatives***

In a final design iteration, once all subsystems were dimensioned and the final trajectory known, the structural layout was adapted by ESTEC to assure the integration of all components including the final material selection. The cross sections are given in Fig. 5.

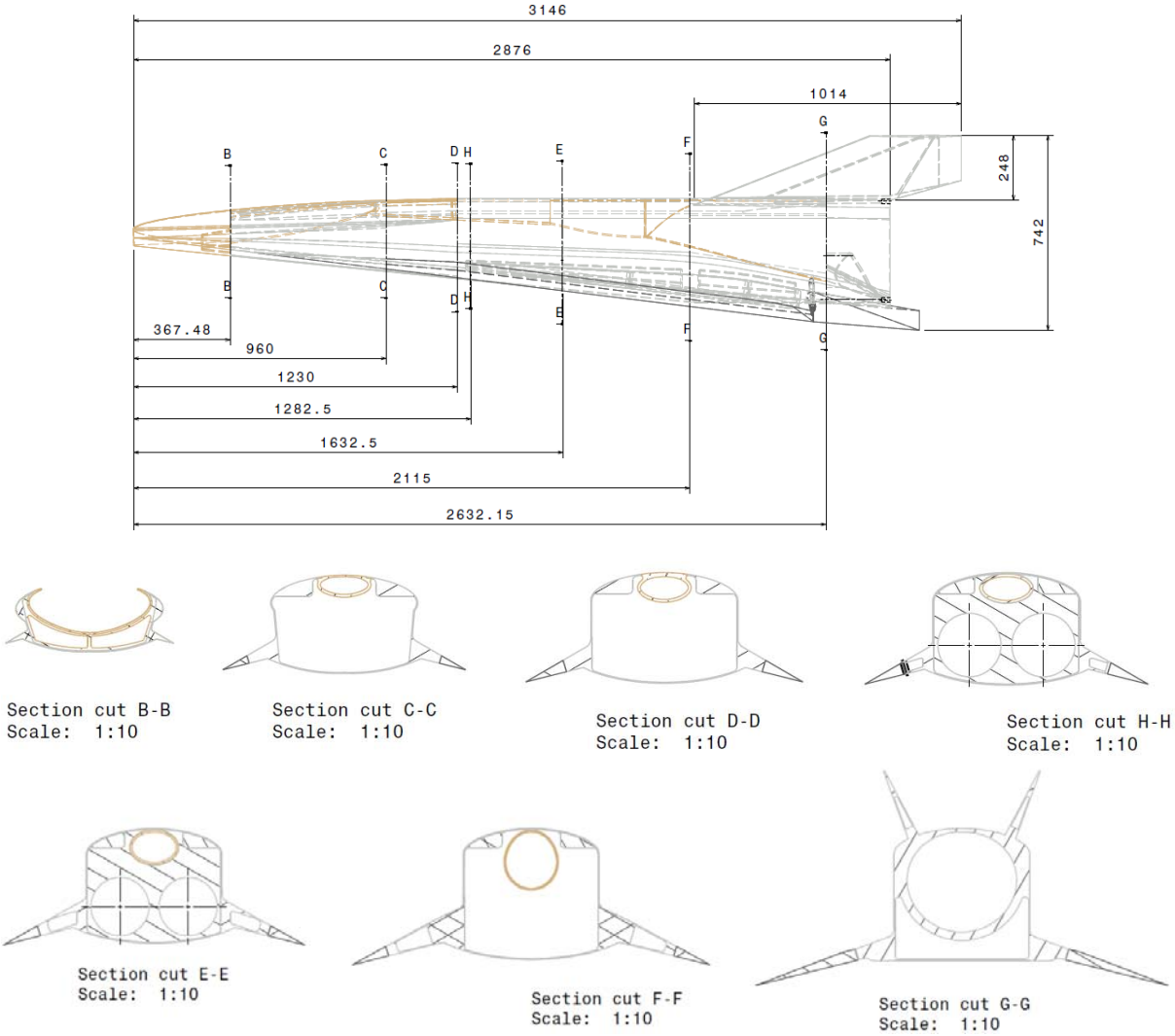


***Fig. 5: Cross-sections at different x-locations***

In addition, potential solutions for the ESM have been briefly discussed by DLR Stuttgart (Figure 60). Due to the elliptically-changing shape of the internal flowpath's 3d-nozzle, the ESM support is

very restricted. Possible problems like jamming might occur here, hence other ESM alternatives must be investigated during further iterations.

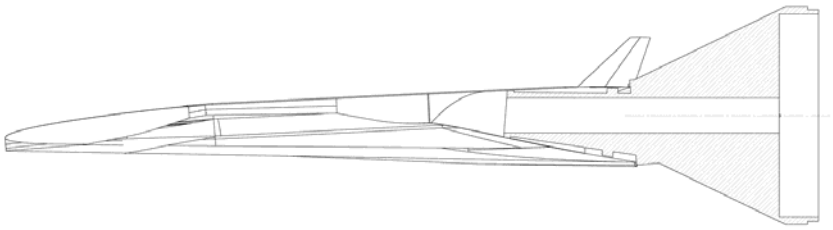

***Figure 60: EFTV + ESM connection***

Further refinements were needed on the ESM as:

- the connection and ejection of the ESM-EFTV was not trivial
- the internal duct could cause internal compression and local hot spots
- the space within the flare was limited due to presence of the captured air passage
- the external diameter needed to reduce from a 1000mm to a 800mm for integration onto the LVSM
- compatibility was preferred towards airborne launch systems

while keeping the same basic functionalities such as a free-jet passage, active control during exo-atmosphere re-entry, passive longitudinal and lateral control in the outer atmosphere and achieve rate control up to the EFTV release. This has led to the following ESM layout (Fig. 6Fig. 6) consisting still of a flare containing the CGS-ACS and connected to the rear of the EFTV with pyrotechnical bolts and 8 CFRP struts. More details are given in **Error! Reference source not found.**. The assembly with the EFTV is given in Fig. 7.

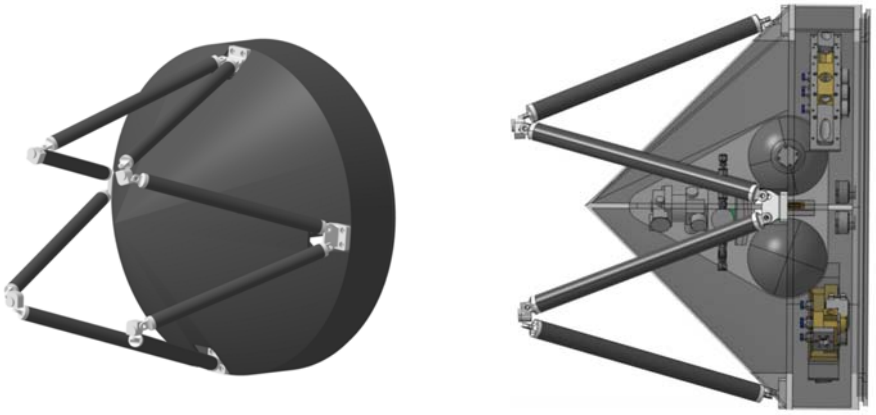

***Fig. 6: General Layout of the final ESM: a: front isoview, b: side view***

***Fig. 7: General layout of the EFTV+ESM; top: front view; bottom: rear view***

*Detailed System Studies – EFTV Design: Instrumentation*

A basic instrumentation layout and data acquisition concept for HEXAFLY EFTV was worked by DLR-Cologne **Error! Reference source not found.**. Focus was laid on pressure, temperature, heat flux and strain measurements based on the SHEFEX-II flight hardware. The system still is flexible enough to integrate other sensors or change the focus of investigation. The EBX is the heart of the DAQ system and is shown in Fig. 8. Basically it consists of a power supply which converts and isolates the power from the vehicle and the box. The Power Distribution Card (PDC) ensures an independent power supply of active sensors and manages the internal housekeeping. For acquiring signals the data is amplified in an Analog Amplifier Card (AAC) and converted to a digital signal in a Multi-Function Card (MFC). The MFC pass the data with a RS422 bus to the Telemetry System.

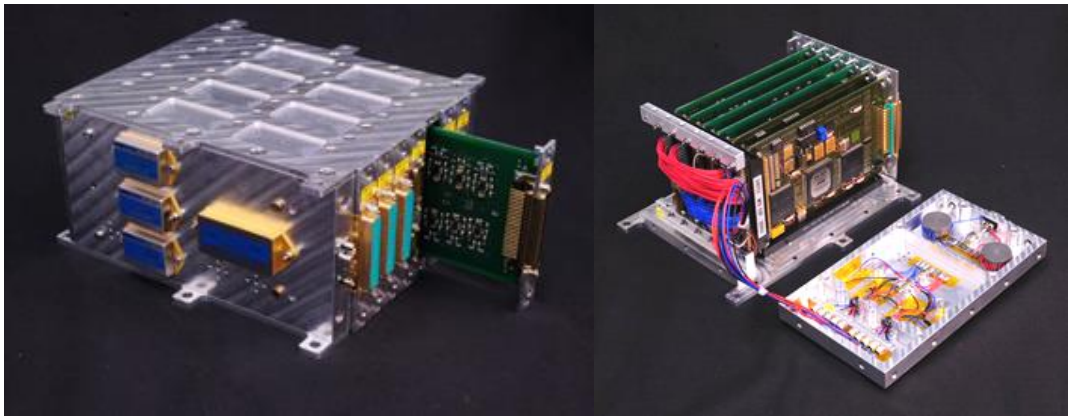

***Fig. 8: Electronic Box (EBX)***

In **Error! Reference source not found.**, **Error! Reference source not found.** and **Fig. 11** , the proposed sensor positions are plotted. Focus is set on the internal flow path for measuring the pressure rise due to the combustion and the internal flow field. Additional pressure sensors on the wings and the bottom of the vehicle will give the pressure distribution on the outer surface. Coaxial thermoelements and heat flux sensors are used to measure the heat flux in the internal flow path and detect transition on the outer surfaces.

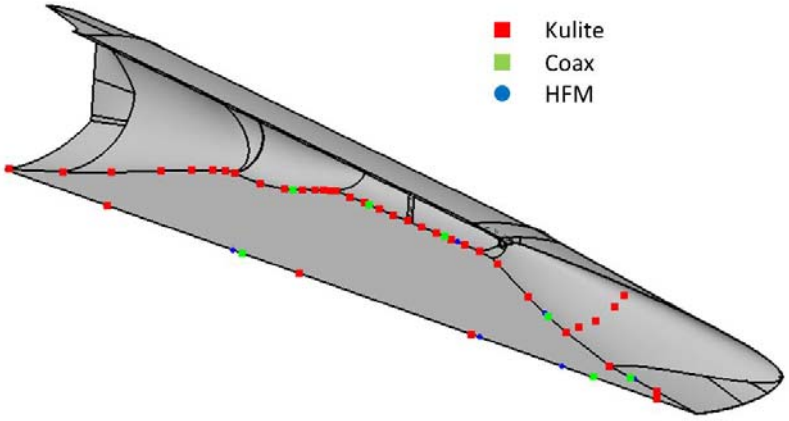


***Fig. 9: Sensor positions – symmetry line and FADS***

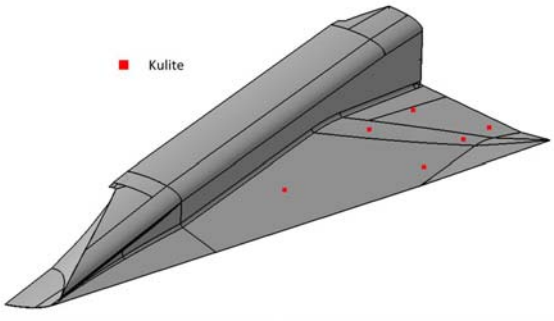


***Fig. 10: Sensors positions - wing upper side***

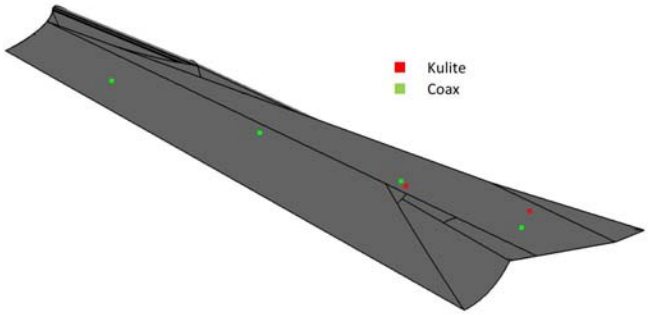


**Fig. 11: Sensor positions - wing lower side**

A further detailed analysis was performed by DLR-Co on the FADS, which is much more complex due to the complex shape of the wave-rider flight vehicle. It could be shown, that the measurement of angle of attack and sideslip are feasible. Also the Mach number is possible, but a correction correlation needs to be developed from CFD or experiments. Validation was performed by comparison with other numeric and experiments of the LAPCAT II intake Fig. 12.

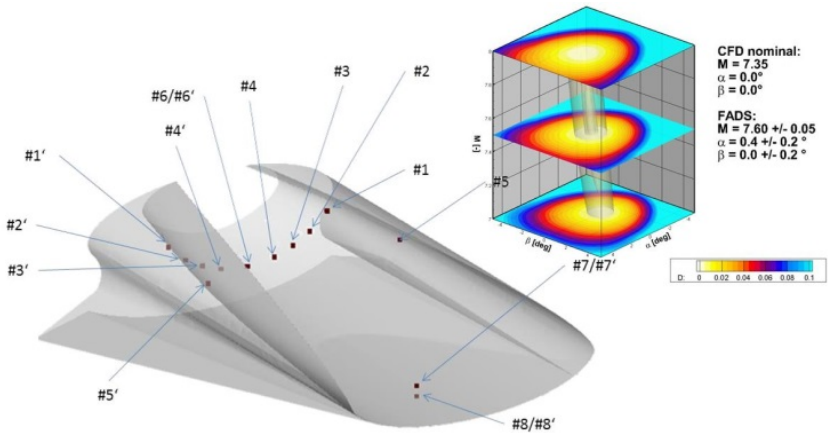

***Fig. 12: Least square values for 13 sensors based FADS***

ONERA investigated the feasibility of an on-board TDLAS system in order to measure the temperature and concentration of a species like $H_2O$. Three different positions were pointed out for measuring in the upstream free flow with a Pitot-probe, in the flow at the wing-tip and across the inlet Fig. 13. Also some studies on a short range Rayleigh LIDAR system to measure free stream density were carried out.

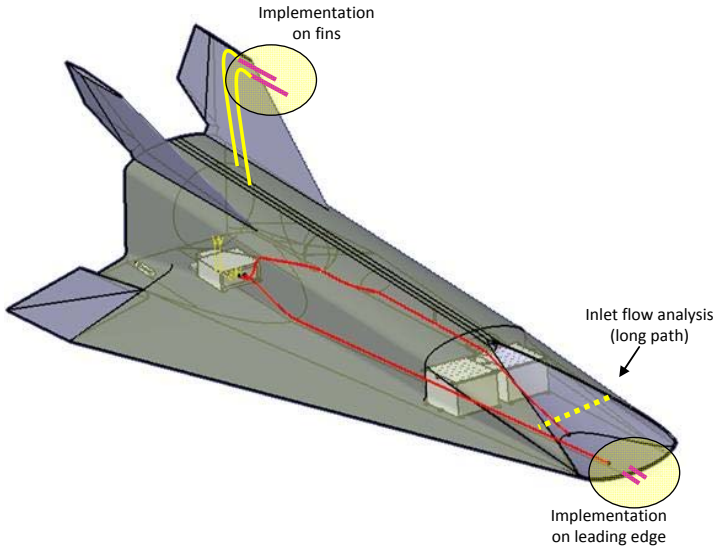


***Fig. 13: Implementation of TDLAS***

In the present document, a thermo-structural deformation experiment to be mounted on-board of EFTV-G vehicle has been proposed and conceptually designed by CIRA. Some interesting areas of the vehicle have been indicated and proper high-temperature strain gauges, which can operate up to about 1400 K, have been selected to measure different deformations during the flight: bend of the wing, aileron bending, fin torsion and fin bending, fuselage bending and wing torsion Fig. 14. An analysis of sensor requirements with respect to the data acquisition system and the full vehicle has been done, also highlighting some criticalities are still open such as the necessity of dummy strain gauges for temperature compensation and the need for laboratory tests to solve some implementation issues due to the brittle nature of the ceramic adhesives usually employed for bonding these gauges to the surface of a vehicle.

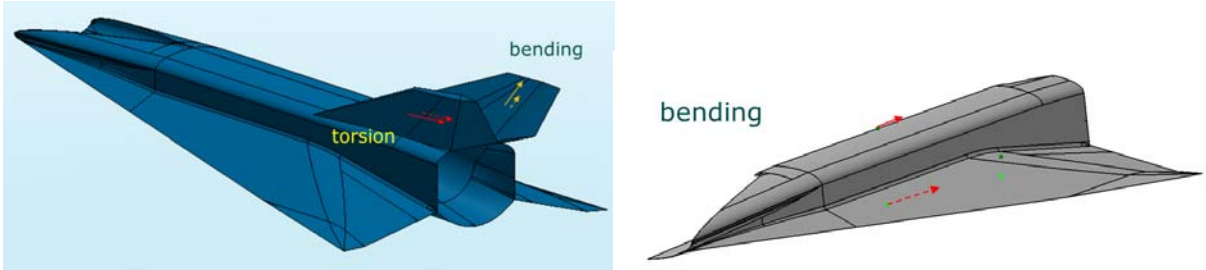


***Fig. 14: HTSGs location for fin torsion and bending***

The basic requirements of the sensors related to the propulsion system and its control have been worked out by ESA-ESTEC. The very fast depletion of the high-pressure tanks result in a large drop in pressure and temperature which needs to be accurately measured to assure a correct mass flow rate in the combustor pending on the ambient conditions and attitude of the vehicle by means of closed feed-back loop (Fig. 15). The criticality of the required accuracy requires the need for dedicated calibration and qualification tests on the proper hardware.

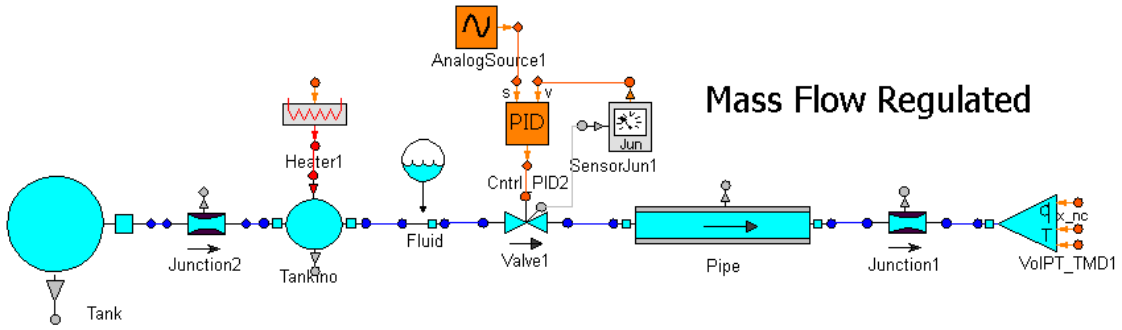


***Fig. 15: Numerical representation of on-board propulsion system***

*Detailed System Studies – EFTV Design (Nose-cap analysis, DLR-Br)*

The final part of the EFTV design was the analysis of different versions of a preliminary inlet cover for the flight vehicle. The investigations focus on static stability and trim using a horizontal fight scenario. For each version of the cap-configuration, Euler calculations are performed using the DLR Tau-Code. Two Mach numbers were preselected covering the lower and higher end of the planned Mach number range. If successful as solution and if required from system perspective, this test matrix will need further extension. Table 5 summarizes the calculations: the angle of attack $\alpha$, the Mach number Ma and the flap angle $\eta$ were varied.

| Ma [-] | $\eta$ [°] | $\alpha$ [°] |
|---|---|---|
| 8 | -15, 0, +5 | 1 – 5 ($\Delta$ = 1) |
| 2 | -15, 0, +5 | 1 – 5 ($\Delta$ = 1) |

***Table 5: Overview of the calculations***

Cap-version 7 has, compared to the other investigated configurations, the best aerodynamic performance. Hence this configuration and the main-results are described and summarized in the following: Figure 61 shows a comparison of the unclosed configuration (green/grey colour) and the cap-configuration 7 (blue colour).

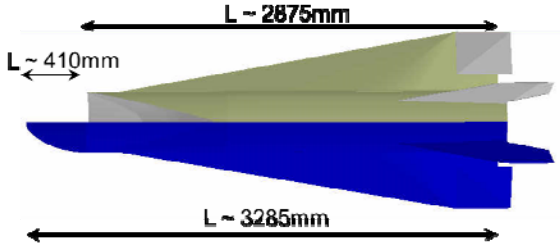


***Figure 61: Comparison unclosed and cap-v7***

In Figure 62 an overview of the cap-v7 in different views is illustrated.

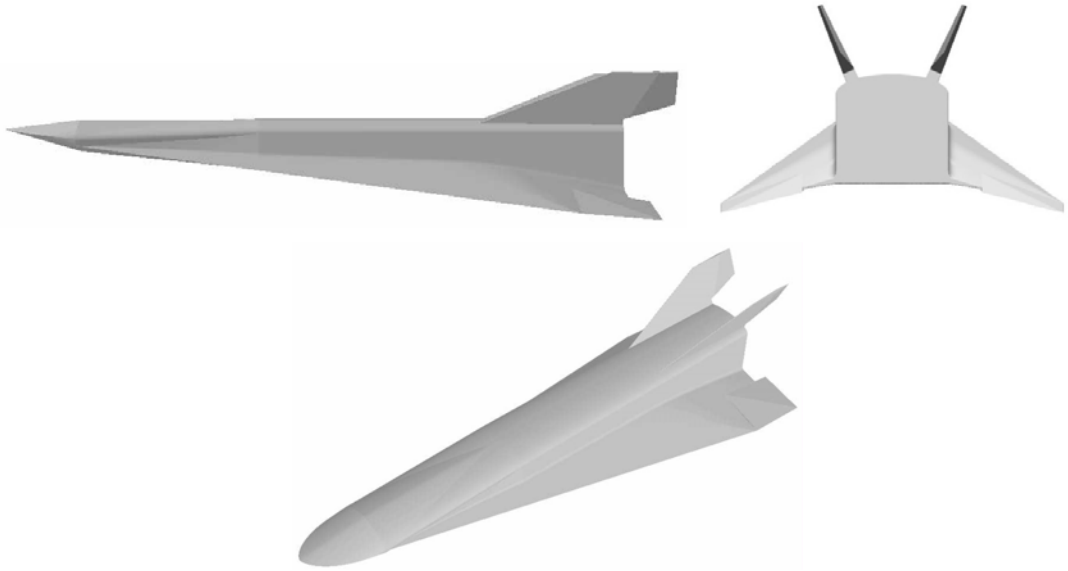

***Figure 62: Overview of the cap-v7.***

For the investigation of the longitudinal stability a moment reference point (MRP) of 57% measured from the nose is used for the x-coordinate. This corresponds approximately to the moment reference point of the open configuration with 50%.

Figure 63 shows the investigation of the longitudinal stability: The pitching moment coefficient Cm as a function of the angle of attack $\alpha$ at Ma = 8 (solid lines) and Ma = 2 (dashed lines) for different flap angles $\eta$. In all cases the longitudinal stability is given. With reduced Mach number the flap efficiency increases. For Ma = 8 trim can be obtained almost without flap deflection. At Ma = 2, a negative flap deflection is needed below -15°.

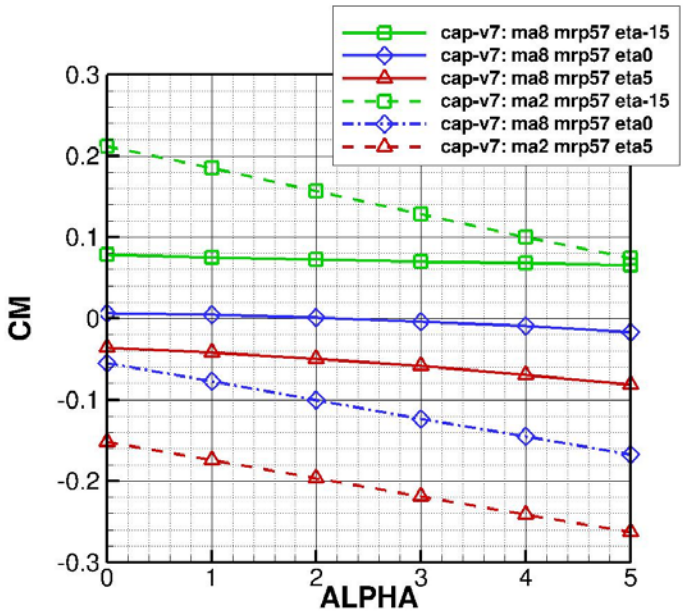


***Figure 63: Investigations of longitudinal stability of cap-v7***

To summarise, a static, horizontal flight stability analysis of different configurations of the nose cap was performed. It is shown that a longitudinally stable and trimmed horizontal flight with a closed inlet is feasible at a vertical load of 1g for the two investigated flight points (Ma = 2 and Ma = 8). For cap-v7 at Ma = 8 trim can be obtained almost without flap deflection. This cap-geometry can

be considered as a preliminary solution for protecting the internal flowpath. But further analyses including the g-forces along a realistic trajectory are necessary.

*Detailed System Studies – ECTV Design (Gas Dynamics)*

As noted in the introduction, a ground-test model similar in design to the HEXAFLY vehicle, was previously tested in the HEG shock tunnel at DLR as part of the LAPCAT-II project. In order to demonstrate that an aero-propulsive balance could be achieved, this model was allowed to fly freely during the ~3-4ms test period, requiring all of the instrumentation, fuel system and power supply to be carried on-board the vehicle. In support of the tunnel testing, a large number of Nose-to-Tail CFD computations were also performed in order to verify the net forces acting on the vehicle, and to determine the fuelling strategy for the engine.

In summary, this test campaign was considered a success in that an aero-propulsive balance was achieved, and the net acceleration levels were in reasonable agreement with the CFD predictions. However, the most interesting part of the study related to the internal performance of the engine, as the pressure profiles within the engine were found to differ from the CFD model predictions. This is not a reflection on how careful the CFD model was applied, but is a rather clear example of how difficult it is to accurately predict the internal engine performance. In contrast the external aerodynamics are easier to predict, and are easier to measure in a ground test facility. For the ECTV, we have therefore focussed our efforts on designing an experiment to study the internal aerodynamics of the vehicle. So long as a precise model of the external aerodynamics can be developed, a prediction of the aero-propulsive balance can be found by careful definition of a control volume, allowing the net forces on the vehicle to be determined accurately.

Furthermore, the ECTV concept described herein has been conceived to minimise both technical risk and development time and cost by sharing common technologies with the experimental free flight vehicle (EFTV), and other flight-proven hypersonic systems. To this effect, particular attention has been given to the Sharp Edge Flight Experiment II [SHEFEX II], flown by DLR in June 2012, having the objective of investigating different shapes and materials for a manoeuvring re-entry vehicle. And based upon the initial trajectory profile developed by DLR for the EFTV (described in **Figure 4**), it was also clear that the VS-40 would be well suited to a captive-carry test campaign.

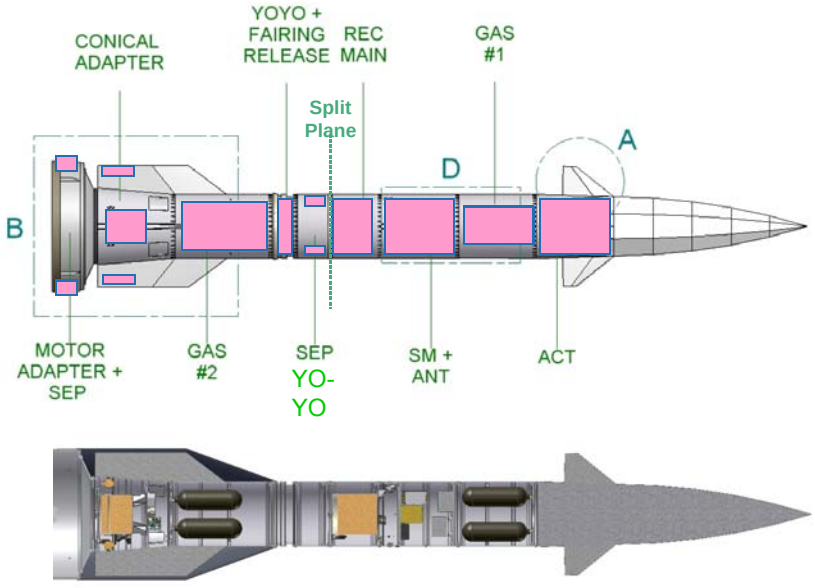


***Figure 64: SHEFEX II payload layout, courtesy DLR***

With that objective in mind, Figure 64 gives an indication of how the SHEFEX-II payload may be re-configured to satisfy the HEXAFLY requirements. Note that the faceted nose-tip is approximately 1.5m long, and is followed by a 600mm extension piece containing the canards and the associated actuators. Rather fortuitously the ground-test model tested at HEG under LAPCAT-II also has a length of almost exactly 1.5m. And if our objective is to focus on the internal performance of the engine, then we only need to extract the internal flow-path from the model, and allow the external contour to be modified in order to provide the aerodynamic performance necessary to achieve a stable re-entry.
An initial layout for such a scheme is shown in *Figure 65* below. The internal flow-path is highlighted in green; and is connected to the external aero-shell (in light grey) by the conical adaptor shown in orange. To vent the engine exhaust over-board, the flow is initially decelerated to a subsonic Mach number through a normal shock ahead of the hemi-spherical cap located on the end of the payload delivery module (in red). The flow is then re-accelerated and vented through an annular gap located between the payload delivery module and the external aero-shell. Based on this initial configuration, a detailed internal layout was then developed to determine the mass properties of the system.

***Figure 65: Initial layout of the ECTV***

Figure *67* shows the final ECTV concept, composed of the fore-mounted experimental payload mated to the SHEFEX II payload delivery module (PDM). The overall length is 5.5m, and the overall mass laden with fuel is 573kg. The experimental payload occupies the first 1.5m and contains the following primary elements:-

1. The flow path: to be made from a carbon-carbon composite matrix;
2. The flow path thermal protection system: Used to isolate the internal structure from the combustion chamber thermal loads;
3. The internal structure: composed of 8 titanium frames, joined by four longerons, with a stressed skin to provide additional rigidity;
4. The external thermal protection system: employed to isolated the internal structure and system during re-entry;
5. The external skins & internal flow adaptor: used to provide aerodynamic fairing;
6. The internal flow adaptor: used to contain the nozzle exhaust gases prior to egress in the external stream;
7. The fuel system: to supply the gaseous hydrogen during the test window;
8. The instrumentation subsystem: providing power and signal conditioning to the outputs.

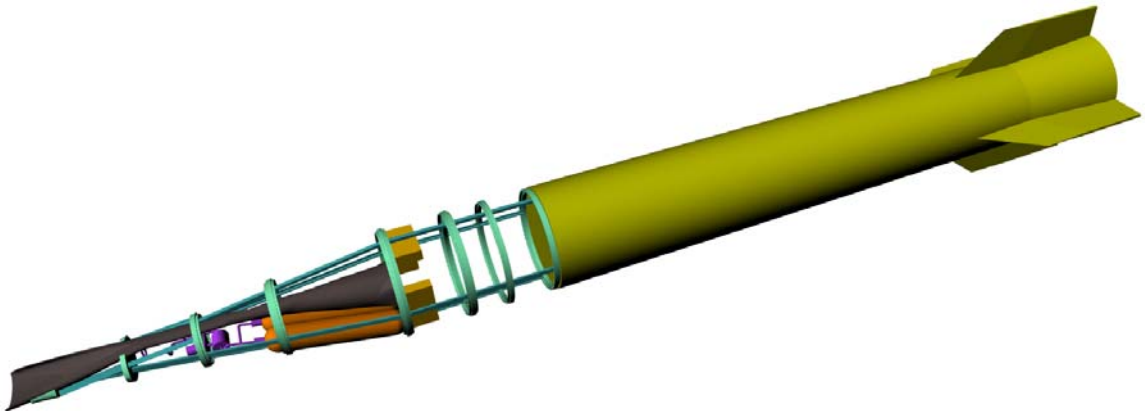

***Figure 66: The ECTV concept shown mounted to the payload delivery system adopted from Shefex II. The inner and external skins and TPS have been removed from the ECTV to reveal the internal***

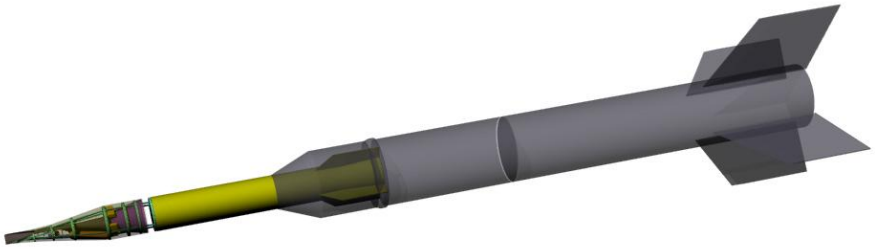

***Figure 67: ECTV illustrated together with the VS40 launcher.***

A more detailed description of each of these sub-systems is provided in the design report [D2.2.1, part A], but a brief summary of the major components is provided below.

Although a detailed stress analysis was not undertaken, in keeping with the design philosophy for the vehicle the internal structure drew heavily from SHEFEX-II. As shown in Figure 68, a conventional (and relatively heavy) aeronautical structural approach has been adopted, composed of eight 10mm frames connected via longerons, wrapped by a semi-structural 1mm skin. The scheme is broadly similar to SHEFEX-II having a cold sub-structure that is isolated from the hot external skin via a layer of thermal insulation. Given that the internal structure is cold a number of material choices are possible, but for this initial scheme Inconel has been adopted with an assumed density of 8,450kg/m$^3$, resulting in a mass budget for the sub-structure of 63kg.

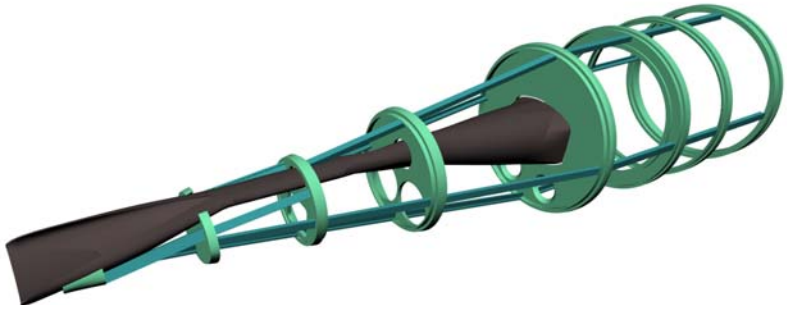

***Figure 68: The flow-path shown located within the sub-structure, with the TPS removed.***

As shown in Figure 69 the vehicle is shrouded in 3mm thick Inconel skins, mounted indirectly to the cold structure below, enabling the necessary thermal expansion to occur whilst reducing

conduction loads to the underlying structure. Further thermal protection is afforded by the lightweight insulation sandwiched between the hot external aero-shell and the cold internal skin. The choice of Inconel for the external hot wall was based upon a temperature prediction from an unsteady heat transfer calculation, taking the boundary layer edge conditions as those found on a 9.5° cone. The peak temperatures were found to be well within the material limits for Inconel (which has a maximum operating temperature of ~900K). The resulting mass budget established for the external skin, including the internal adaptor (which is sized similarly) was found to be 67kg.

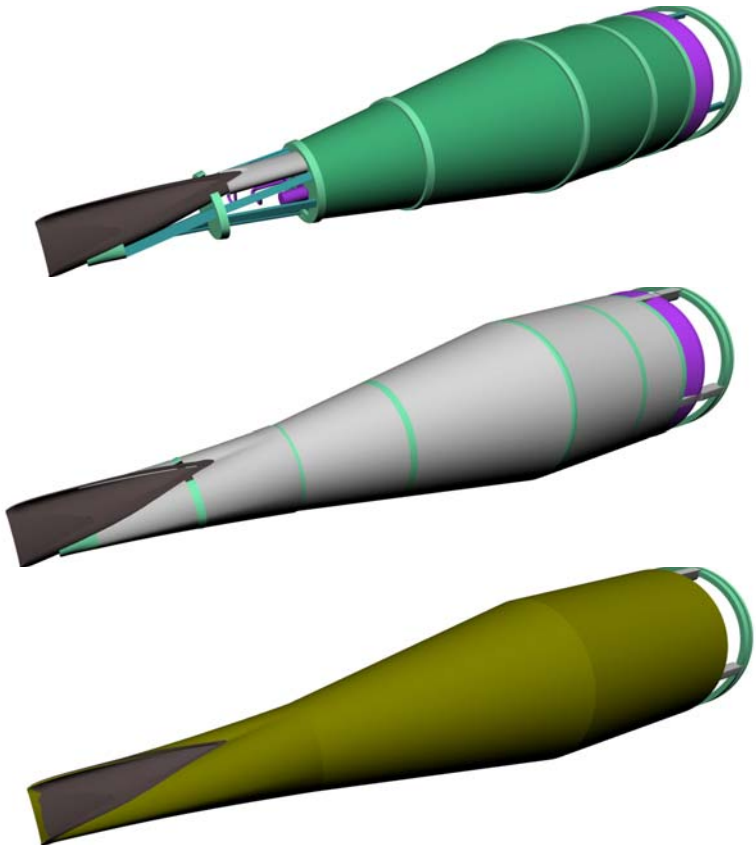

***Figure 69: Top to bottom: underlying frame and longeron structure with cold skin; inclusion of the TPS layer; and finally the hot outer aero-shell.***

The fuel system is shown in Figure 70 below. The tanks containing the gaseous hydrogen fuel are Luxfer carbon fibre wrapped aluminium cylinders, having a diameter of 117 mm and a length of 580 mm. The fuel tanks present a total volume of 8.4 litres and their charging pressure is 300 bar. Assuming they are filled to 30Mpa (abs) at a temperature of 298K they will store 172g of hydrogen. The fuel mass required for the test is calculated by integrating the atmospheric density profile during the near vertical descent between 37km and 25km altitude. Assuming that the intake operates at full capture, then for near stoichiometric combustion the required fuel mass is approximately 125g; a requirement that is comfortably satisfied by the storage capacity of the Luxfer tanks.

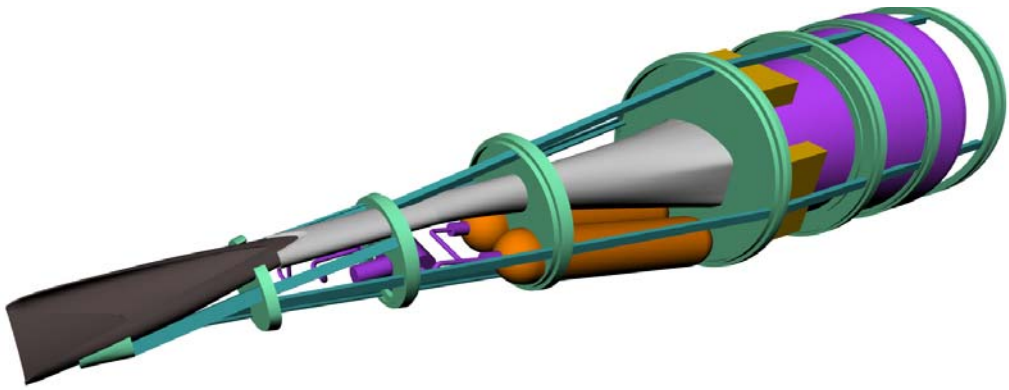

***Figure 70: Fuel system layout showing tanks in orange and ancillary pipework in purple.***

Mass and inertia estimates have been made for the experimental payload based on the design information detailed above and the associated CAD drawing. The properties for the entire system are given in Table 6 below.

| **Mass (kg)** | **PDM** | **Experimental payload** | **Entire system** |
|---|---|---|---|
| **Mass (kg)** | 373 | 200 | 573 |
| **Centre of gravity (m)** | 3.7, 0 ,0 | 1.39, 0 ,0 | 2.89,0 ,0 |
| **Rxx (m)** | 0.202 | 0.184 | 0.196 |
| **Ryy (m)** | 0.957 | 0.521 | 1.380 |
| **Rzz (m)** | 0.957 | 0.521 | 1.380 |

***Table 6: Mass and inertia estimates for the entire assembly***

*Significant results*

Different concepts have been worked at different scales and for different flight approaches, i.e. captive and free-flying. For the captive configuration, ECTV, the focus is mainly on the investigation of the internal flowpath and the combustion process. The Free-flying concept, EFTV, covers a wider range of disciplines, such as vehicle concepts, high-speed aerodynamics, flight control and high temperature materials.

*Reasons for deviations*

*N/A*

*Critical issues*

Some critical technologies have been highlighted but are not of this nature that they might evolve into a showstopper.

*Use of Resources*

The use of Resources is detailed in section **Error! Reference source not found.**

## 3.2 Flight Platform Definition

*3.2.1 Ground launch system*

*Summary of progress*

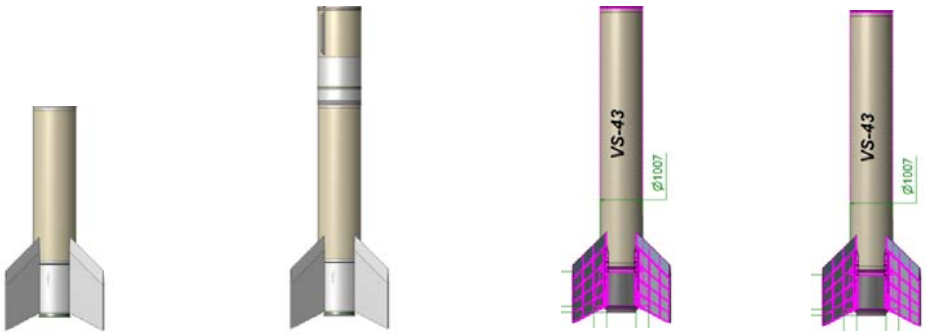


| S40 | VS40 | S43 Steel Case | S43 CFRP Case |
|---|---|---|---|
| Single stage | 2 stage | Single stage | Single stage |
| Thrust Vector Control | Fixed nozzle, 2nd stage pointing controlled | Thrust Vector Control | Thrust Vector Control |
| SFXII Fin Assy | SFXII Fin Assy | SFXII Similar Fin Assy | SFXII Similar Fin Assy |
| 4to Propellant | 4to + 1to Propellant | 7to Propellant | 7to Propellant |
| Existing | Existing & Flight Proven | Existing | To Be Developped |
| 5.83m //1.007m | 6.94m //1.007m | 7.2m //1.007m | 7.2m //1.007m |
| 5400kg<br>1050kg | 6350kg<br>2050kg | 8700kg<br>1500kg | 8400kg<br>1200kg |

***Figure 71: Motor configurations investigated over the course of the study***

Based on the successful flight of SHEFEX II on a VS40 rocket motor configuration (see figure below), the study started investigating the potential application of this motor to the HEXAFLY mission.

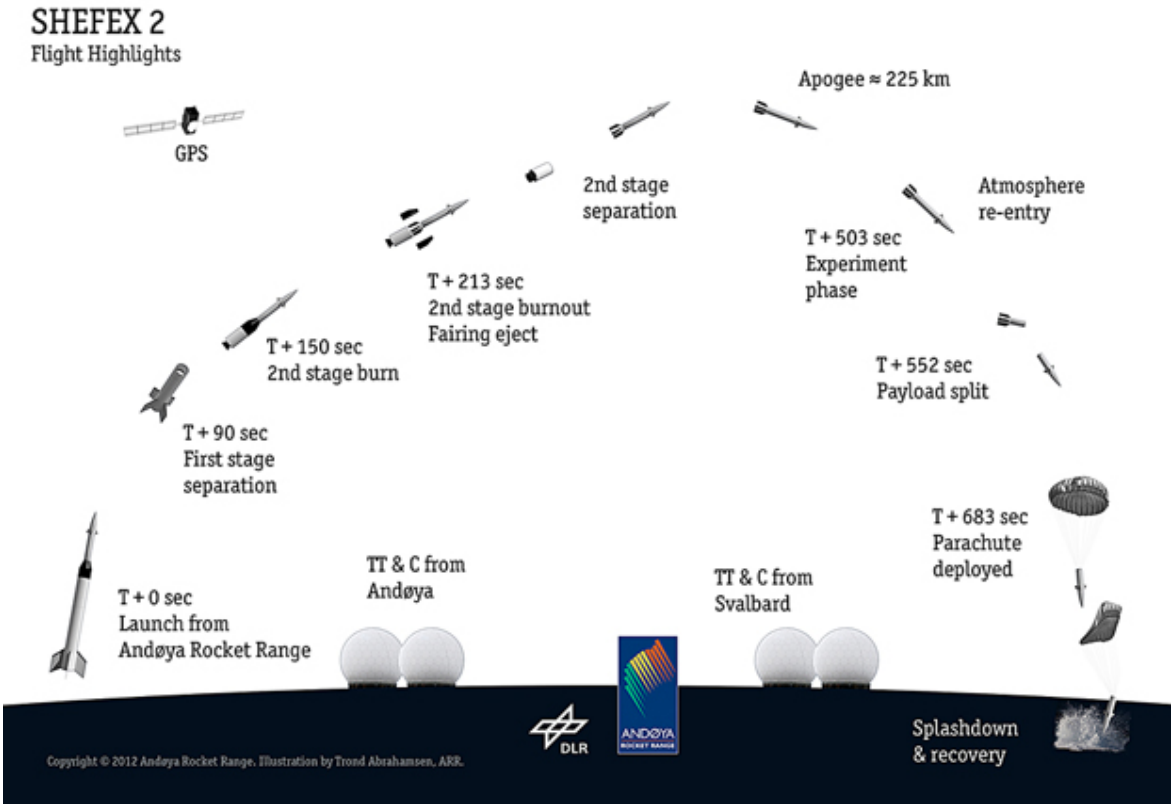


***Figure 72: SHEFEX II mission sequence***

Since the EFTV provides no sufficient rotational symmetry, which is a requirement to provide aerodynamically benign behaviour, a nosecone was put in place over the vehicle. Due to the wingspan of the EFTV, this results in a hammer head configuration, which is challenging from an aerodynamic stability and rail launching perspective. A large hammer head requires large and therefore massive launch lugs to span the distance between the motor and the launch rail. Exploiting the geometry of the EFTV, it was therefore proposed to fly a squashed nosecone with an elliptical cross section and rotate the finset by 45°, see figure below.

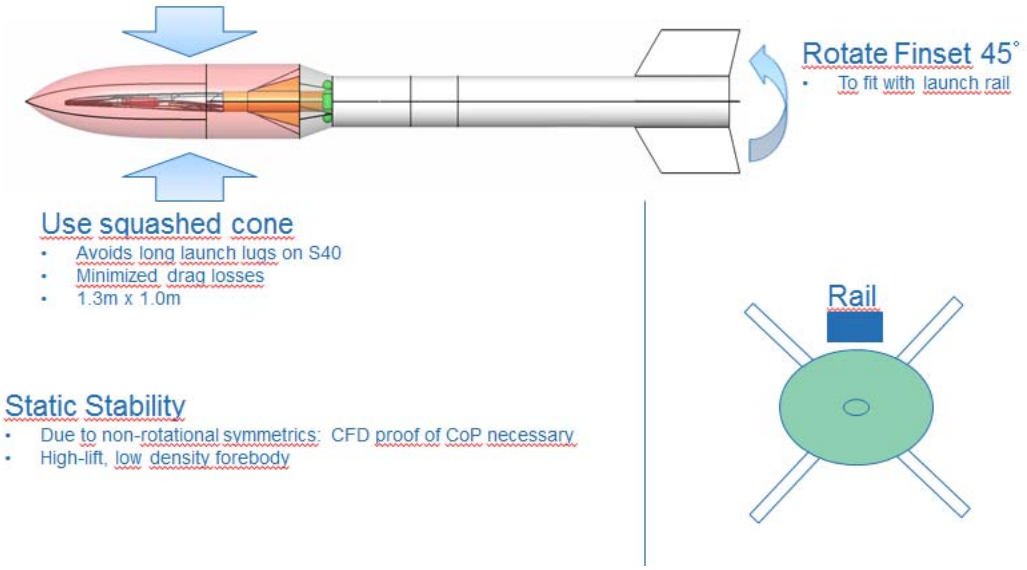


***Figure 73: Squashed nose cone proposal***

While maintaining the hammer head configuration when viewed at from top (and therefore not improving stability in this plane), the required length of the launch lugs is considerably reduced by implementing this as a solution. It was however noted, that this will also require the development of an elliptical separation joint the remove the nosecone from the vehicle after leaving the lower atmosphere.

As an alternative concept a constant diameter nosecone was proposed with hoods (called “Mickey Mouse Ears” in project talk) to house the EFTV wings. A detailed stability study was carried out for this configuration.

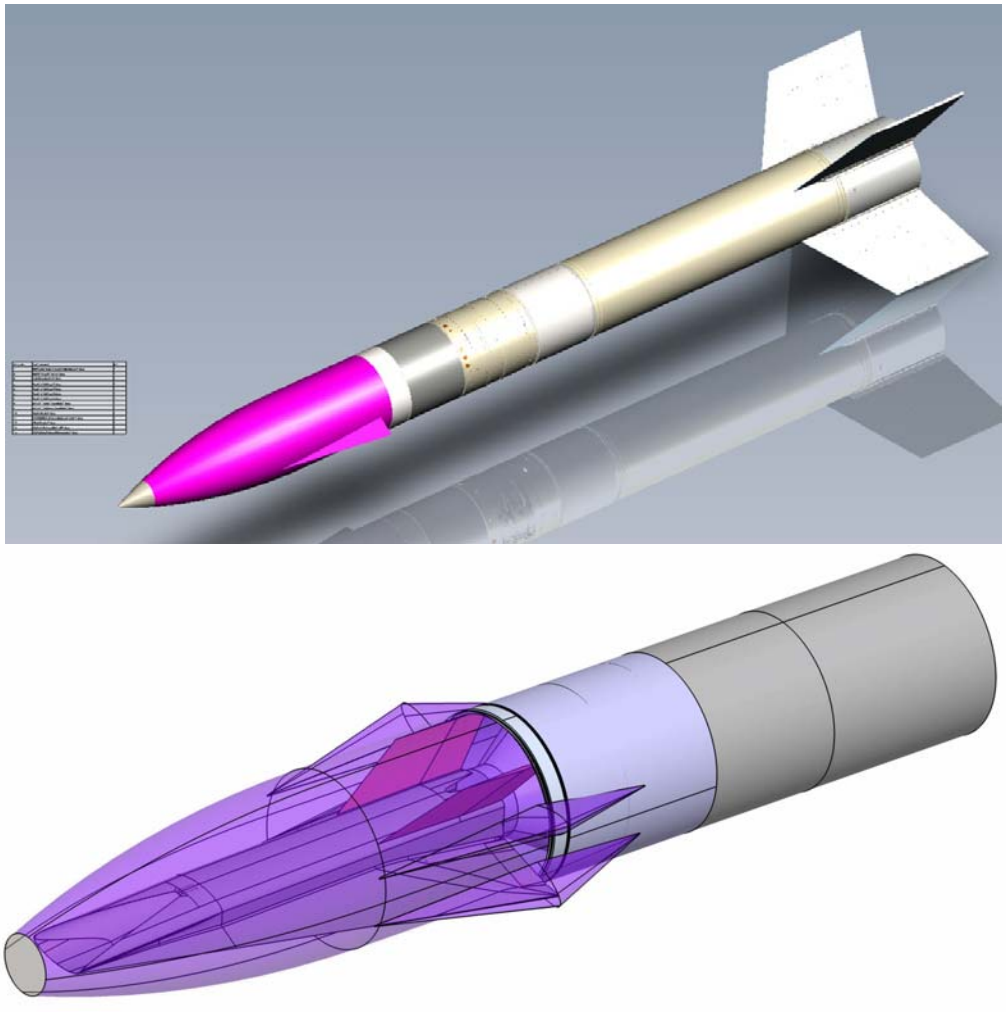

*Figure 74: VS40 launch vehicle with stabilizing fins*

As these hoods generate a configuration only symmetric in one axis, a second pair of ears had to be introduced resulting in the shape given in the figure below.

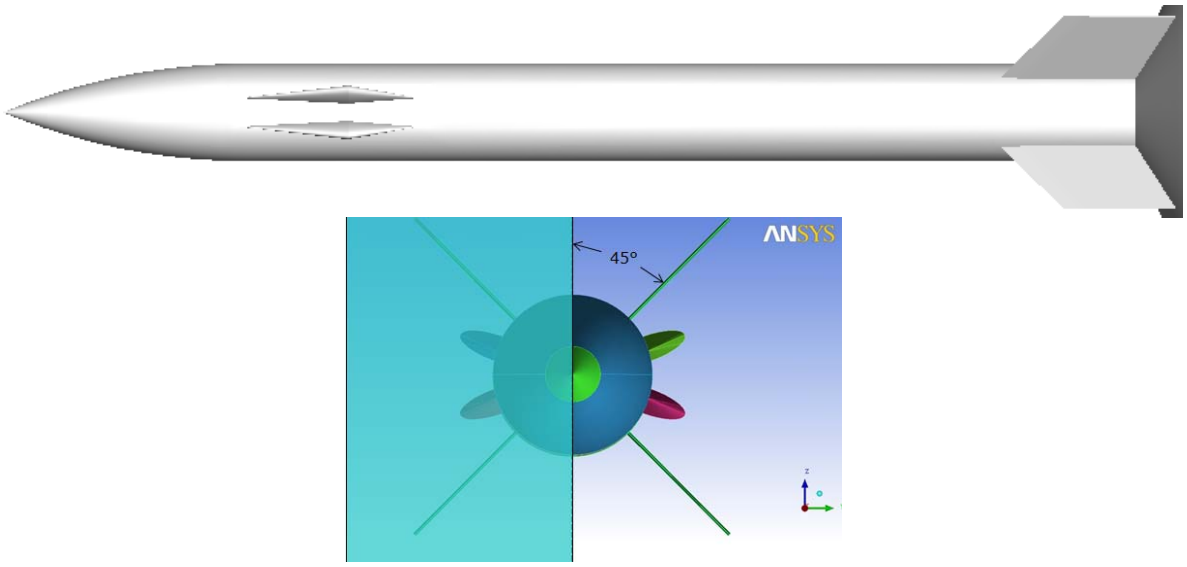


*Figure 75: VS40 launch vehicle with stabilizing fins and nose-cone with covers*

CIRA provided the CoP over an early defined Mach number regime by means of a simplified aerodynamic analysis of the VS40 launch vehicle with fairing with covers. Together with the CoG estimation of the configuration, this has allowed to assess the static stability of the vehicle. Figure 76 below plots both values as function of the flight Mach number (with $L_{ref}$ = 1.007m).

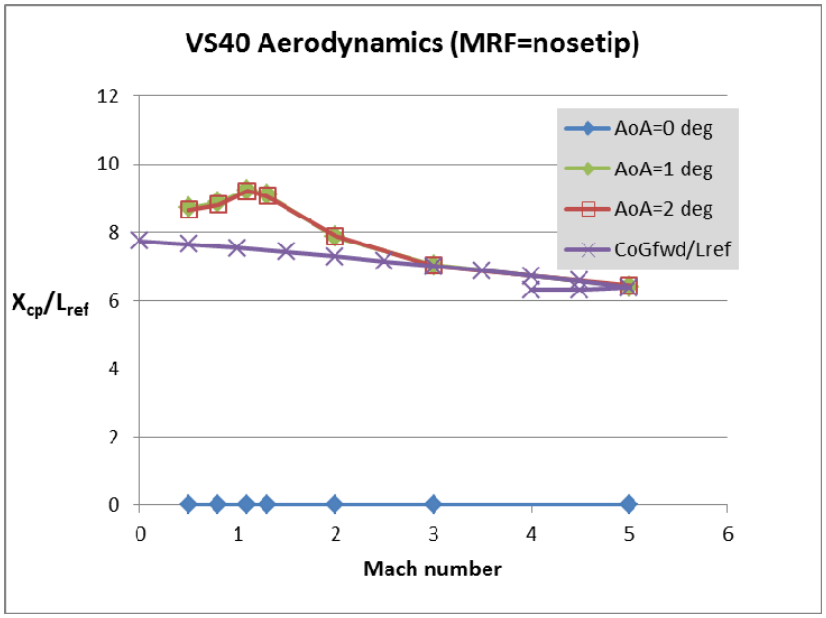


***Figure 76: Normalised centre of pressure and centre of gravity vs. Mach number***

DLR MORABA's minimum static stability requirement is 1 calibre [i.e. $(X_{CoP}-X_{CoG})/L_{ref} \geq 1$], which is violated by the VS40 launch vehicle actual stability behaviour. In fact, the vehicle is neutrally stable from predictions.

This is not tolerable and counter measures have to be pursued in order to obtain a sound design. These may include:

- Truncating of the Nose Cone
- Diameter Reduction of the Nose Cone
- Elimination of the ears
- Larger Fins
- Flare Tail can

Trajectory studies were carried out, confirming that the carrier performance would be just sufficient to reach the mission objectives, depending on the overall payload weight and the manoeuvring capability of the EFTV. It was initially proposed to fly a mission scenario with only one telemetry location at Andoya Rocket Range, and hence keeping the mission cost and complexity to a minimum. It was however found, that a short range trajectory – which is required to grant a continuous TM-link to and from Andoya (see figure below) can only be granted at the expense of flight path velocity and flight path angle, both in conflict with the mission requirements.

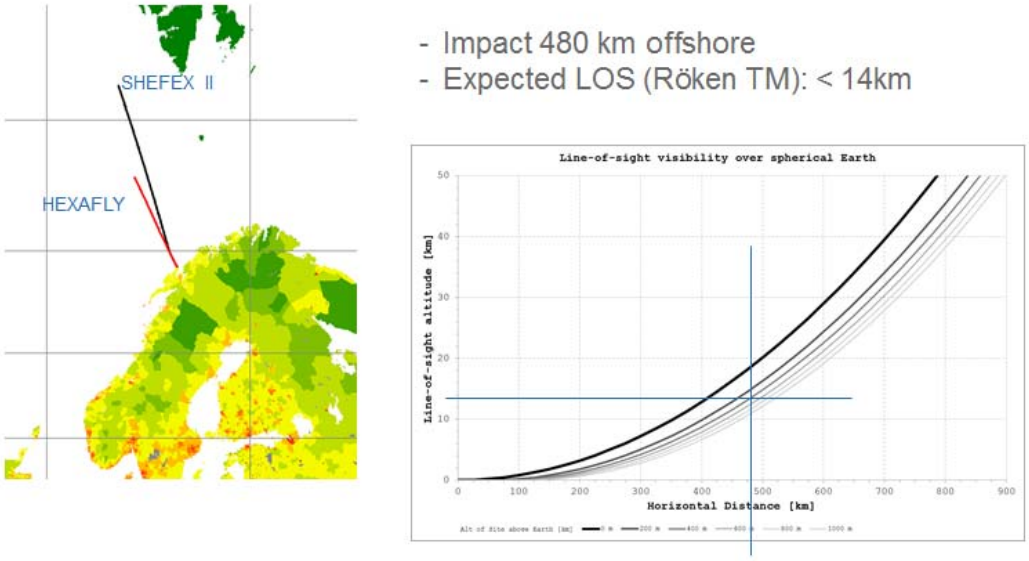


***Figure 77: Sample short range trajectory on VS40 motor configuration and associated TM line of sight calculation***

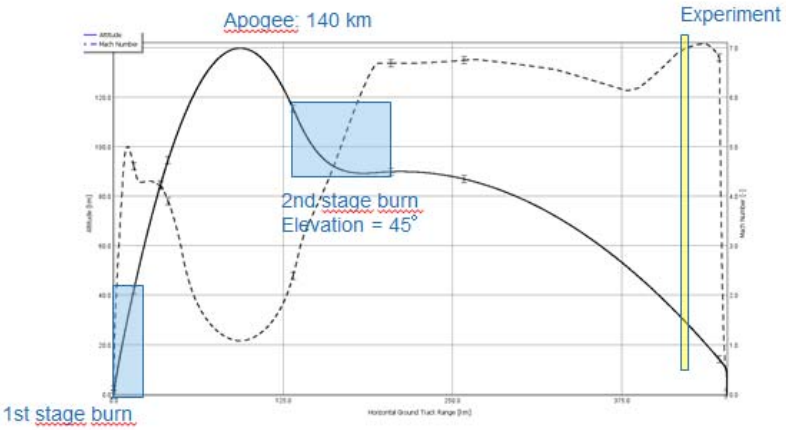


| | Experiment (Ballistic!) | MRD |
|---|---|---|
| Alt | 33..27 km | 33..27 km |
| Ma | 7 | 7..8 |
| FPA | -29° | >-15° |
| t | 6 | >7 |

***Figure 78: Sample short range trajectory and comparison of obtained flight performance against MRD requirements***

The S40 motor configuration was investigated but soon found to provide insufficient performance even when assuming a very optimistic payload weight, see figure 50. The figure below depicts a sample trajectory of this configuration, clearly showing that even the maximum reached flight Mach number does not exceed 6. The S40 was therefore not further investigated.

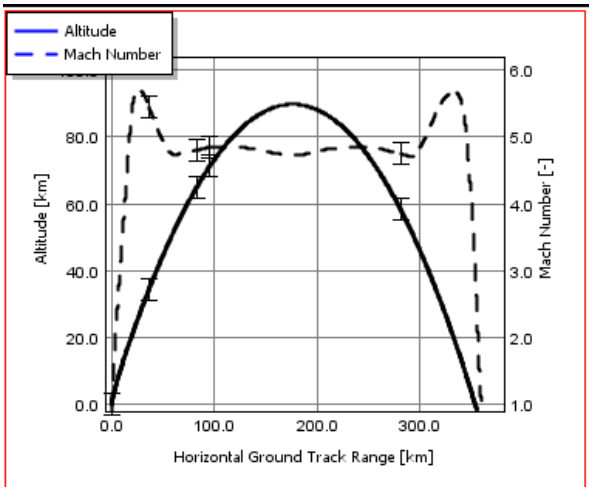


***Figure 79: S40 based configuration sample trajectory***

As another potential candidate, an S43 based vehicle configuration was investigated, proving that – depending on payload mass and trajectory design – the required flight Mach numbers are just within the motor performance, see figure below.

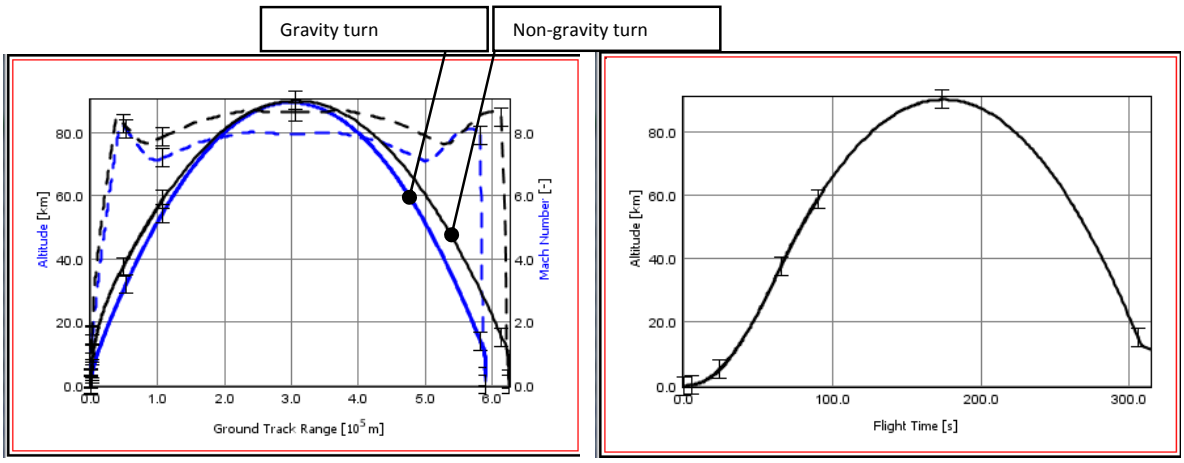


***Figure 80: Trajectory prediction with S43 single stage steel motorcase motor***

A decision tree was built in order to select the best option to meet the Hexafly requirements.

Two ground-based solutions are conceivable, unguided and guided sounding rocket Launch Vehicles. The unguided VS-40 requires a spin stabilized vehicle which requires a spin balanced payload. Due to the highly unsymmetrical layout of the EFTV spin balancing is nearly impossible. Therefore unguided, spin stabilized Launch Vehicle are excluded for further use in HEXAFLY.

The initial guided options have been the Brazilian S40 and the VS-40, both equipped with the same Thrust Vector Control (TVA). The S40 did not match the scientific objectives of providing Mach 7 at 90km apogee (limitation to Mach 5). On the other hand the VS-43 does.

Independent if the Launch Vehicle is guided or unguided, the following on-board subsystems are necessary to support the mission: Telemetry, TV, GPS, and Ignition Units for separation. In addition stabilizing Fins and Payload Fairing are required too.

In case of a guided Launch Vehicle the above subsystems are completed during the boosted flight phase with Thrust Vector Assembly, requiring Guidance Navigation and Control (GNC) and Thrust Termination, as well as Radar Transponder. In the unpowered flight phase, stabilization is archived with a Cold Gas System.

GNC and CGS need to be validated on-ground using hardware-in-the-loop and air-bearing test facilities.

The Launch vehicle will be validated with structural and thermal analysis to optimize the trajectory profile. The aerodynamic optimization is achieved with CFD tools.

Prior to the flight trial a safety assessment is prepared by the selected launch range. A test flight demonstrates in-flight functionality and reduces the risk for the main HEXAFLY mission.

The Launch Vehicle can be launched from a single rail launcher or a launch stool. The single rail launcher has the disadvantage that retractable launch lugs need to be implemented. Since the conical skirt diameter of the VS-43 is of 1.3 m the retractable launch lugs would get rather large and the retraction process is fault-prone. Launching from a launch stool is therefore recommended, which offers the opportunity to protect the entire payload with a hammerhead Fairing rather than an ogive nosecone with overlaying wing-tip protection covers. A split version is not recommended since the stiffness will be reduced and separations complexity increased.

While providing sufficient performance it was also noted, that an S43 based solution adds some technical challenges to the project. The S43 has been developed and utilized by the Brazilian space agency AEB as a cluster 1$^{st}$ stage and as a second stage central motor in its VLS ELV. Partially successful, the three historical flights of the VLS have proven the S43 operation in a comparably slowly accelerating vehicle.

When utilized as a single stage launch vehicle, the associated launch acceleration, and particularly the suppressed trajectory design required to thrust the HEXAFLY EFTV to high horizontal speed, results in considerably kinetic heating of the motor structure and also much higher flight loads. This requires a considerable amount of additional analyses and possibly countermeasures to reduce the effects of heating and flight loads.

Also due to the suppressed trajectory design, the motor burnout occurs within the relevant atmosphere below 40 km. To maintain attitude stability, the vehicle has to be passively stable, therefore necessitating large fins on the vehicle.

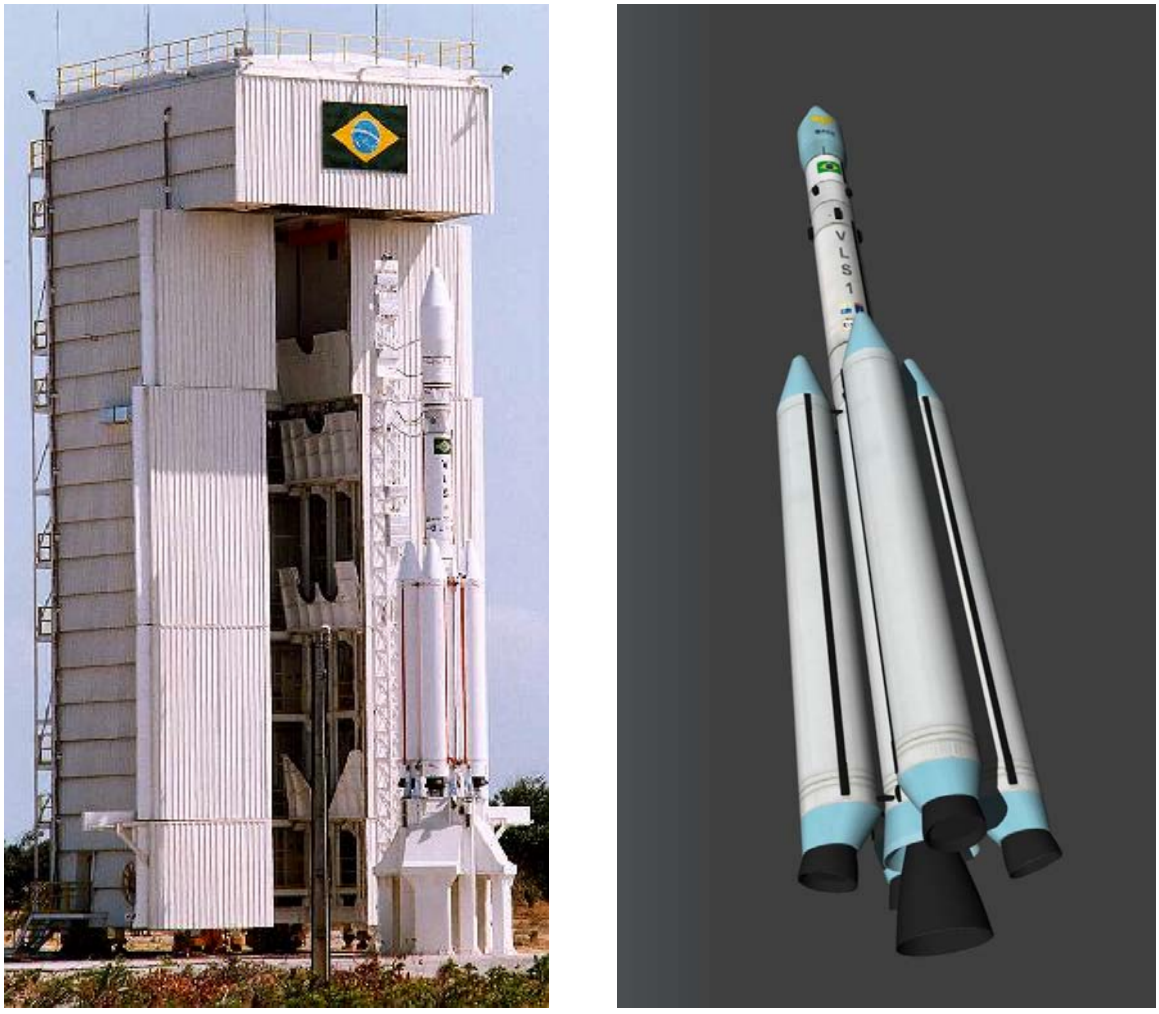


***Figure 81: VLS Launch vehicle***

*Significant results*

The guided single-stage S43 rocket launched from a launch stool is the preferred way to go. The preferred launch site is Alcantara in Brazil

*Reasons for deviations*

*N/A*

*Critical issues*

All study objectives were addressed. Since the S40 based flight platform was found to provide insufficient performance, the more powerful S43 motor was put in the scope of further studies. While providing sufficient performance, it is to be determined how aerodynamic stability upon burnout of the motor in low altitude layers will be granted. Also, due to the hammer headed configuration, a launch of the vehicle from a rail launcher is critical due to the requirement of uncommonly long and heavy launch lugs. A launch stool is therefore a preferred solution, which is to date not an existing infrastructure at Andoya Rocket Range.

The VS-43 with Thrust Vector Control will be flown for the first time in a single stage configuration. DLR-MORABA requests a qualification test flight prior to the actual flight trial.

If such qualification test cannot be envisaged before or within the Flight Test Program, alternatives would have to be revisited, like:

- consequences on the risk of failure when flying VS-43 without qualification test ?
- reconsidering the S-40 with more limited performances ?

### *3.2. Air launched system*

*General scope*

The baseline of WP3.2 is to provide elements regarding the design of an air-launched platform to perform EFTV flight test upon principles described in the Mission Requirement Document, and based on the Raduga D2 booster which is used by MBDA and ONERA for the LEA flight test program, and operated from a Tupolev 22M3 supersonic carrier.

*Summary of progress*

At the beginning of HEXAFLY, a general definition of air-launched platform was presented based on the approach used in the LEA flight –test program. The first constraints that should be taken into consideration to handle a new Experimental Flight Test Vehicle derived from Lapcat 2 studies were identified.

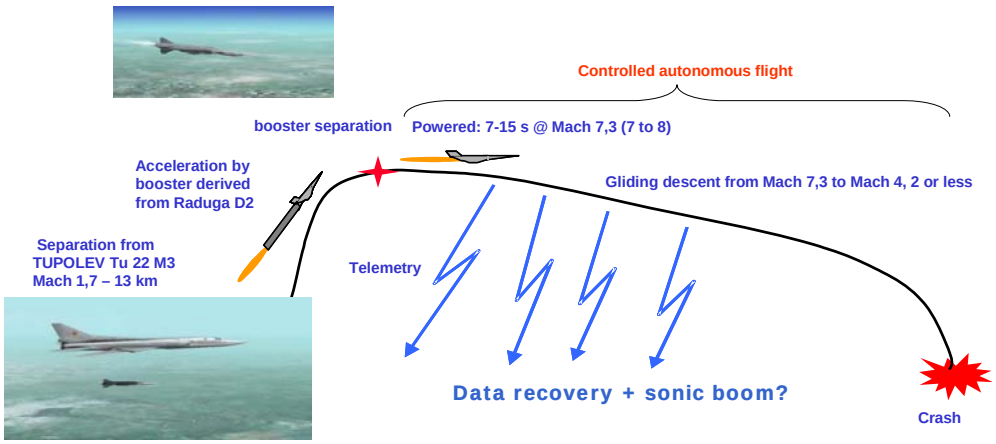


***Figure 82 LEA flight test concept***

Before performing the integration study, it was necessary to start by re-building a general model of the Russian booster. As ONERA is not allowed to make use of Russian Information obtained from Raduga through the LEA Program, ONERA defined a new booster using only data available in the open literature on Raduga D2 concept.

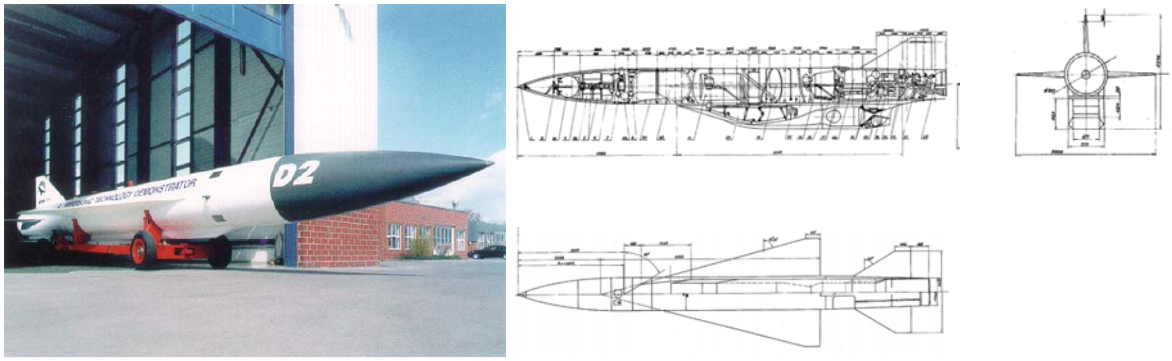


***Figure 83 Raduga D2 booster and use as hypersonic test bench for propulsion tests***

Then, a generic definition of air-launched platform was established as a first attempt to integrate a small scale EFTV-A with length of 2,88m.

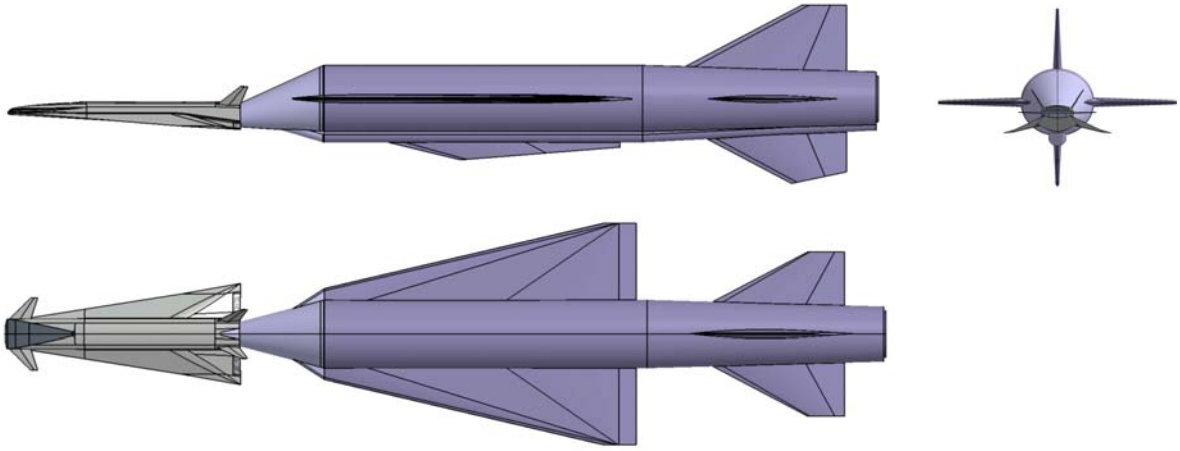

***Figure 84 First integration study for L=2,88m***

The adaptation of the EFTV-A experimental vehicle to the Raduga booster, thanks to a specific interstage, was presented and discussed.

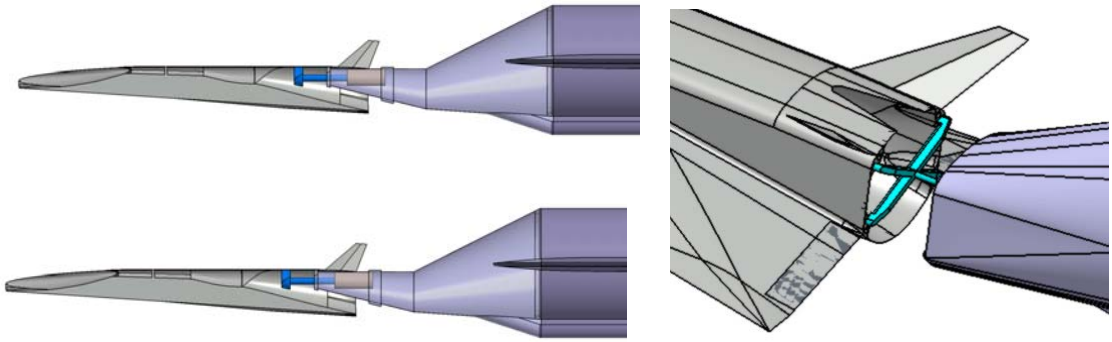

***Figure 85 Separation scenario: based on DLR studies for ground launch (left) and preferred option for air-launched (right)***

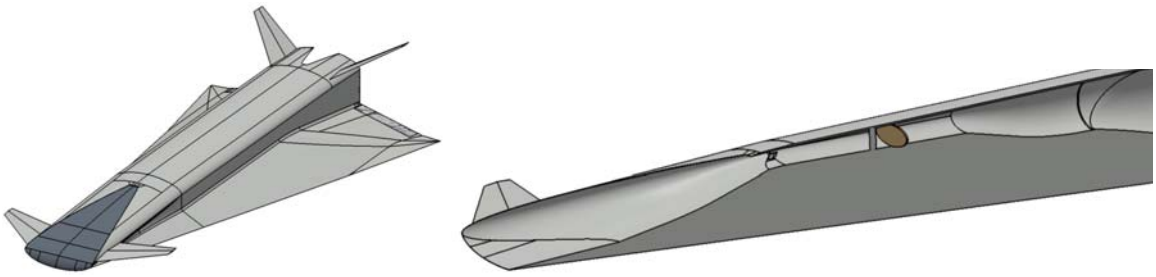

***Figure 86 Different options regarding the management of internal flowpath –Fairing ( Left) and internal closure (right)***

A preliminary performance assessment was presented, showing the possibility to match the Hexafly requirements regarding both aeropropulsion and sonic boom issues. First elements regarding costs were also described.

In a second step, the preliminary integration study was refined and extended to a large scale concept with a length of L=4,5m. For both scales, it seems possible to accommodate with the different geometrical constraints associated to the booster and the aircraft with satisfactory margins.

**L= 2,88 m**
**short interstage, shortened booster**

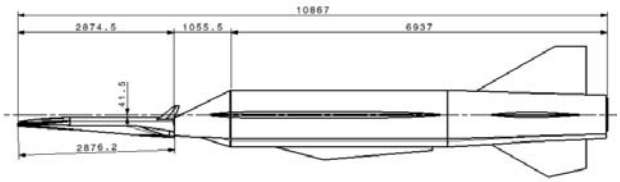


**L= 2,88 m**
**short interstage, nominal booster**

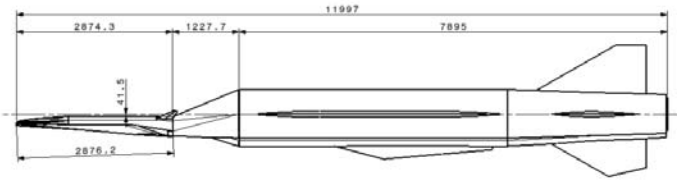


**L= 4,5 m**
**short interstage, nominal booster**
**Closed flowpath**

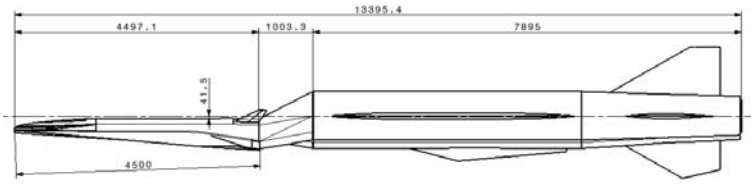


**L= 4,5 m**
**short interstage, nominal booster**
**Open flowpath**

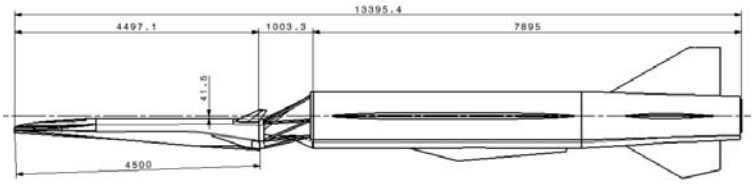


***Figure 87 Different variants for EFTV-A integration at different scales***

In order to check aerodynamic stability and to enable performance assessment, aerodynamic models were established based of semi-empirical models, Euler computations, and finally some full 3D Navier-Stokes computations. This provided models covering the overall flight domain (Mach 1,7 to Mach 8) for both scales.

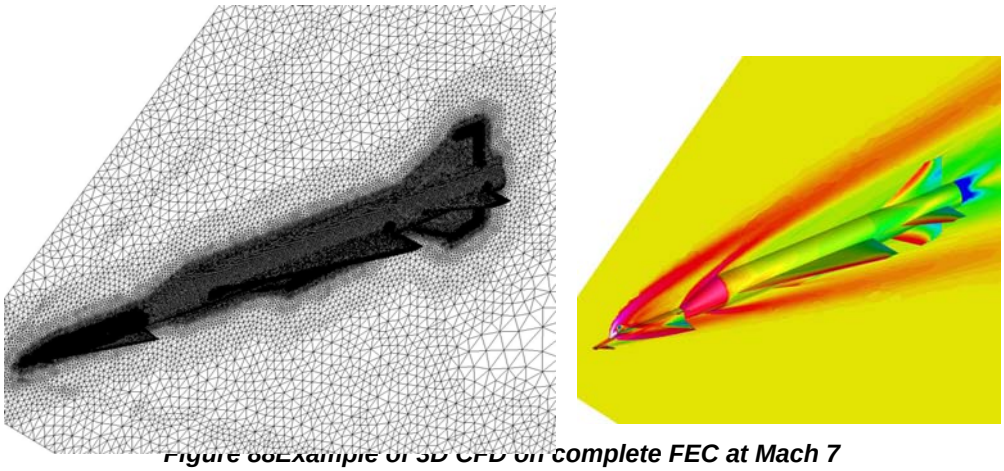

*Figure 88Example of 3D CFD on complete FEC at Mach 7*

The mass considered for the large scale option was defined within WP2. Maximum and very pessimistic value proposed was 1400 kg so far, which would probably exceed allowed structural design limitations. This mass is much higher than for LEA, when its length is roughly the same. It is recommended to select the EFTV technologies in a way to reduce the mass. Such a too large mass would be an issue for the mechanical loads applied to the upper structure of the booster. It would also lower the frequency of the first bending mode, which might appear too low.

Finally, after first performance assessment, it is also confirmed that this mass would not allow reaching the targeted maximum Mach number range. A limitation to Mach 5,5 is anticipated. A mass of 800 kg would enable reaching Mach 6,4, and the target of Mach 7,5 could be achieved only if the mass of EFTV is reduced to less than 600 kg. This figures would need refinement with Russian side.

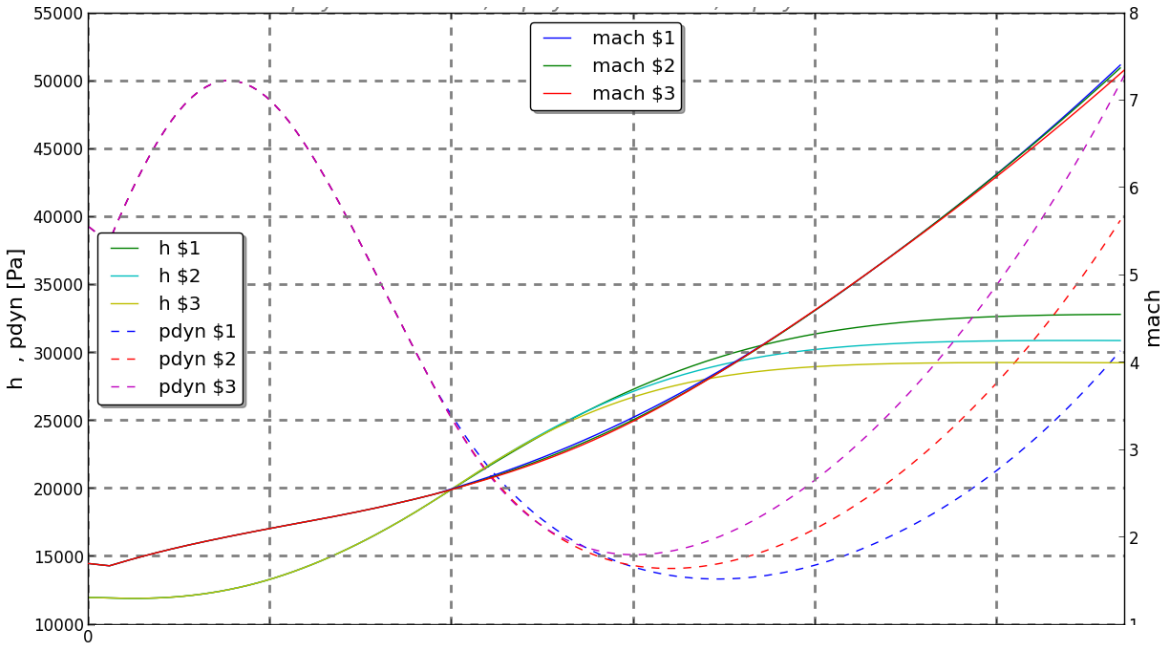


*Figure 89 Performance assessment for EFTV-A – L=2,88m – m=400 kg*

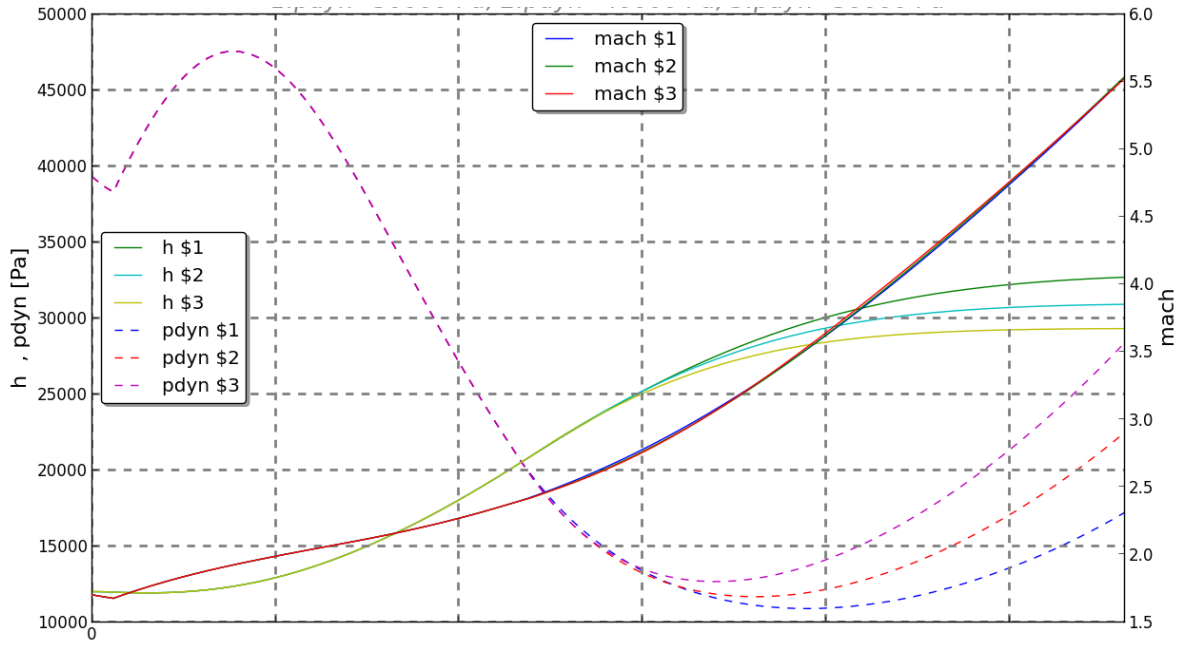


***Figure 90 Performance assessment for EFTV-A L=4,5m – m=1400 kg***

A stability issue is also identified for both scales, due to the presence of large lifting surfaces in the front part of the booster during acceleration. If some solutions can be envisaged with the smallest vehicle (implementation of mass at different locations), this seems more difficult at larger scale, when the estimated mass of the EFTV-A already exceeds the acceptable limits. This point is to be addressed specifically to enable better understanding of the integration constraints. This study would require further information about the evolution of the booster's center of gravity. These issued should be addressed with Raduga designers.

Whatever the scale, it is clear that some of the specific tests that have been performed for LEA vehicle will have to be also performed for such specific platform (e.g. aerodynamic tests, safety tests). Some additional tests will be required because of the extension of the flight test duration. The long gliding descent might require adaptation of the data transmission system due to a much longer range.

Finally, it is also confirmed that using the air-launched platform would offer an interesting option to address sonic boom issues, in particular during the FEC flight, because the FEC is a large system which should provide both an operational shape as reference, and a sufficient pressure signal at ground level on track, where the signature of the EFTV alone could be more difficult to detect.

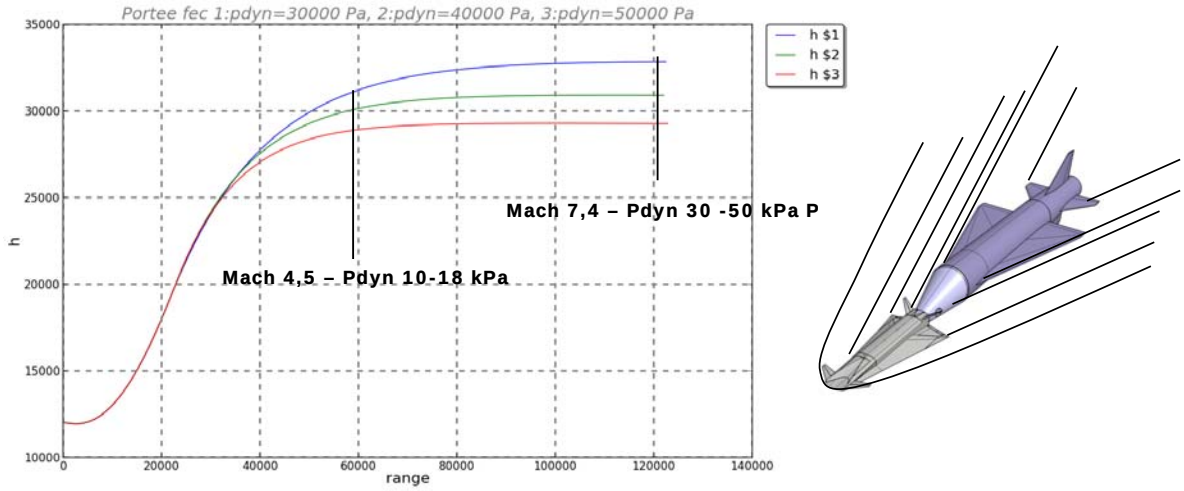


***Figure 91 – Use of final acceleration to perform sonic boom analysis ion FEC***

First analysis of cost issues associated to the reference EFTV-A vehicle. Although a large part of the necessary know-how has been developed within the LEA Program to address this flight test approach, some specific work has to be performed to enable integration of EFTV-A in a FEC system. A list of necessary tasks has been defined, which would require further discussions with the Russian side through French partners.

Two EFTV variants have also been analysed as possible cost reduction options.

Variant 1: ELTV-A (LEA-based test vehicle) is making a wide re-use of existing hardware of the LEA flight test program, the LEA engine being replaced by a scaled EFTV-A engine.

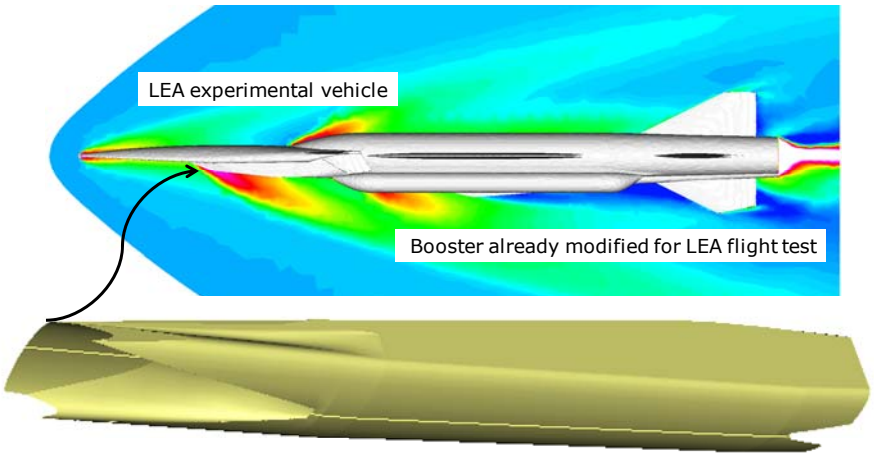


***Figure 92 ELTV approach: integrating EFTV-A engine concept on-board LEA platform***

The feasibility of such approach was confirmed by MBDA, and all on-board equipment and systems, including fuel supply system, proved to be well adapted to the needs in the new engine concept. This approach would clearly enable considering the existing hardware is developed and validated, and this should lead to significant expenses avoidance. Such variant seem to make sense and should lead to avoid a large part of development costs associated to the vehicle, even though the need for some specific tests would still need further discussions with the Russian side.

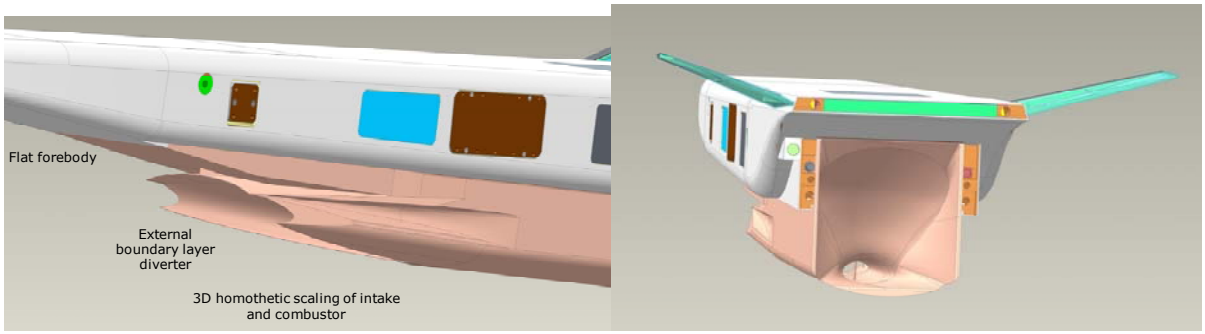


***Figure 93 EFTV-A integration into LEA platform***

Variant 2: ECTV-A considers a captive carry test, where the EFTV concept remains attached to its booster. This specific architecture enables testing the propulsion system over a wide range of Mach number during the acceleration phase provided by the booster. The flexibility of the liquid fuel rocket engine on the booster, and its large lift and control surfaces opens the way to a large display of trajectory that can be adapted to the needs of such flight test concept.

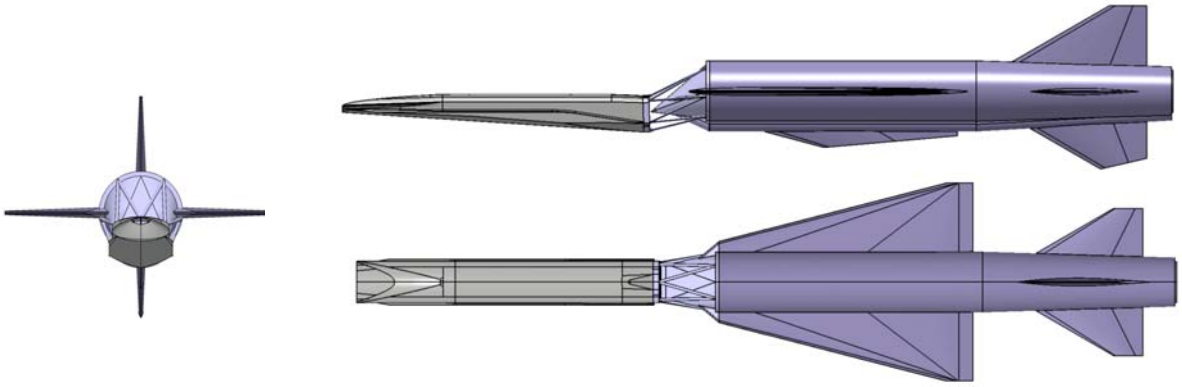

***Figure 94 – flight tests with non-separated configuration (ECTV-A)***

With the same acceleration scenario as for free flights, the final section of the trajectory provides:

- a horizontal flight at constant altitude (at least selected in the range 27km to 34km)
- acceleration between Mach 4 and Mach 6,5 with stabilized attitude
- a continuously increasing dynamic pressure in a range depending on the selected altitude (e.g. 22 kPa to 5O kPa for z=27km)

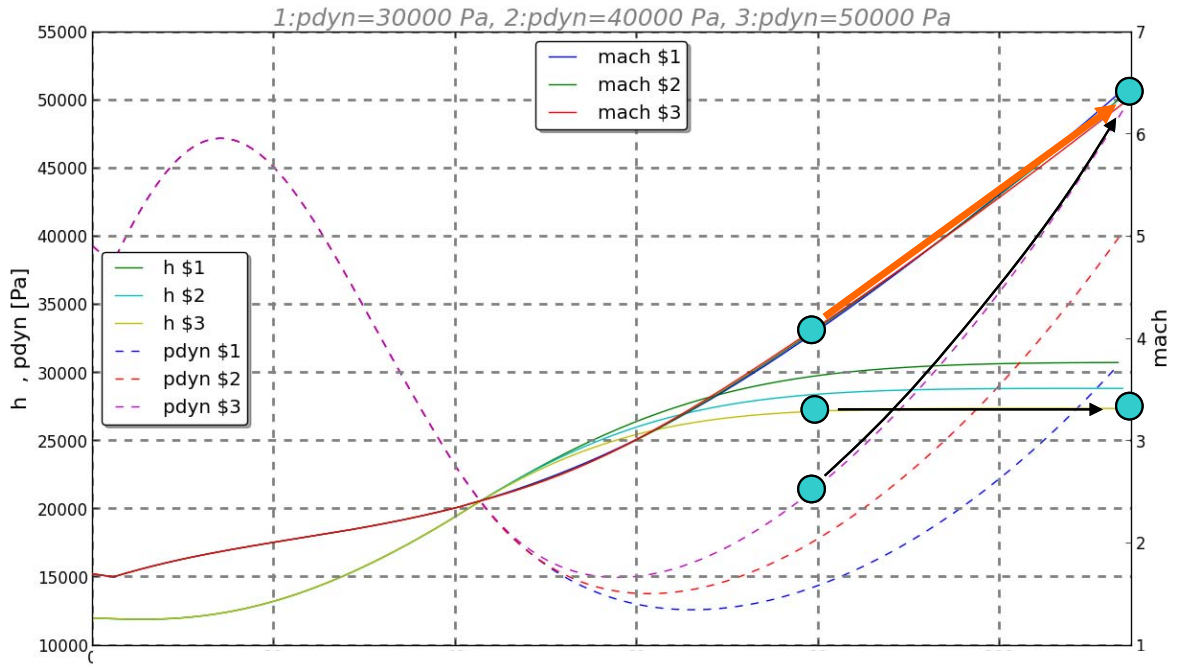


***Figure 95 Performance assessment with ECTV-A (L=4,5m)***

Both ELTV-A and ECTV-A offer an interesting trade-off between costs and technical / scientific goals.

*Critical issues*

Aerodynamic stability of the FEC with a large lifting body like EFTV-A would have to be studied in details with Raduga, in order to check the controllability along the whole trajectory.

The maximum Mach number that can be reached with the booster might be below 6,5 if the mass of the EFTV is maintained close to 800 kg. An objective of 600kg could favour reaching the targeted flight point. Accordingly, this mass of 600 kg should be considered as a target also for the EFTV-A in order to ease the design of the interstage between EFTV concept and booster, and avoid structural limits. In any case, those limits should be further discussed with Russian side.

If the stability issues remain too difficult to solve, in particular with a large scale EFTV-A, a good cost effective option would be to further study the interest of captive flight.